Investigations sur la perméabilité des formations salifères stratifiées du site de StocaMine

In situ permeability investigations in layered saliniferous formation of StocaMine

Table of content

1 Extended Abstract (French Version)

1.1 Résumé

Dans le cadre de la planification de la fermeture du site, IBeWa Consulting a été mandatée par la société StocaMine, France, pour réaliser des mesures de perméabilité étendues sur le site.

Les mesures réalisées dans l'ancienne mine de potasse "mine Amélie" (Fossé du Rhin Supérieur) visaient essentiellement à caractériser la zone perturbée par les excavations (excavation damaged zone, ou zone EDZ), en tenant compte des conditions particulières de la formation rocheuse tertiaire, entrecoupée de couches salifères. Aussi, nous avons réalisé 150 essais de perméabilité au gaz sur place, à l'aide de packers de forage, en vue d'analyser la distribution spatiale de la perméabilité en fonction de la distance au contour k = f(dtc) (conditions hydrauliques latérales dans le voisinage du site de stockage de déchets, 4 sites d'implantation potentiels de barrages). De plus, les investigations ont également porté sur les conditions de perméabilité de la couche S du toit, riche en marne/anhydrite (conditions hydrauliques verticales au centre du site de stockage de déchets, 3 sites). Enfin, nous avons déterminé la teneur en saumure des carottes de forage prélevées sur les sites de mesure, en vue d'évaluer l'état de la roche durant les essais de perméabilité au gaz conduits sur site.

En nous basant sur les données les plus récentes disponibles, nous avons trouvé une distribution spatiale hétérogène de la perméabilité à l'intérieur de la zone EDZ (qui caractérise les conditions hydrauliques latérales) au niveau des sites d'implantation potentiels des barrages. La perméabilité dans la zone EDZ dépend des conditions géomécaniques du site (c'est-à-dire des différences entre les conditions géomécaniques rencontrées au niveau du toit, du mur, des parements et des angles des galeries de section rectangulaire), de la distance au contour (tendances générales) et des conditions géologiques du site (variation des strates lithologiques / variations rhéologiques observées). Nous supposons que les variations de dilatation induites par la déformation autour de la galerie sont dues aux différences de résistance des différentes couches composant la formation salifère stratifiée du terrain.

Sauf au niveau des angles de la galerie, la perméabilité au gaz dans la zone EDZ peut atteindre des valeurs maximales de 7E-14 m², pour retomber à des valeurs d'env. 1E-18 m² à une distance au contour comprise entre 1 m et 2 m. Toutefois, il y a des indices pour une élévation de la perméabilité induite par la lithologie (2.4E-16 m² et 2.1E-13 m²) à une distance de > 1.5 m au sein de la couche de marne/anhydrite du mur. La distribution de la perméabilité au niveau des angles de la galerie diffère de la situation décrite, avec des perméabilités maximales de 1E-15 m², retombant rapidement à env. 1E-18 m² (entre 0.25 m et 0.5 m de distance), probablement du fait de contraintes géomécaniques élevées, limitant la dilatation. Les conditions hydrauliques verticales (toit) au centre du site de stockage se caractérisent apparemment par une faible perméabilité à des distances supérieures à env. 1.5 m. Ceci correspond bien à l'augmentation de pression observée, due aux émissions de gaz en provenance du banc S riche en inclusions de marne/anhydrite, au cours des essais de perméabilité dans les trous de forage. En principe, la situation générale de la perméabilité au niveau du toit au centre et dans le voisinage du site de stockage semble compatible. Les conditions de perméabilité dans le pilier de la double galerie ne diffèrent pas de celles examinées dans d'autres forages au niveau du parement, qui se caractérisent par des perméabilités élevées.

Enfin, aucun indice ne permet de conclure à une incidence majeure de teneurs élevées en solution présentes dans le sel gemme sur la perméabilité effective au gaz de cette roche. En effet, les teneurs en solution mesurées, inférieures à 0.1 wt %, pour la majeure partie des carottes analysées, indiquent un état généralement sec de la roche. Nous avons néanmoins observé une augmentation de la teneur en solution jusqu'à 1 wt % sur quelques échantillons de sel gemme pur, qui présentaient des pores et de l'humidité visibles. En revanche, certains échantillons, constitués soit de sel gemme comportant des impuretés de type marne/anhydrite, soit de couches de sel gemme alternant avec de la marne/anhydrite, soit de marne/anhydrite pures, peuvent atteindre des valeurs jusqu'à 14.2 wt %. Ces dernières pourraient être dues à la présence d'eau cristalline par suite du séchage au four à 105 °C.

1.2 Introduction - conditions géologiques

Le site de StocaMine fait partie de l'ancienne mine de potassium "mine Amelie", située dans le bassin potassique de Wittelsheim (Fossé du Rhin Supérieur). Ensemble, les bassins de Wittelsheim et de Münchhausen forment le Bassin Potassique de Mulhouse (Figure 1).

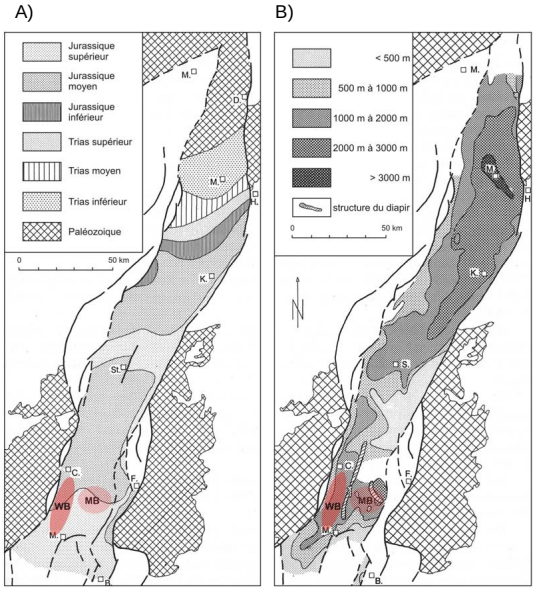

Figure 1 Localisation du Bassin de Mulhouse dans le Fossé du Rhin Supérieur [4]

[Explication : A) Mur tertiaire, B) Isobathes de la base tertiaire, WB – Bassin de Wittelsheim, MB – Bassin de Münchhausen]

La base tertiaire du Bassin Potassique de Mulhouse se situe à une profondeur comprise entre 1000 m et 2000 m en-dessous du niveau de la mer. De l'extraction de potasse a été réalisée dans les deux bassins (MB et WB).

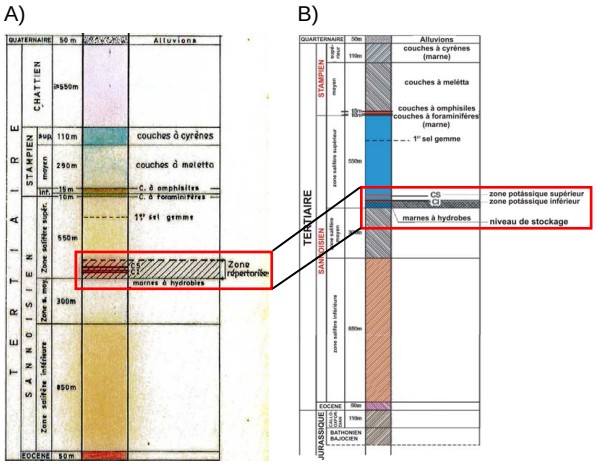

Figure 2 Situation stratigraphique générale

[Explication : A) Bassin de Mulhouse [1], B) StocaMine [3]]

La position stratigraphique du site de stockage de déchets souterrain StocaMine est illustrée dans le profil normal. Les excavations de StocaMine sont situées dans le mur de la zone de potasse, formée de deux bancs de sylvinite (Figure 2B) [3].

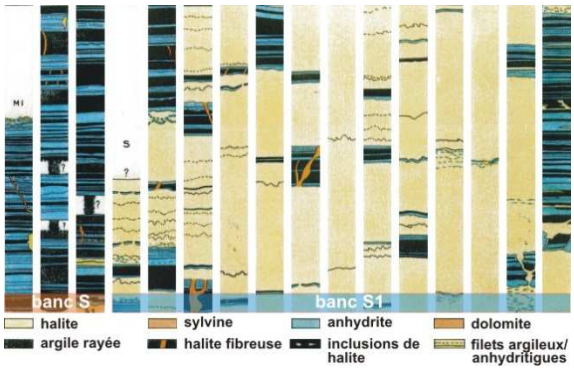

Figure 3 Couches lithologiques dans la zone de stockage [1]

Le sel gemme de la zone de stockage est essentiellement strié de couches de marnes calcaires et d'anhydrite (Figure 3).

Au niveau du site de stockage, le banc de sel gemme subhorizontal, présentant un léger dénivelé dans le sens nord-ouest, ne semblerait avoir d'impact tectonique connu ; cependant, des failles, orientées sud-ouest - nord-est, ont été identifiées dans d'autres parties du bassin [3]. La situation hydrogéologique au sein de la formation évaporitique a été caractérisée par [3] comme étant normalement anhydre (à l'exception de quelques petites inclusions de saumure dues aux opérations d'extraction et d'autres, originaires de marnes exemptes de sel). Les excavations du site de StocaMine sont séparées des horizons aquifères par plusieurs centaines de mètres de sel gemme et de marnes présentant une faible perméabilité.

1.3 Description du site et programme des essais

La Figure 4 récapitule la localisation de l'ensemble des sites de mesure. Les sites de test désignés par T2 se situent dans les galeries dans le voisinage du site de stockage. En revanche, les sites de test désignés par T1 se situent dans le centre du site de stockage.

Pour les sites T1-1 et T1-2, un pilier massif, préservé dans le toit de la mine de potasse, joue un rôle géomécanique important (marque bleue, Figure 4).

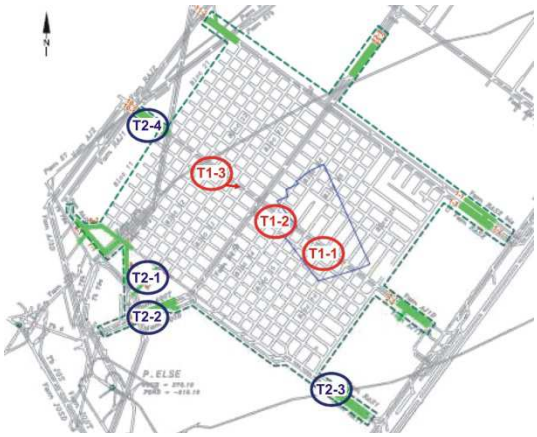

Figure 4 Localisation des sites de test
[Explication : marque bleue – pilier massif dans le toit de la mine de potasse]

Le Tableau 1 récapitule les informations relatives aux différents sites.

Tableau 1 Récapitulatif des informations relatives aux sites

Site	Position[1]	Galerie	Excavation	Trous de forage	Stratigraphie[2]	Remarques
T1-1	centre	AJ1T/AJ1D	Banc de 23 m et Banc de 25 m	2	S et S1	pilier massif dans le toit de la mine de potasse
T1-2				2		
T1-3				2		
T2-1	volsinage	A-12		4	S1	-
T2-2		AQ0T/AQ0D		9		
T2-3		RAS1/RAT1	en-dessous du banc de 25 m	9		
T2-4		AJ1T/AJ1D	Banc de 23 m et Banc de 25 m	9		

Un total de 140 m de forages a été réalisé (forage à sec), sur un total de 37 trous de forage, d'un diamètre de 70 mm. Sur chacun de ces trous de forage, des essais ont été réalisés sur un à six points. Ainsi, env. 150 mesures de perméabilité au gaz ont été réalisées sur site, à l'aide de packers doubles ou quadruples, d'un diamètre < 70 mm. En général, les tronçons d'essai présentaient une longueur d'env. 0.18 m. Cependant, sur certains trous de forage, des séquences de mesure intégrales ont été réalisées sur des tronçons de plusieurs mètres de long. Avant les tests de perméabilité, les trous de forage ont fait l'objet d'un nettoyage normalisé à l'air comprimé sec, et d'une inspection par vidéo-endoscopes. La Figure 5 illustre une galerie double et le plan de forage mis en œuvre.

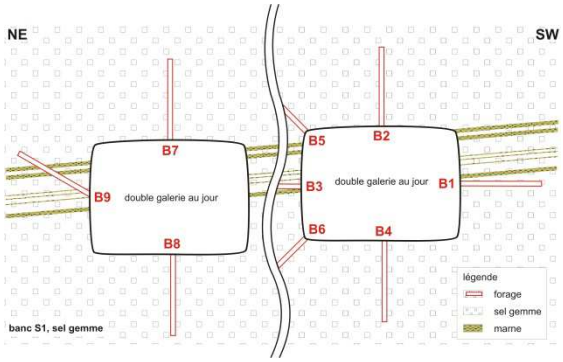

Figure 5 Profil schématique des sites d'exploration (p. ex. double galerie T2-2, -3 et -4)

En plus des tests sur site, des analyses de laboratoire ont été réalisées pour déterminer la teneur en saumure au niveau des points de mesure. Ainsi, les carottes ont été caractérisées du point de vue géologique, scellées dans un film en plastique, transportées au laboratoire et photographiées, puis débitées en échantillons en vue du séchage au four.

Les échantillons de carotte ont été triés en trois groupes : marnes, sel gemme contenant une certaine fraction de marne et sel gemme pur. La Figure 6 illustre les lithologies retrouvées dans les échantillons.

[1] relative au site de stockage de déchets souterrain
[2] rapporté à [1]

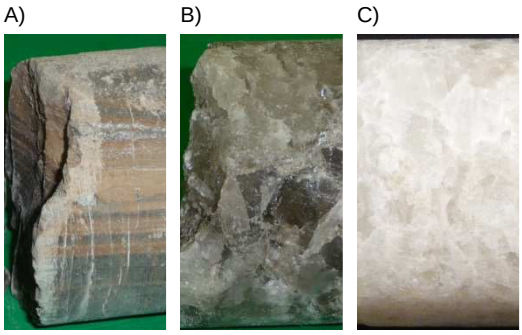

Figure 6 Lithologies retrouvées dans les échantillons

[Explication : A) échantillon de marne ± anhydrite, B) sel gemme contenant une certaine fraction de marne, C) sel gemme visuellement pur]

Environ 200 échantillons ont été prélevés sur les carottes extraites de l'ensemble des trous de forage, et séchés à env. 105 °C au four, conformément au chapitre 1.4.2. L'objectif consistait à détecter des teneurs en saumure élevées en vue d'évaluer les perméabilités au gaz mesurées sur site, en tenant compte de l'impact potentiel de la saturation en liquide sur la perméabilité effective au gaz.

1.4 Méthodes d'analyse

1.4.1 Détermination de la perméabilité à l'aide d'essais in situ

Les tests de perméabilité in situ constituent des expérimentations rhéologiques. Durant ces expérimentations, un processus rhéologique transitoire est initialisé et enregistré. Différents fluides sont mis en œuvre. Aussi, on peut réaliser des tests à l'aide de plusieurs types de gaz et de liquides (généralement de la saumure). La sélection des fluides dépend toujours de l'usage prévu et de la mission d'expérimentation définie.

Le gaz et notamment l'air comprimé sec est un fluide inerte au regard de l'espace interstitiel des roches salifères ; il est couramment utilisé pour les tests de perméabilité dans les formations salifères (p. ex. [5], [6], [7], [8], [9], [10], [11], [12]).

Sachant d'une part que la perméabilité au gaz dépend de la saturation en liquide et sachant d'autre part que la présence de liquide dans l'espace interstitiel ne saurait être exclue totalement, la perméabilité au gaz mesurée sur site démontre a priori l'existence d'une perméabilité effective au gaz. L'ampleur de cette perméabilité pourrait diminuer au fur et à mesure de la saturation en liquide de la roche. En cas d'humidité élevée, révélée par la présence de saumure dans les carottes de forage prélevées sur les sites de mesure de perméabilité in situ, des tests de perméabilité à la saumure (fluide liquide) sont recommandés.

Les tests de perméabilité in situ peuvent être essentiellement réalisés sous forme de :

- tests d'impulsion (IT),
- tests à pression constante (CP) et
- tests à débit constant (CR).

Avant de procéder aux mesures, des tests de fuite sont réalisés sur place pour prouver l'étanchéité requise de l'équipement de test assemblé. Il est possible d'additionner le gaz à l'aide de 1,1,1,2-tétrafluoroéthane en vue de détecter des fuites. Même de faibles traces (> 1.5 ppm) sont décelables et permettent la mise en évidence de fuites.

Des transducteurs de pression piézoélectriques d'une précision située généralement entre 0.1 % et 0.2 % sont utilisés pour enregistrer l'évolution de la pression dans le temps dans les tronçons d'essai et les éléments de packer. Les plages de mesure des capteurs sont soigneusement adaptées à la plage de pression attendue. Le débit est enregistré à l'aide de débitmètres massiques thermiques d'une précision de 1 % de la valeur relevée (< 20 % du débit) et de 0.2 % de la pleine échelle (> 20 % du débit). Le dispositif de test de perméabilité comprend une unité de contrôle de pression, de mesure et d'acquisition de données.

Pour évaluer les données mesurées et pour déterminer la perméabilité, nous avons créé un modèle 2D dans une géométrie de type r-φ-z (profil r-z) pour chaque mesure, prenant en compte la structure géométrique et les propriétés du fluide. Ce modèle peut être discrétisé au moyen de variables. Le rayon est étendu dans la direction x à partir du centre du trou de forage, et la profondeur est étendue dans la direction y (Figure 7). En appliquant un

code informatique spécifique, on peut simuler la solution numérique d'une équation différentielle partielle (PDE) du débit isotherme en 2D, symétrique au rayon, pour une phase unique (gazeuse ou liquide). Le paramètre "perméabilité" est déterminé en rapprochant les données de pression mesurées et calculées.

La perméabilité est déterminée en rapprochant les courbes de pression simulées aux courbes de pression mesurées. La fonction cible de ce "rapprochement" consiste à minimiser l'erreur quadratique moyenne des deux courbes (méthode des moindres carrés).

La Figure 7 illustre la simulation d'un débit symétrique au rayon au cours d'un test à l'aide d'un packer.

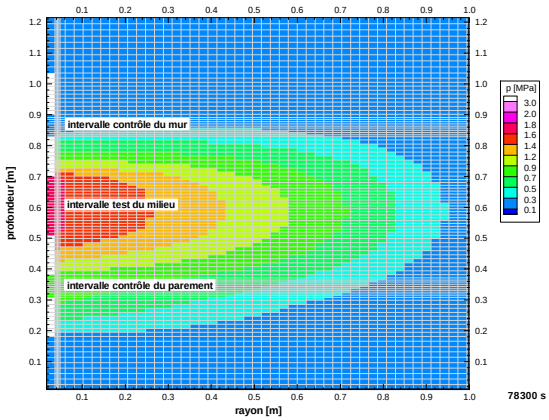

Figure 7 Evaluations du test – discrétisation du modèle et distribution spatiale simulée de la pression

- rouge : pression élevée se propageant depuis le tronçon d'essai
- bleu : pression initiale (faible) dans la roche (pression d'air)

1.4.2 Détermination de la teneur en saumure par séchage au four

La teneur en saumure a été déterminée par séchage au four à 105 °C [2] jusqu'à la stabilisation du poids de l'éprouvette séchée. Des échantillons ont été prélevés sur les carottes, extraites au plus près du tronçon d'essai. La précipitation de saumure dans l'espace interstitiel a été prise en compte en considérant la minéralisation et la densité de saumure saturée en NaCl (halite) [13].

1.5 Essais de perméabilité sur le site T1

Figure 8 illustre les résultats de la mesure de perméabilité.

A)

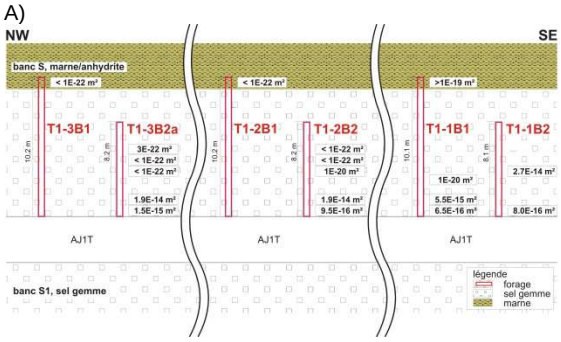

B)

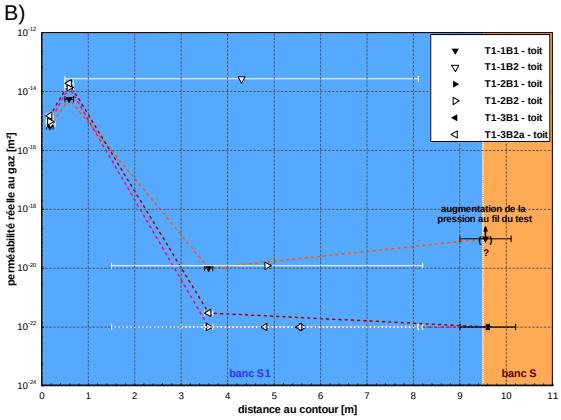

Figure 8 Résultats obtenus au niveau des sites T1-1, T1-2 et T1-3 – toit

[Explication : A) Profil schématique de la galerie présentant une perméabilité effective au gaz, B) Diagramme k_{eff} / distance]

Comme l'illustre la Figure 8, il existe une bonne corrélation entre les résultats obtenus sur les différents sites (T1-1, T1-2 et T1-3). La zone plus proche du contour (< 0.5-1.0 m) se caractérise par une augmentation de la perméabilité effective en fonction de la distance. Il n'y a cependant aucun indice pour une teneur plus élevée en saumure au niveau de ces points de mesure. Aussi, nous pouvons exclure une influence majeure de la teneur en saumure sur la perméabilité effective au gaz.

Les mesures réalisées dans la zone proche du contour ont généralement révélé un niveau de perméabilité assez élevé > 6E-16 m² (T1-1B1-010-G1). Cela peut s'interpréter comme la désagrégation de la roche dans la zone EDZ. Au-delà de cette zone, la perméabilité retombe à des valeurs très faibles, de l'ordre de ≤ 1^{E}-20 m² (T1-1B1-350-G). La transition entre

des valeurs de perméabilité > 1E-18 m² et < 1E-18 m² semblerait intervenir plus tôt sur les sites T1-2 et T1-3 qu'au niveau du site, T1-1, à une distance comprise entre env. 0.6 m et env. 1.5 m (au-dessus des tronçons d'essai T1-2B2-150-G et T1-3B2a-150-G).

Les perméabilités effectives au gaz, mesurées sur les sites T1, peuvent se distinguer comme suit :

- distance au contour < env. 0.6 m: => perméabilité élevée (> 6E-16 m²) au niveau de la zone EDZ et
- distance au contour > env. 1.5 m : => niveau de perméabilité (≤ 1E-20 m²), au-delà duquel l'augmentation de la pression mesurée (T1-1B1-900-G et T1-2B2-150-G) confirme un faible niveau de perméabilité.

1.6 Essais de perméabilité sur le site T2

1.6.1 Conditions de perméabilité au niveau du toit

La Figure 9 illustre l'évolution de la perméabilité en fonction de la distance au niveau des sites T2.

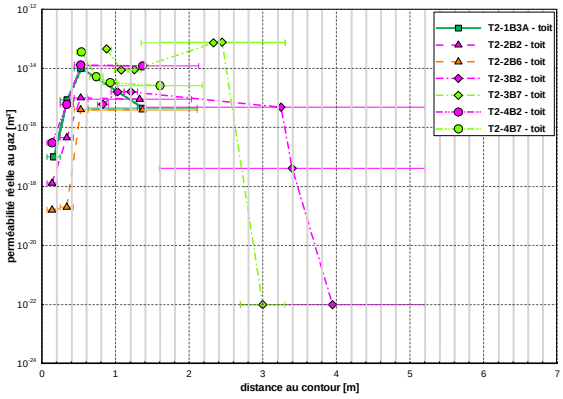

Figure 9 Perméabilité effective au gaz / distance au contour au niveau des sites T2 – toit

Comme l'indique la Figure 9, il existe une bonne corrélation entre les sites de mesure T2. Tous les profils présentent des conditions plus ou moins similaires. La perméabilité effective au gaz augmente à une distance < env. 2 m. Cela correspond aux profils étendus du site T2-3. Cependant, une baisse de la perméabilité à ≤ 1E-22 m² est observée à une distance > env. 2 m.

Les perméabilités effectives élevées au gaz mesurées au niveau du point de mesure MP4 (0.63 m jusqu'au fond du trou de forage) sur les sites T2-1, T2-2 et T2-4 pourraient être dues à des perméabilités localement plus élevées au niveau des couches minces de marne/anhydrite (p. ex. plans de stratification). Le profil décalé au niveau du site T2-4B7 révèle une faible baisse de la perméabilité à l'intérieur du tronçon initialement retenu pour le point de mesure MP4 (0.63 m jusqu'au fond du trou de forage). Néanmoins, la mesure T2-4B7-103-G, réalisée sur un tronçon de 1.04 m jusqu'au fond du trou de forage, révèle toujours une perméabilité au gaz effective relativement élevée de 2.6E-15 m². Les tronçons de mesure présentant une distance au contour plus importante (p. ex. T2-3B2-160-G, T2-3B2-270-G, T2-3B7-270-G) révèlent une baisse de la perméabilité jusqu'à env. ≤ 1E-22 m², ce qui concorde avec l'hypothèse d'une couche rocheuse non perturbée.

1.6.2 Conditions de perméabilité au niveau du parement

La Figure 10 illustre les changements de perméabilité pour l'ensemble des trous de forage pratiqués dans le parement.

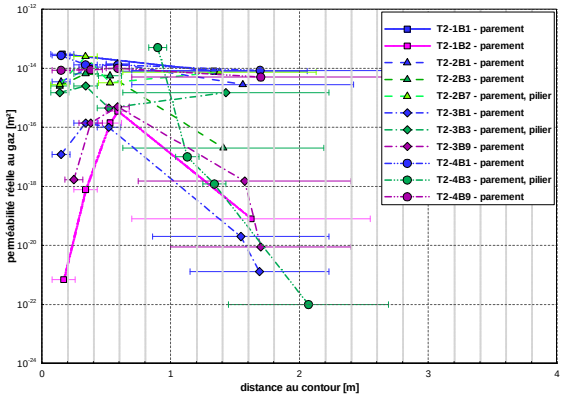

Figure 10 Perméabilité effective au gaz / distance au contour au niveau des sites T2 – parement

La majeure partie des mesures ont donné lieu à des perméabilités > 1E-15 m² telles que décrites par la Figure 10. Encore une fois, nous supposons que les perméabilités localement plus élevées au niveau des couches de marne/anhydrite (p. ex. plans de stratification)

sont à l'origine des perméabilités élevées fréquemment observées.

Un deuxième groupe de mesures englobe les mesures sur l'intégralité des trous de forage T2-1B2, T2-3B1 et T2-3B9, MP4 au niveau du trou de forage T2-2B3 et les 3 dernières mesures dans le trou de forage T2-4B3. La perméabilité dans les trous de forage de ce groupe s'accroît en fonction de l'augmentation de la distance au contour dans un intervalle compris entre 0 m et env. 0.6 m. Là non plus, nous n'avons trouvé aucun signe de teneur plus élevée en saumure.

Les mesures sur des tronçons plus courts (T2-4B3) révèlent une transition de perméabilité de > 1E-18 m² à ≤ 1E-18 m², à l'intérieur d'une distance au contour comprise entre env. 1.2 m et 1.4 m, ce qui concorde parfaitement avec les résultats obtenus au niveau du point de mesure MP4 dans les trous de forage T2-2B3, T2-3B9 et T2-1B2.

Aucun indice n'a été fourni quant à des perméabilités plus élevées au niveau des piliers des doubles galeries (entre AQ0T et AQ0D ou entre AJ1T et AJ1D) par rapport aux parements massifs.

1.6.3 Conditions de perméabilité au niveau du mur

Les conditions de perméabilité au niveau du mur pour les sites T2 sont illustrées par la Figure 11.

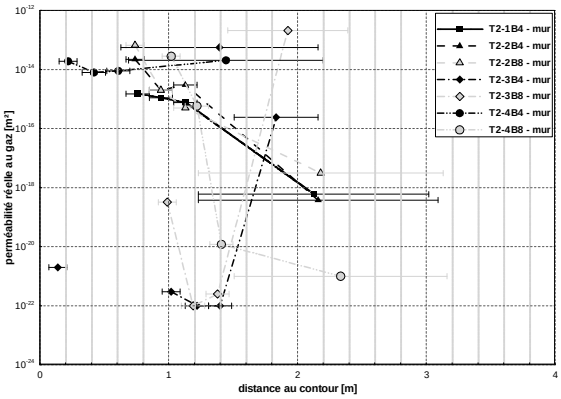

Figure 11 Perméabilité effective au gaz / distance au contour au niveau des sites T2 – toit

Un effritement visible du mur (p. ex. failles, fissures) dans une profondeur jusqu'à 0.6 m nous a amené à décaler les profils de T2-1B4, T2-2B4 et T2-2B8. Le profil au niveau du trou de forage T2-4B8 a même été décalé d'env. 1.0 m. En revanche, le profil T2-4B4 débute dès une profondeur d'env. 0.15 m (pas d'effritement visible). Les profils au niveau du site T2-3 ont été décalés respectivement d'env. 0.85 m ou 0.88 m.

Là aussi, nous avons observé une bonne corrélation entre les résultats de T2-1 et de T2-2. Néanmoins, la perméabilité diminue en fonction de l'augmentation de la distance au contour dans le mur. C'était un effet attendu, résultant de la perturbation du mur par suite des travaux d'excavation (zone EDZ).

Pour le site T2-4, le changement de perméabilité de > 1E-18 m² à des valeurs ≤ 1E-18 m² intervient à une distance au contour comprise entre env. 1.13 m et env. 1.5 m (points de mesure MP2 et MP3 du site T2-4B8, Figure 11). De l'autre côté, les mesures réalisées sur le site T2-4B4 se sont soldées par des perméabilités relativement élevées, comprises entre 7.9E-15 m² et 1.4E-14 m², indiquant que le décalage du profil a été judicieux. Sans contredire les mesures réalisées au niveau des sites T2-1, T2-2 ou T2-4B8, le point de mesure MP4 du site T2-4B4 (env. 0.69 m jusqu'à env. 2.2 m) est tout simplement plus fortement tributaire des perméabilités accrues. Aussi, les résultats de T2-4 sont en bonne corrélation avec les tendances observées au niveau de la distribution des perméabilités, et fournissent des informations essentielles pour les zones > env. 1.2 m (T2-4B8) et < env. 0.6 m.

Sur la base de ces observations, nous supposons la distribution suivante : des perméabilités relativement élevées dans une zone comprise entre 0 m et env. 1.13 m (> env. 1E-15 m²), un changement de perméabilité de > 1E-18 m² à ≤ 1E-18 m² à une distance au contour de 1.5 m et des perméabilités relativement faibles, < 1E-18 m², à des distances > env. 1.5 m. Cela ne s'applique pas en cas de changements dans la stratification géologique, comme l'indiquent les profils des deux sites de

mesure T2-3 (T2-3B4 et T2-3B8). La situation géologique différente du niveau du mur du site T2-3 est décrite par la Figure 12 (intercalation de marne/anhydrite au fond du trou de forage).

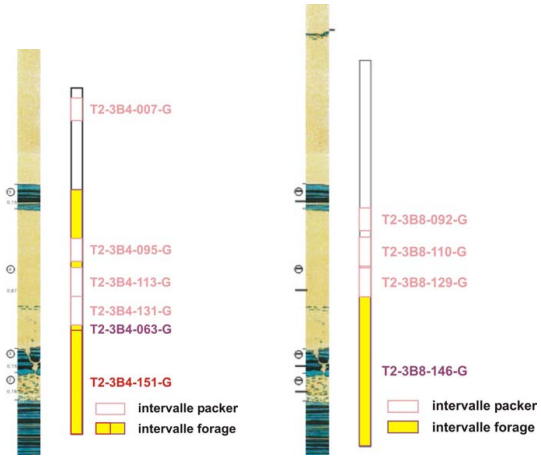

A) T2-3B4 B) T2-3B8

Figure 12 Description schématique de la situation géologique au niveau du site T2-3, situé à env. 25 m de profondeur dans le mur de la mine de potasse

Après des niveaux de perméabilité de ≤ 1E-22 m², les valeurs augmentent à > 1E-18 m² à des distances > 1.5 m (T2-3B4-151-G et T2-3B8-146-G). En rapportant ces résultats à la situation géologique illustrée par la Figure 12, nous en déduisons que la perméabilité élevée au niveau des plans de stratification entre le sel gemme et la marne et/ou entre la marne et l'anhydrite explique les niveaux élevés de perméabilité effective au gaz mesurés. Ce changement de stratification géologique a été observé lors des investigations endoscopiques.

De plus, les mesures réalisées au niveau des sites T2-3B4 (env. 0.07 m jusqu'à env. 0.14 m et env. 0.63 m jusqu'à env. 2.16 m) indiquent l'existence de perméabilités faibles à l'intérieur de courts tronçons de T2-3B4-007-G (supposé être du sel gemme pur), et une forte perméabilité à l'intérieur d'un grand tronçon de T2-3B4-063-G. Le comparatif de T2-3B4-063-G (tronçon long) avec T23B4-095-G, -113-G et -131-G (tronçons courts) illustre bien les effets des mesures intégrales dans de longs tronçons de trous de forage dans les formations géologiques stratifiées. Nous supposons l'existence de perméabilités localement plus élevées au niveau des couches de marne/anhydrite (p. ex. plans de stratification) dans une plage comprise entre 0.63 m et env. 0.9 m et entre env. 1.5 m et env. 2.16 m ; en revanche, des mesures réalisées dans de courts tronçons (T2-3B4-095-G, -113-G et -131-G) révèlent des perméabilités faibles à très faibles (sel gemme pur).

1.6.4 Conditions de perméabilité au niveau des angles

La Figure 13 illustre les changements de perméabilité en fonction de la distance au contour au niveau des angles des galeries.

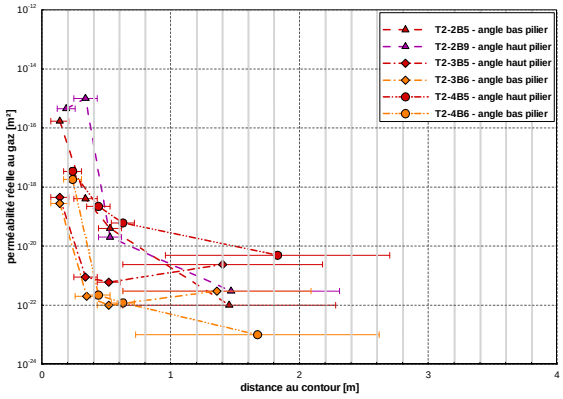

Figure 13 Perméabilité effective au gaz / distance au contour au niveau des sites T2 – angles

Les conditions de perméabilité dans les angles de la galerie ont été analysées au niveau des sites T2-2, T2-3 et T2-4. La perméabilité diminue en fonction de la distance au contour comme on pouvait s'y attendre dans un environnement homogène de sel gemme. Nous supposons que les contraintes géomécaniques élevées dans les angles de la galerie limitent la dilatation dans les régions du toit et du mur du pilier.

1.7 Teneur en saumure déterminée pour les carottes extraites des différents sites

Au total, 198 échantillons ont été prélevés sur les carottes extraites pour évaluer la teneur en saumure sur les différents sites d'exploration. L'objectif de ces investigations consistait à détecter des teneurs en saumure élevées en

vue d'évaluer les perméabilités au gaz mesurées sur site, en tenant compte de l'impact potentiel de la saturation en liquide (perméabilité effective au gaz).

La Figure 14 et la Figure 15 récapitulent la teneur en saumure respective de 45 échantillons (T1) et de 153 échantillons (T2).

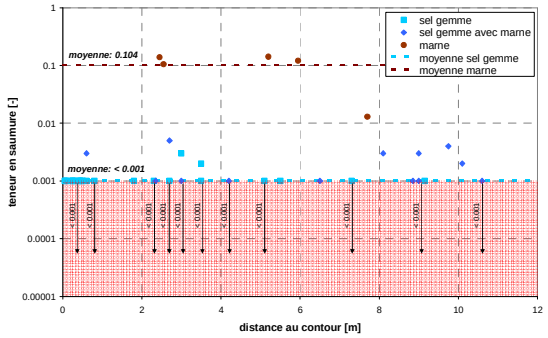

Figure 14 Teneur en saumure / distance au contour pour les sites T1

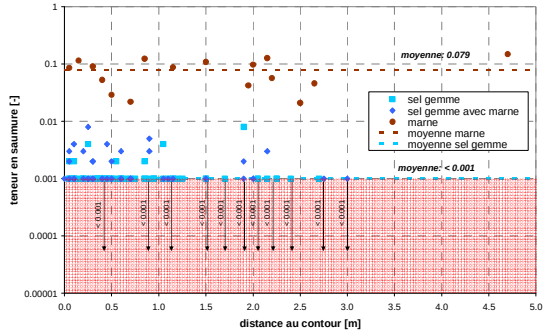

Figure 15 Teneur en saumure / distance au contour pour les sites T2

En tenant compte des données récapitulées par la Figure 14 et la Figure 15, on peut conclure ce qui suit :

- on ne note pas de forte tendance de diminution de la teneur en solution en fonction de la distance au contour,
- la teneur en solution est faible < 0.1 wt % (sel gemme pur), mais elle peut augmenter jusqu'à 1 wt % (présence de pores macroscopiques), jusqu'à atteindre une valeur de 14.2 wt % (impuretés, intercalations ou marne pure) et
- la valeur moyenne des échantillons de marnes prélevés sur les sites T2 (couche S1), de l'ordre de 7.9 ± 4.1 wt % (n=16), est légèrement plus faible que celle mesurée au niveau du site T1 (couche S), avec 10.4 ± 5.3 wt % (n=5).

Sur la base des données recueillies sur la teneur en saumure, nous excluons à ce stade un impact majeur de la teneur en saumure sur la perméabilité effective au gaz. Aucune teneur en solution plus élevée n'a été détectée, susceptible d'expliquer les faibles perméabilités effectives au gaz près du contour illustrées par la Figure 9, la Figure 10 et la Figure 11.

1.8 Conditions de perméabilité au niveau du toit – comparatif entre T1 et T2

Le comparatif des résultats obtenus au niveau des sites T1 et T2, illustré à la Figure 16, révèle qu'il n'y a pas de différence notable entre les sites T1 et T2. La seule différence consiste en ce que les points de mesure analysés sur le site T1 étaient plus profonds qu'au niveau du site T2 (à l'exception de T2-3).

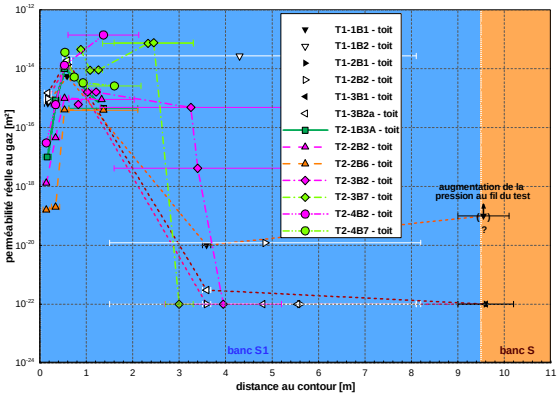

Figure 16 Comparatif de la distribution des perméabilités au niveau des sites T1 et T2 (toit)

Ainsi, la situation générale de la perméabilité au niveau du toit peut être résumée comme suit :

- plage de distance au contour dtc < env. 1.5 m : niveau de perméabilité généralement > 1E-16 m² (à l'exception de quelques mesures < 0.4 m au niveau des sites T2),
- plage de distance au contour dtc env. 1.5-2.5 m : transition de perméabilité, de > 1E-16 m² à < 1E-22 m² et
- plage de distance au contour dtc > env. 1.5-2.5 m : niveau de perméabilité généralement < 1E-22 m² (émission de gaz au niveau de T1-1B1-900-G et T1-2B2-150-G)

1.9 Récapitulatif

Les résultats des tests et des analyses réalisés peuvent se résumer comme suit :

1) la perméabilité dans les roches évaporitiques stratifiées dépend :
– des conditions géomécaniques du site, p. ex. des situations géomécaniques différentes au niveau du toit, des parements, du mur et des angles.
– de la distance au contour, en fonction du phénomène d'effritement (zone EDZ) => tendances générales
– des conditions géologiques du site, p. ex. des changements lithologiques/ rhéologiques (cet aspect a été démontré par les mesures T2-3B4-151-G et T2-3B8-146-G).
2) sur la base des données existantes, nous avons supposé la distribution de perméabilité ci-après :
– toit au niveau de T1 : < env. 1.0-1.5 m => perméabilité généralement élevée
– toit au niveau de T2 : < env. 1.5-2.0 m => perméabilité généralement élevée
– parement : < env. 1.0-1.5 m => perméabilité généralement élevée
– mur : < env. 1.0-1.5 m => perméabilité généralement élevée (élévation causée par la situation géologique > 1,5 m possible, env. 1.5-2.25 m)
– angles : < env. 0.25-0.5 m => perméabilité généralement élevée (aucun lien de dépendance géologique observé, il y a lieu de supposer l'impact d'une contrainte géomécanique élevée au niveau des angles des galeries, limitant la dilatation)
3) niveau de perméabilité apparemment faible > env. 1.5 m au niveau du toit du site T1 (l'émission de gaz constitue un indice de faible perméabilité)
4) la situation de perméabilité générale au niveau du toit sur les sites T1 et T2 est compatible
5) aucun indice quant à des perméabilités plus élevées au niveau des piliers par rapport aux parements de galerie massifs (perméabilités équivalentes sur le premier mètre de distance au contour > 1E-16 m²)
6) les teneurs en solution mesurées n'ont généralement pas d'impact majeur sur la perméabilité effective au gaz et peuvent se caractériser comme suit :
– teneurs généralement faibles < 0.1 wt % (sel gemme),
– augmentation des teneurs jusqu'à 1 wt % (pores visibles) et
– pointes à 14.2 wt % (impuretés, intercalations ou marne pure) ; en revanche, les analyses des échantillons de marne peuvent être influencées par le séchage d'eau cristalline à 105 °C

1.10 Abréviations

B	-	Trou de forage
CP	-	Test à pression constante
CR	-	Test à débit constant
dtc	-	Distance au contour
EDZ	-	Zone perturbée par l'excavation (zone EDZ)
FS	-	A grande échelle
IT	-	Test d'impulsions
MP	-	Point de mesure (correspond au centre d'un tronçon de mesure)
PDE	-	Equation différentielle partielle
PR	-	Tronçon de mesure
T	-	Site de mesure

1.11 Références bibliographiques

[1] Rybka, S. (1981) : Bassin Potassique de Mulhouse – Répertoire des bancs de halite et d'insolubles au–dessus et au-dessous des couches potassiques. Mines de Potasse d' Alsace S.A., Département Géologie, France

[2] DIN 18121, partie 1 (1998) : Soil, investigation and testing - Water content - Part 1 : Determination by drying in oven. Deutsches Institut für Normung e. V., Berlin.

[3] Ercosplan (2010) : Backfilling of Underground Waste Disposal StocaMine, Wittelsheim/ France. feasibility study, Ercosplan Ingenieurgesellschaft Geotechnik und Bergbau mbH, Erfurt / Germany, EGB07-042, p. 16-20

[4] Walter, R. (1992) : Geologie von Mitteleuropa. Schweizerbat'sche Verlagsbuchhandlung, Stuttgart, 561 p.

[5] Cosenza, Ph.; Ghoreychi, M.; Bazargansabet, B. (1997): Mesure de la perméabilité in situ du sel. Revue Francaise de Geotechnique, Nr. 79 (1997).

[6] Förster, S. (1970) : Dichtheitsprüfung des Jüngeren Steinsalzes im Schacht Burggraf. Bergakademie Freiberg, Sektion Geotechnik und Bergbau, Lehrstuhl für Tiefbohrtechnik und Erdölgewinnung.

[7] Förster, S. (1985) : Gasdruckbelastbarkeit und Rißbildung der für die unterirdische Gasspeicherung bedeutsamen Salinargesteine des Zechsteins. Dissertation, Bergakademie Freiberg, Sektion Geotechnik und Bergbau ; publication : Leipzig : VEB Deutscher Verlag für Grundstoffindustrie, Freiberger Forschungsheft A 724.

[8] Häfner, F.; Belohlavek, K.-U.; Förster, S.; Pohl, A.; Behr, A. (2001) : In situ Ermittlung von Strömungskennwerten natürlicher Salzgesteine in Auflockerungszonen gegenüber Gas und Salzlösungen unter den gegebenen Spannungsbedingungen im Gebirge. Abschlussbericht 2001, TU Bergakademie Freiberg, Institut f. Bohrtechnik u. Fluidbergbau.

[9] Häfner, F.; Belohlavek, K.-U.; Förster, S.; Pohl, A.; Behr, A. (1998) : Dichtheitsuntersuchungen der Ortsbrust EU, 1. Teilbericht zum BMBF- und TMLNU-geförderten Vorhaben, Förderkennzeichen 02 C 0527 6, In-situ-Ermittlung von Strö-

mungskennwerten natürlicher Salzgesteine in der ALZ gegenüber Gas und Salzlösungen unter den gegebenen Spannungsbedingungen im Gebirge, April 1998.

[10] Stormont, J.C. (1997a): Conduct and interpretation of gas permeability measurements in rock salt. Int. J. Rock Mech. & Min. Sci. Vol. 34, No 3-4, paper No. 303.

[11] Stormont, J.C. (1997b) : In Situ Gas Permeability Measurements to Delineate Damage in Rock Salt. Int. J. Rock Mech. Min. Sci. Vol. 34, No. 7, 1997.

[12] Weber, J.R.; Wallner, M. (1998) : Hydraulische Untersuchungen im Grubengebäude Morsleben. Bundesanstalt für Geowissenschaften und Rohstoffe, Hannover.

[13] Kaltofen, R.; Schumann, K.; Ziehmann, J. (1962) : Tabellenbuch Chemie. VEB Deutscher Verlag für Grundstoffindustrie, Leipzig

2 Extended Abstract

2.1 Abstract

Within the scope of the planning of closure IBeWa Consulting was assigned to perform extensive in situ permeability investigations by StocaMine, France.

The main focus of the investigations in the former potash mine Amelie (Upper Rhine Graben) was the characterisation of the excavation damaged zone (EDZ) under the specific site conditions of a layered Tertiary saliniferous formation. For this reason about 150 in situ gas permeability tests using borehole packers were performed in order to investigate the spatial permeability distribution in dependence on the distance to contour k = f(dtc) (lateral hydraulic conditions in the vicinity of a deposit area, 4 potential dam sites). Furthermore, the permeability conditions of the marl/anhydrite rich layer S in the roof (vertical hydraulic conditions in the centre of the same deposit area, 3 sites) were investigated. Finally, the brine content at core samples from measurement intervals was determined to evaluate the rock condition during in situ gas permeability tests.

On the base of the recent available data an inhomogeneous spatial permeability distribution was found within the EDZ characterising the lateral hydraulic conditions at potential dam sites. The permeability in the EDZ depends on the geomechanical site condition (e.g. differences in roof, faces, floor and corners of a drift with rectangular cross section), distance to the contour (general trends) and the geological site condition (changes in lithology/rheological behaviour). We assume contrasts in competence of different lithologies in the layered saliniferous formation as reason for a different grade of dilatancy due to deformation around the drift.

Except in the corners of drift, gas permeability in the EDZ reaches values up to 7E-14 m² and decreases down to values of about 1E-18 m² in distances to the contour somewhere between 1 m and 2 m. However, there is evidence for lithology caused permeability elevation (2.4E-16 m² and 2.1E-13 m²) in a distance > 1.5 m within a marl/anhydrite sequence in the floor. The permeability distribution in the drift corners differs from the described situation in the way that a maximum of only 1E-15 m² was yielded and the permeability drops quite quickly down to about 1E-18 m² (between 0.25 m and 0.5 m) presumably due to high geomechanical stress limiting dilatancy. The vertical hydraulic conditions (roof) in the centre of the deposit area are characterised by an apparently low permeability level at distances > ca. 1.5 m. This correlates with the observation of pressure increase due to gas emission from interbedded marl/anhydrite rich layer S during borehole measurement. Principally, the general permeability situation in the roof of the centre and in the roof in the vicinity of the deposit area seems to be compatible. The permeability conditions in the pillar of the double drift do not differ from those investigated in other face boreholes and are characterised by high permeabilities.

Finally, there was no evidence for major influence of effective gas permeability by elevated brine content in pure rock salt. Brine contents < 0.1 wt % indicate mainly dry condition for the bulk of analysed core samples. However, the brine content rises up to 1 wt % for few samples of pure rock salt showing visible pores and moisture. Whereas, samples consisting of rock salt and impurities of marl/anhydrite, intercalations of salt and marl/anhydrite or of pure marl/anhydrite reach values up to 14.2 wt %. Last values might be influenced by crystalline water due to oven drying at 105 °C.

2.2 Geological introduction

StocaMine is part of former potash mine Amelie and situated in the Wittelsheim basin (Upper Rhine Graben). The Wittelsheim and the Münchhausen basin form the Mulhouse Potash Basin (Figure 1).

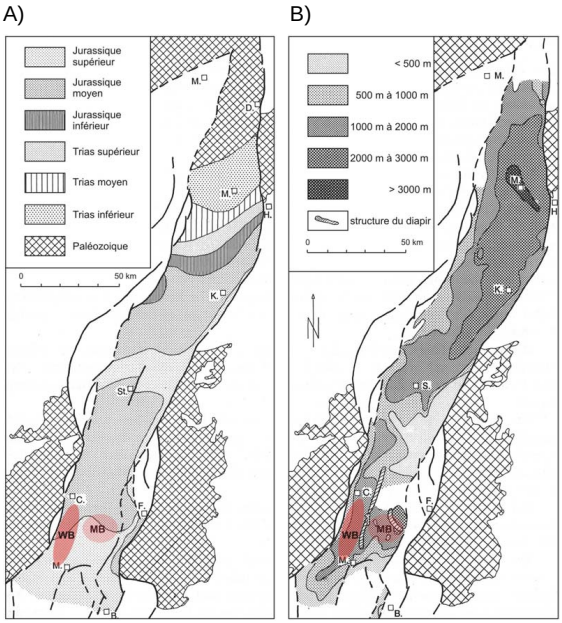

Figure 1 Location of Mulhouse Basin in the southern Upper Rhine Graben [4]

[Explanation: A) footwall of Tertiary, B) isobaths of Tertiary basis, WB – Wittelsheim basin, MB – Münchhausen basin]

The Tertiary basis in the Mulhouse Potash Basin is located between 1000 m and 2000 m below sea level. Potash salt was mined in both sub-basins.

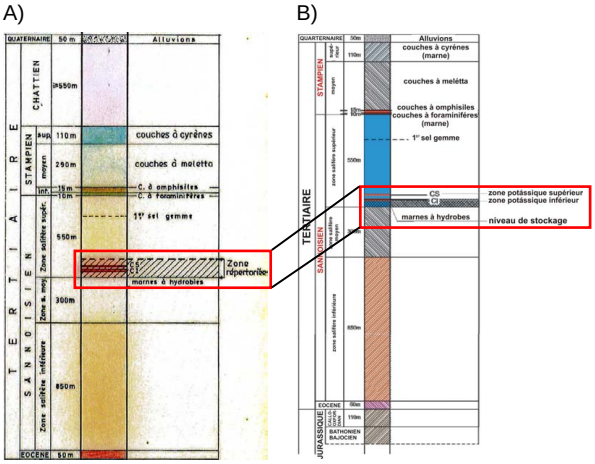

Figure 2 General stratigraphic situation

[Explanation: A) Mulhouse basin [1], B) StocaMine [3]]

The stratigraphic position of the StocaMine underground waste disposal is shown in the normal profile. The excavations of StocaMine are located in the footwall of the potash zone consisting of two sylvinite seams (Figure 2B) [3].

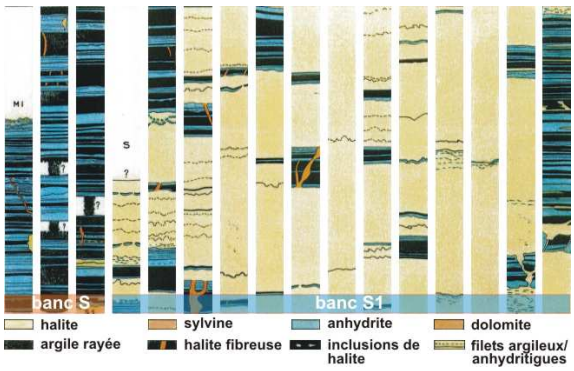

Figure 3 Lithologies in the disposal area [1]

The rock salt formation of the disposal area is mainly inter-layered by calcareous clay and anhydrite (Figure 3).

No tectonic influence of the sub-horizontal, slightly NW dipping rock salt is known in the disposal area, although deep reaching, SW-NE oriented faults have been identified in other parts of the basin [3]. The hydrogeological situation within the evaporite formation has been characterised by [3] as normally water free (some small brine inclusions during mining and from salt free marls). Excavations of StocaMine are separated from groundwater bearing horizons by several 100 metres of low permeable rock salt and marl.

2.3 Site description and test program

Figure 4 shows the location of all test sites. Test sites named T2 are situated in drifts in the vicinity of the disposal area. Whereas, test sites named T1 are located in the centre of the disposal area. For sites T1-1 and T1-2 a massive pillar of potash mining field in the hanging has a rock mechanical relevance (blue mark, Figure 4).

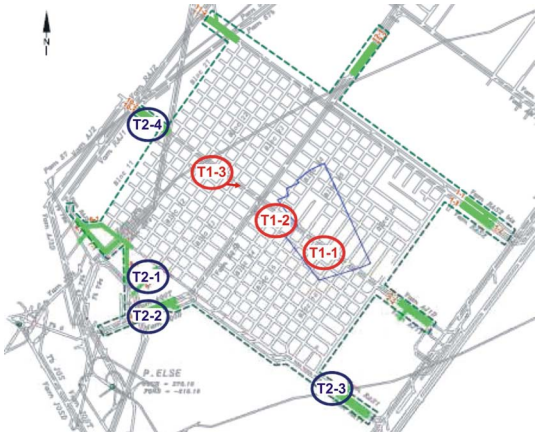

Figure 4 Location of test sites
[Explanation: blue mark – massive pillar of potash mining field in the hanging wall]

Table 1 summarizes the information for each site.

Table 1 Summarized site information

site	position[1]	drift	excavation	boreholes	stratigraphy[2]	remarks
T1-1	centre	AJ1T/ AJ1D	Banc de 23 m and Banc de 25 m	2	S and S1	massive pillar of a potash mining field in the hanging wall
T1-2				2		
T1-3				2		
T2-1	vicinity	A-12		4	S1	-
T2-2		AQ0T/ AQ0D		9		
T2-3		RAS1/ RAT1	below Banc de 25 m	9		
T2-4		AJ1T/ AJ1D	Banc de 23 m and Banc de 25 m	9		

About 140 metres were drilled (dry drilling method) for 37 boreholes having a diameter of 70 mm. Between one and six measuring points were investigated in each borehole. Thus, approximately 150 in situ gas permeability determinations were performed applying borehole packer tests using double and quadruple packers with a diameter of < 70 mm. Basically, intervals of ca. 0.18 m length were tested. However, if testing a whole borehole sequence even intervals of up to several meters length were integrally tested. Prior to in situ permeability test boreholes were standardizing cleaned by dry pressurized air and surveyed by video endoscopy. Figure 5 depicts a double drift and the applied drilling plan.

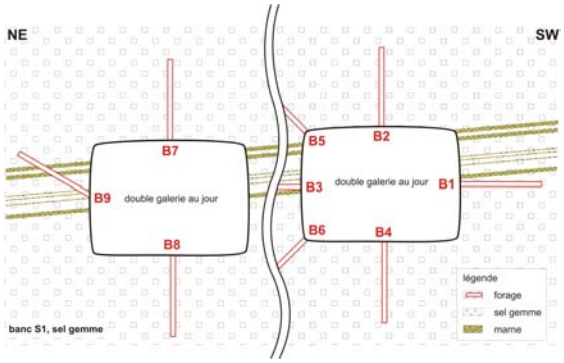

Figure 5 Schematic profile of exploration sites (e.g. double drift T2-2, -3 and -4)

In addition to the in situ tests, laboratory investigations were performed to determine the brine content at the measuring points. Therefore, core material was geological described, welded in plastic foil, transported, photographed and sampled for oven drying.

Core samples were distinguished in marl, rock salt with certain amount of marl and pure rock salt. Figure 6 depicts the sampled lithologies.

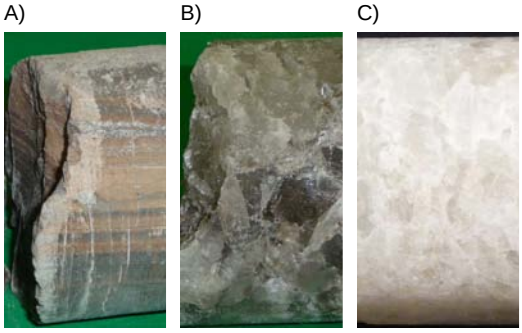

Figure 6 Sampled lithologies
[Explanation: A) marl sample ± anhydrite, B) rock salt with certain amount of marl, C) visually pure rock salt]

Approximately 200 samples were taken from core material of all boreholes and dried at ca. 105 °C referring to chapter 2.4.2. The goal was to detect elevated brine contents in order to evaluate the in situ measured gas permeabilities in respect to the possibility of influence by liquid saturation in the sense of effective gas permeability.

[1] relative to the underground waste disposal
[2] referred to [1]

2.4 Analytic methods

2.4.1 Determination of permeability by in situ-Tests

In situ permeability tests exhibit fluidic in situ experiments. During these experiments an unsteady flow process is initiated and recorded. Different fluids are in use. Thus, tests with different gases and liquids (commonly brines) are possible. The selection of fluid is always use- and task-dependent.

Gas, especially dry pressurised air, exhibits an inert fluid in respect to pore space of salty rocks and was often applied to many salt formations (e.g. [5], [6], [7], [8], [9], [10], [11], [12]).

Due to the dependence of gas permeability on the liquid saturation and the circumstance that the existence of liquid in the pore space can never completely be excluded the in situ determined gas permeability a priori exhibits an effective gas permeability. This permeability may decrease in the order of magnitude with increasing liquid saturation. In case of elevated moisture revealed by brine content from core samples of the test site in situ permeability tests with brine as fluid are advised.

In situ permeability test can principally be performed as:

– pulse test (IT),
– constant pressure test (CP) and
– constant rate test (CR).

Prior to measurement leak tests performed at the test site proof the necessary tightness of the assembled equipment. It is possible to dope the gas by 1,1,1,2-Tetrafluorethane in order to detect leakages. Even very low traces (> 1.5 ppm) are detectable and reveal leakages.

Piezoelectric pressure transducers having precisions from normally 0.1 % to 0.2 % are applied to record the temporal pressure development in test intervals and packer elements. Measuring ranges of sensors are carefully fitted to the expected pressure range. The flow rate is recorded by thermal mass flow rate sensors having an accuracy of 1 % Rd (< 20 % of flow) and of 0.2 % FS (> 20 % of flow). The test setup for gas consists of a pressure controlling, measuring and a data acquisition unit.

To evaluate measured data and determine the permeability a two-dimensional model in r-φ-z geometry (r-z profile) is built for each measurement considering the geometric structure and the fluid properties. The model can be variable discretised. The radius is spread in x-direction starting from bore centre and the depth is spread in y-direction (Figure 7). Applying a specific computer code the numerical solution of the partial differential equation (PDE) for the isothermal, two-dimensional, radial-symmetrical flow of a single phase (gas or liquid) is simulated. The parameter permeability is determined by fitting measured and calculated pressure data.

The permeability is determined by fitting of simulated to measured pressure curves. The target function of the fitting is the minimisation of the error square sum for both curves (least-squares method).

Figure 7 shows the simulation of radial-symmetrical flow during a packer test.

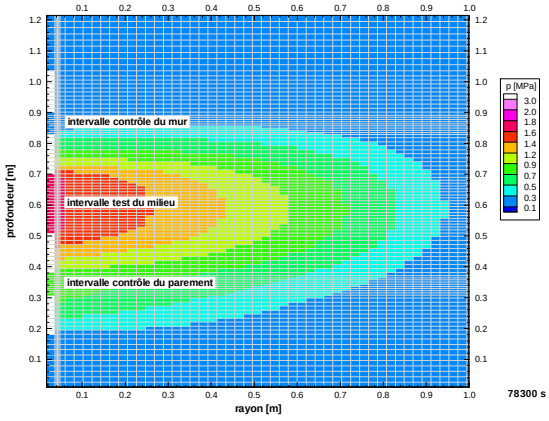

Figure 7 Test evaluations – model discretisation and simulated, spatial pressure distribution

- red: high pressure starting from test interval
- blue: initial (low) pressure in rock (air pressure)

2.4.2 Determination of brine content by oven drying

The brine content was determined by oven drying at 105 °C [2] until mass stability. Samples were obtained from core material as close as possible to the test interval. Precipitation of brine in pore space was considered by mineralisation and density of saturated halite brine [13].

2.5 In situ permeability test at T1

Figure 8 shows the permeability results.

A)

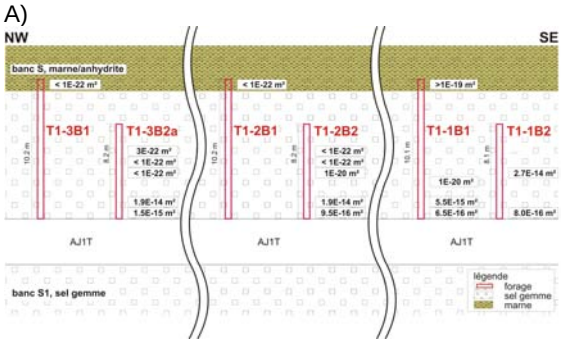

B)

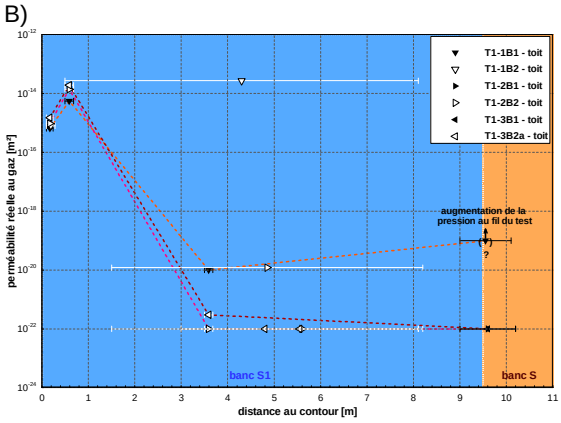

Figure 8 Results at T1-1, T1-2 and T1-3 – roof
[Explanation: A) schematic profile of drift showing effective gas permeabilities, B) diagram k_{eff} vs. distance]

As seen in Figure 8, a good correlation exists between the results from all sites (T1-1, T1-2 and T1-3). The range close to the contour (< 0.5-1.0 m) is characterised by an increase in effective gas permeability with distance. However, there is no evidence for increased brine content at these measurement points. Therefore, we exclude an important influence of brine content to the effective gas permeability.

Measurements within the contour near range principally revealed a higher permeability level of > 6E-16 m² (T1-1B1-010-G1). This is interpreted as loosening in the EDZ. After this range the permeability decreases to very low values of ≤ 1E-20 m² (T1-1B1-350-G). The transition in permeability from values > 1E-18 m² to < 1E-18 m² seems to occur earlier at sites T1-2 and T1-3 than at T1-1 somewhere between ca. 0.6 m and ca. 1.5 m (top of test intervals T1-2B2-150-G and T1-3B2a-150-G).

The measured effective gas permeabilities at the sites T1 can generally be distinguished in:

- dtc < ca. 0.6 m: => elevated permeability (> 6E-16 m²) of EDZ and
- dtc > ca. 1.5 m: => permeability level (≤ 1E-20 m²) whereat, pressure increases (T1-1B1-900-G and T1-2B2-150-G) confirm low permeability level.

2.6 In situ permeability test at T2

2.6.1 Permeability conditions in the roof

Figure 9 shows the change in permeability with increasing distance at T2 sites.

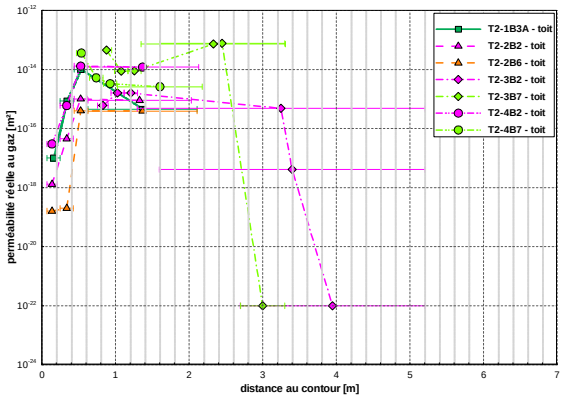

Figure 9 Effective gas permeability vs. distance to contour at T2 – roof

As seen in Figure 9, there is a good correlation between T2-sites. All profiles show more or less similar conditions. The effective gas permeability increases within the distance < ca. 2 m. This correlates to the extended profiles of T2-3. However, a permeability decrease to ≤ 1E-22 m² is revealed at distances > ca. 2 m.

The high effective gas permeabilities at MP4 (0.63 m to final depth) at sites T2-1, T2-2 and T2-4 might be caused by local higher perme-

abilities along small marl/anhydrite layers (e.g. bedding planes). The shifted profile in T2-4B7 reveals a slight decrease in permeability within the interval of initial MP4 (0.63 m to final depth). However, the measurement T2-4B7-103-G testing an interval from 1.04 m to final depth still yielded a relative high effective gas permeability of 2.6E-15 m². Testing intervals having a larger distance to contour (e.g. T2-3B2-160-G, T2-3B2-270-G, T2-3B7-270-G) revealed a decrease in permeability down to values of ≤ 1E-22 m² as assumed for undisturbed rock.

2.6.2 Permeability conditions in the face

Figure 10 shows the permeability change with distance for all face boreholes.

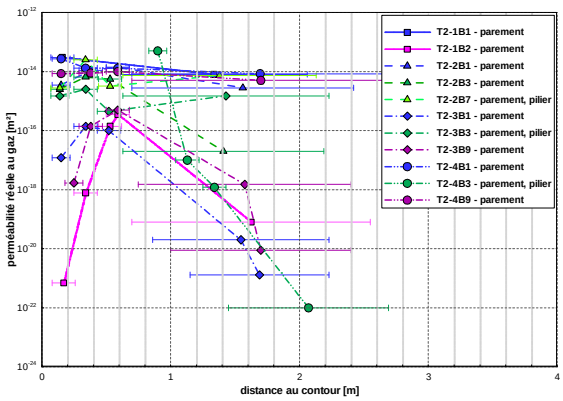

Figure 10 Effective gas permeability vs. distance to contour at T2 – face

The bulk of tests yielded effective gas permeabilities > 1E-15 m² as depicted in Figure 10. Again, we assume higher local permeabilities along marl/anhydrite layers (e.g. bedding planes) as reason for frequently observed high permeability level.

A second group of measurements includes complete measurements in boreholes T2-1B2, T2-3B1 and T2-3B9, MP4 in borehole T2-2B3 and the last 3 measurements in T2-4B3. The permeability in boreholes of this group increases with distance to contour in the range from 0 m to ca. 0.6 m. Again, there is no evidence for increased brine content.

Measurements with smaller intervals (T2-4B3) reveal a permeability transition from > 1E-18 m² to ≤ 1E-18 m² within a distance from ca. 1.2 m to 1.4 m which is in good concordance with the results from MP4 in T2-2B3, T2-3B9 and T2-1B2.

No evidence for particular high permeabilities in the pillars of the double galleries (between AQ0T and AQ0D or AJ1T and AJ1D) compared to the massive faces.

2.6.3 Permeability conditions in the floor

The permeability conditions in the floor are shown for T2-sites in Figure 11.

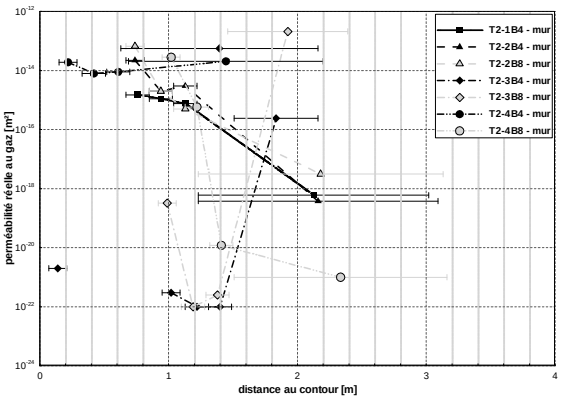

Figure 11 Effective gas permeability vs. distance to contour at T2 – floor

Visible loosening of ground (e.g. cracks, fissures) in the range until ca. 0.6 m was the reason for shifting profiles of T2-1B4, T2-2B4 and T2-2B8. The profile in T2-4B8 was even shifted by about 1.0 m. Whereas, the profile T2-4B4 starts at about 0.15 m (no visible loosening). The profiles at site T2-3 were shifted by about 0.85 m or 0.88 m, respectively.

Again, there is a good correlation between the results for T2-1 and T2-2. However, permeability decreases with distance to contour in the floor. This is expected caused by loosening of ground due to excavation (EDZ).

For site T2-4 the transition in permeability from values of > 1E-18 m² to values ≤ 1E-18 m² occurs at a distance between ca. 1.13 m and ca. 1.5 m (MP2 and MP3 of T2-4B8, Figure 11). On the other hand, measurements in T2-4B4 yielded relative high permeabilities from 7.9E-15 m² to 1.4E-14 m² showing that shifting was reasonable. MP4 in T2-4B4 (ca. 0.69 m to

ca. 2.2 m) is not in contradiction to the measurements at T2-1 and T2-2 or in T2-4B8 but is simply more affected by higher permeabilities. Therefore, the results of T2-4 correlate to the general observed trend of permeability distribution and supply essential information for ranges > ca. 1.2 m (T2-4B8) and < ca. 0.6 m.

Based on these observations we assume relative high permeabilities between 0 m and ca. 1.13 m (> ca. 1E-15 m²), a transition in permeability from > 1E-18 m² to values ≤ 1E-18 m² somewhere at 1.5 m and relative low permeabilities < 1E-18 m² for distances > ca. 1.5 m. This is not applicable if changes in geology occur as both profiles from site T2-3 (T2-3B4 and T2-3B8) are showing. The different geological situation in the floor level of site T2-3 is depicted in Figure 12 (intercalation of marl/anhydrite at the bottom of borehole).

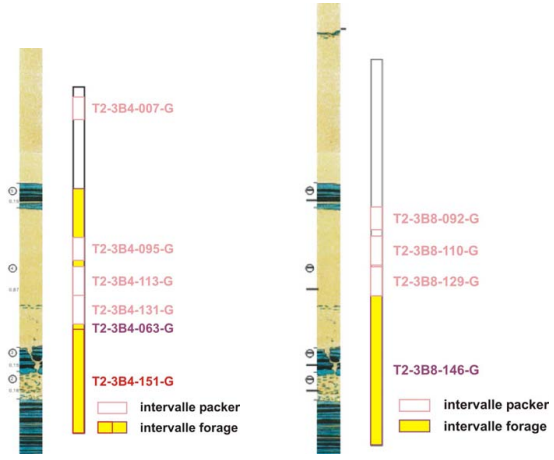

A) T2-3B4 B) T2-3B8

Figure 12 Schematic geological situation at site T2-3 situated about 25 m in the footwall of the potash excavation

After achievement of permeability levels of ≤ 1E-22 m² values increase to > 1E-18 m² at distances of > 1.5 m (T2-3B4-151-G and T2-3B8-146-G). Correlating this with the geological situation in Figure 12 we interfere that high permeability at bedding planes either between rock salt and marl and/or between marl and anhydrite is accounting for high permeability levels of effective gas permeability. This change in geology was observed in video inspection.

Additionally, measurements in T2-3B4 (ca. 0.07 m to ca. 0.14 m and ca. 0.63 m to ca. 2.16 m) are showing the occurrence of low permeability within small interval of T2-3B4-007-G (assumed to be pure rock salt) and high permeability within large interval of T2-3B4-063-G. The comparison of T2-3B4-063-G (large interval) with T2-3B4-095-G, -113-G and -131-G (small intervals) illustrates the effects of integral measurements in large borehole intervals in layered formation. We assume higher local permeabilities along marl/anhydrite layers (e.g. bedding planes) within the ranges from ca. 0.63 m to ca. 0.9 m and from ca. 1.5 m to ca. 2.16 m whereas, the measurements in small intervals (T2-3B4-095-G, -113-G and -131-G) reveal low to very low permeabilities (pure rock salt).

2.6.4 Permeability conditions in the corners

Figure 13 shows the permeability changes with increasing distance in drift corners.

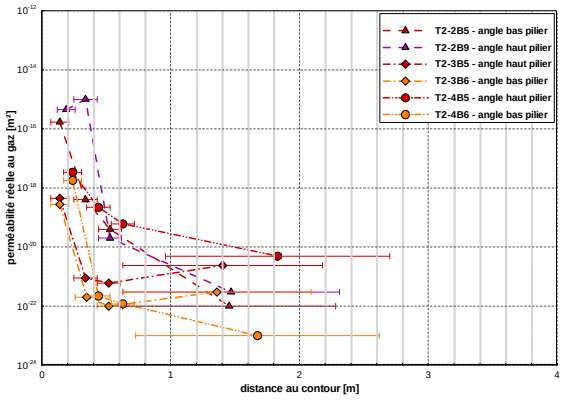

Figure 13 Effective gas permeability vs. distance to contour at T2 - corner

The permeability conditions in the drift corners were investigated at sites T2-2, T2-3 and T2-4. The permeability decreases with the distance as expected for homogeneous rock salt. We assume the influence of high geomechanical stress in the drift corners limiting dilatancy in the roof and the floor regions of the pillar.

2.7 Brine content determined on core material from all sites

Totally, 198 samples were taken from core material to evaluate the brine content at the exploration sites. The goal of these investigations was to detect elevated brine contents in order to evaluate the in situ measured gas permeabilities in respect to the possibility of influence by liquid saturation (effective gas permeability).

Figure 14 and Figure 15 present the brine content of 45 (T1) and 153 (T2) samples.

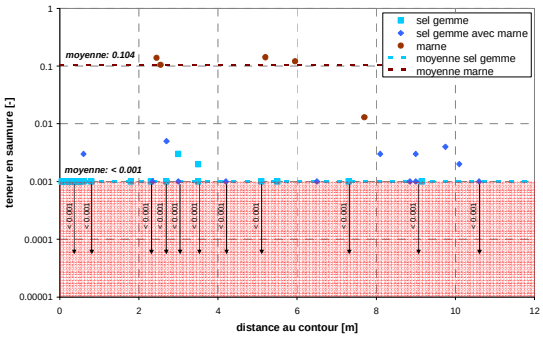

Figure 14 Brine content vs. distance to contour for sites T1

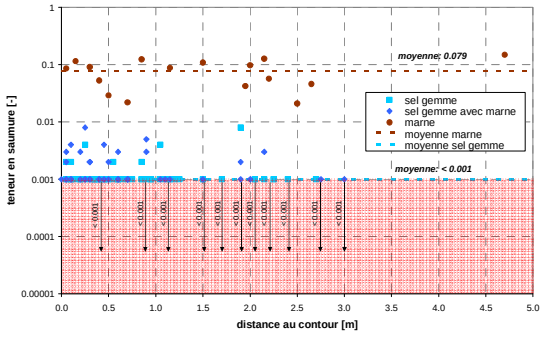

Figure 15 Brine content vs. distance to contour for sites T2

Considering data in Figure 14 and Figure 15 the following points can be concluded:

- there is no straight trend of decrease in brine content with distance,
- brine content is low < 0.1 wt % (pure rock salt), can rise up to 1 wt % (macroscopic pores present) and finally reaches up to 14.2 wt % (impurity, intercalation or pure marl) and
- mean value of marl samples at sites T2 (layer S1) is with 7.9 ± 4.1 wt % (n=16) slightly lower than 10.4 ± 5.3 wt % (n=5) at T1 (layer S).

Based on the data on brine content we exclude an important influence of brine content to the effective gas permeability at this stage. No elevated brine content was detected to explain the low effective gas permeabilities near to the contour in Figure 9, Figure 10 and Figure 11.

2.8 Permeability conditions in the roof – comparison between T1 and T2

The comparison of result from T1 and T2 in Figure 16 reveals there is no conspicuous difference between T1- and T2-sites. The only difference is that deeper measurement points were investigated at T1 than at T2 (except T2-3).

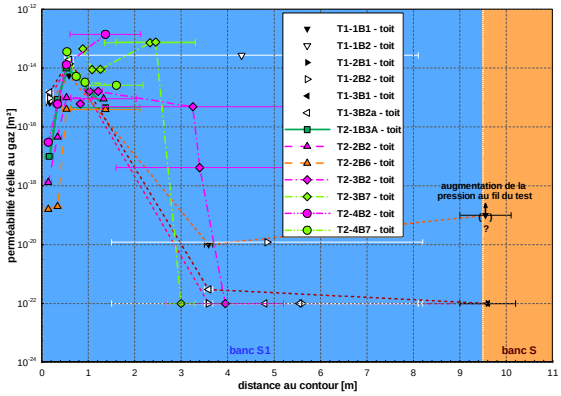

Figure 16 Comparison of permeability distribution at T1- and T2-sites (roof)

Thus, the general permeability situation in the roof can be summarised as follows:

- range dtc < ca. 1.5 m: permeability level mainly > 1E-16 m² (except some measurements < 0.4 m at T2-sites),
- range dtc ca. 1.5-2.5 m: transition of permeability from values > 1E-16 m² to < 1E-22 m² and
- range dtc > ca. 1.5-2.5 m: permeability level mainly < 1E-22 m² (gas emission at T1-1B1-900-G and T1-2B2-150-G)

2.9 Summary

The results of the performed tests and investigations can be summarised as follows:

1) permeability in layered evaporite rocks depends on:

- geomechanical site condition, e.g. different situations in roof, faces, floor & corners.
- distance to contour caused by loosening (EDZ) => general trends
- geological site condition, e.g. changes in lithology/rheological behaviour (was demonstrated by the measurements T2-3B4-151-G and T2-3B8-146-G).

2) based on existing data following permeability distribution is assumed:
- roof T1: < ca. 1.0-1.5 m => mainly elevated
- roof T2: < ca. 1.5-2.0 m => mainly elevated
- face: < ca. 1.0-1.5 m => mainly elevated
- floor: < ca. 1.0-1.5 m => mainly elevated (geology caused elevation > 1.5 m possible, ca. 1.5-2.25 m)
- corner: < ca. 0.25-0.5 m => mainly elevated (no geology dependence observed, assume the influence of high geomechanical stress in the drift corners limiting dilatancy)

3) apparently low permeability level > ca. 1.5 m in the roof at T1 (gas emission as evidence for low permeabilities)
4) general permeability situation in the roof at T1 and T2 is compatible
5) no evidence for particular higher permeabilities within the pillars in comparison to massive drift faces (equal within the first metre > 1E-16 m²)
6) measured brine content has mainly no major effect on effective gas permeability and can be characterised:
- generally low < 0.1 wt % (rock salt),
- rises up to 1 wt % (visible pores) and
- finally reaches up to 14.2 wt % (impurity, intercalation or pure marl) whereat, analyses of marl samples might be influenced by drying of crystalline water at 105 °C

2.10 Abbreviations

B	-	borehole
CP	-	constant pressure test
CR	-	constant rate test
dtc	-	distance to contour
EDZ	-	excavation damaged zone
FS	-	full scale
IT	-	pulse test
MP	-	measuring point (equates to the central point of test interval)
PDE	-	partial differential equation
PR	-	test interval
T	-	test site

2.11 References

[1] Rybka, S. (1981): Bassin Potassique de Mulhouse – Répertoire des bancs de halite et d'insolubles au–dessus et au-dessous des couches potassiques. Mines de Potasse d' Alsace S.A., Département Géologie, France

[2] DIN 18121, Teil 1 (1998): Baugrund; Untersuchung von Bodenproben - Wassergehalt - Teil 1: Bestimmung durch Ofentrocknung. Deutsches Institut für Normung e. V., Berlin.

[3] Ercosplan (2010): Backfilling of Underground Waste Disposal StocaMine, Wittelsheim/ France. feasibility study, Ercosplan Ingenieurgesellschaft Geotechnik und Bergbau mbH, Erfurt / Germany, EGB07-042, p. 16-20

[4] Walter, R. (1992): Geologie von Mitteleuropa. Schweizerbat'sche Verlagsbuchhandlung, Stuttgart, 561 p.

[5] Cosenza, Ph.; Ghoreychi, M.; Bazargansabet, B. (1997): Mesure de la perméabilité in situ du sel. Revue Francaise de Geotechnique, Nr. 79 (1997).

[6] Förster, S. (1970): Dichtheitsprüfung des Jüngeren Steinsalzes im Schacht Burggraf. Bergakademie Freiberg, Sektion Geotechnik und Bergbau, Lehrstuhl für Tiefbohrtechnik und Erdölgewinnung.

[7] Förster, S. (1985): Gasdruckbelastbarkeit und Rißbildung der für die unterirdische Gasspeicherung bedeutsamen Salinargesteine des Zechsteins. Dissertation, Bergakademie Freiberg, Sektion Geotechnik und Bergbau; veröffentl. in: Leipzig : VEB Deutscher Verlag für Grundstoffindustrie, Freiberger Forschungsheft A 724.

[8] Häfner, F.; Belohlavek, K.-U.; Förster, S.; Pohl, A.; Behr, A. (2001): In situ Ermittlung von Strömungskennwerten natürlicher Salzgesteine in Auflockerungszonen gegenüber Gas und Salzlösungen unter den gegebenen Spannungsbedingungen im Gebirge. Abschlussbericht 2001, TU Bergakademie Freiberg, Institut f. Bohrtechnik u. Fluidbergbau.

[9] Häfner, F.; Förster, S.; Pohl, A.; Behr, A. (1998): Dichtheitsuntersuchungen der Ortsbrust EU, 1. Teilbericht zum BMBF- und TMLNU-geförderten Vorhaben, Förderkennzeichen 02 C 0527 6, In-situ-Ermittlung von Strömungskennwerten natürlicher Salzgesteine in der ALZ gegenüber Gas und Salzlösungen unter den gegebenen Spannungsbedingungen im Gebirge, April 1998.

[10] Stormont, J.C. (1997a): Conduct and interpretation of gas permeability measurements in rock salt. Int. J. Rock Mech. & Min. Sci. Vol. 34, No 3-4, paper No. 303.

[11] Stormont, J.C. (1997b): In Situ Gas Permeability Measurements to Delineate Damage in Rock Salt. Int. J. Rock Mech. Min. Sci. Vol. 34, No. 7, 1997.

[12] Weber, J.R.; Wallner, M. (1998): Hydraulische Untersuchungen im Grubengebäude Morsleben. Bundesanstalt für Geowissenschaften und Rohstoffe, Hannover.

[13] Kaltofen, R.; Schumann, K.; Ziehmann, J. (1962): Tabellenbuch Chemie. VEB Deutscher Verlag für Grundstoffindustrie, Leipzig

3 Report structure

The final report summarizes the results for all investigated sites at StocaMine in a short and compact manner. Separate extended abstracts in French and English were pretended for an even more compact summary of the results. The results were previously reported in several interim reports [5], [7], [8], [9], [10] und [11]. For a better understanding the interim reports are included in the final report in the kind of separate report parts for each site. Based on this the structure of this final report is defined as follows:

1) Report part 1 – Final report: Determination of in situ permeability in the StocaMine – In situ permeability investigations at 7 sites in the StocaMine. IBeWa Consulting Germany, Order JR/CT156-12, 43 p.
2) Report part 2 – Interim report: Determination of in situ permeability in the StocaMine – In situ permeability investigations at site T1-1. IBeWa Consulting Germany, Order JR/CT156-12, 58 p.
3) Report part 3 – Interim report: Determination of in situ permeability in the StocaMine – In situ permeability investigations at site T1-2. IBeWa Consulting Germany, Order JR/CT156-12, 45 p.
4) Report part 4 – Interim report: Determination of in situ permeability in the StocaMine – In situ permeability investigations at site T1-3. IBeWa Consulting Germany, Order JR/CT156-12, 44 p.
5) Report part 5 – Interim report: Determination of in situ permeability in the StocaMine – In situ permeability investigations at site T2-1. IBeWa Consulting Germany, Order JR/CT156-12, 73 p.
6) Report part 6 – Interim report: Determination of in situ permeability in the StocaMine – In situ permeability investigations at site T2-2. IBeWa Consulting Germany, Order JR/CT156-12, 147 p.
7) Report part 7 – Interim report: Determination of in situ permeability in the StocaMine – In situ permeability investigations at site T2-3. IBeWa Consulting Germany, Order JR/CT156-12, 203 p.
8) Report part 8 – Interim report: Determination of in situ permeability in the StocaMine – In situ permeability investigations at site T2-4. IBeWa Consulting Germany, Order JR/CT156-12, 184 p.

Except the final report all separate report parts contain individual appendices with all site specific protocols of in situ and laboratory investigations.

4 Assignment of tasks

IBeWa Consulting (IBeWa) was assigned to perform in situ permeability investigations by the order JR/CT156-12 from 9th of October, 2012 by StocaMine, France [1].

In the scope of site exploration reference holes were drilled and in situ permeability tests were performed. The main focus of the investigations was the characterisation of the excavation damaged zone (EDZ). The focal points were:

- the characterisation of permeability conditions of the marl as well as at the test sites T1 (vertical hydraulic conditions), and

– the spatial permeability distribution in dependence on the distance to contour k = f(dtc) prominently in the rock salt, especially at the test sites T2 (lateral hydraulic conditions).

The investigations were part of the site exploration in advance of sealing measures necessary for the closure of the underground disposal site.

5 Geology and site characterisation

StocaMine is part of the former potash mine Amelie and is geologically situated within the Wittelsheim basin in the southern part of the Upper Rhine Graben. The Wittelsheim basin together with the shallower Münchhausen basin forms the Mulhouse potash basin (Figure 1). The Tertiary basis in the Mulhouse potash basin is approximately located between 1000 m and 2000 m below sea level. Potash salt was mined in both sub-basins (e.g. Amelie in the Wittelsheim basin, Buggingen in the Münchhausen basin).

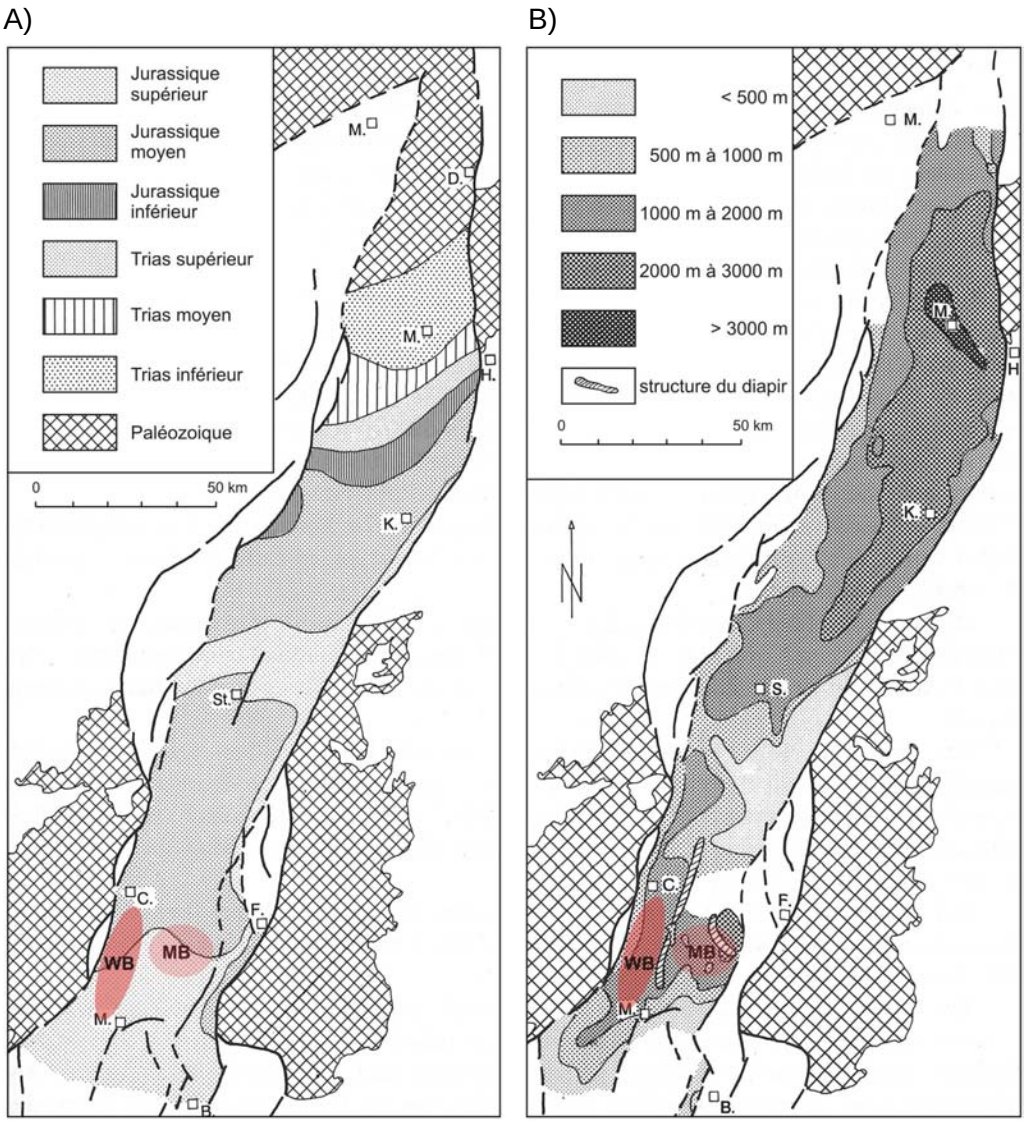

Figure 1 Location of Basin of Mulhouse in the southern Upper Rhine Graben (after [13])

[Explanation: A) footwall of the Tertiary fillings, B) isobaths of the Tertiary basis referred to sea level, WB – Wittelsheim basin, MB – Münchhausen basin]

Figure 2 shows the normal profile of the geologic/stratigraphic sequence within the Mulhouse potash basin, depicts the position of the StocaMine underground waste disposal and gives an impression of the lithological variety of rocks in the explored formation.

A)

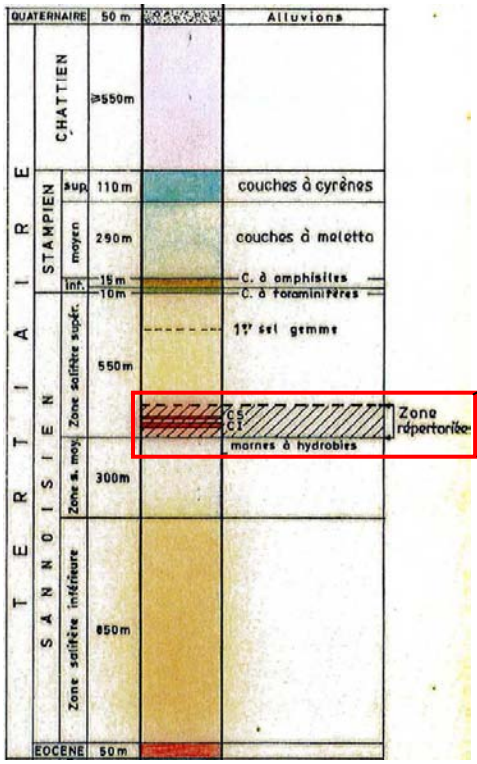

B)

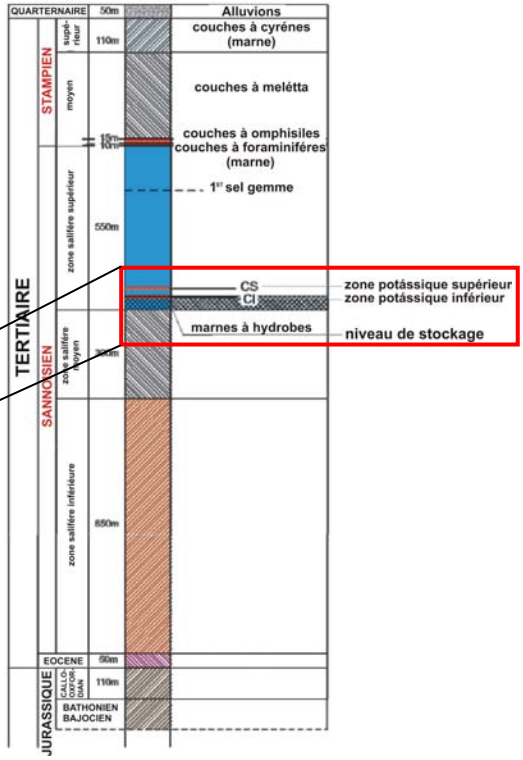

C)

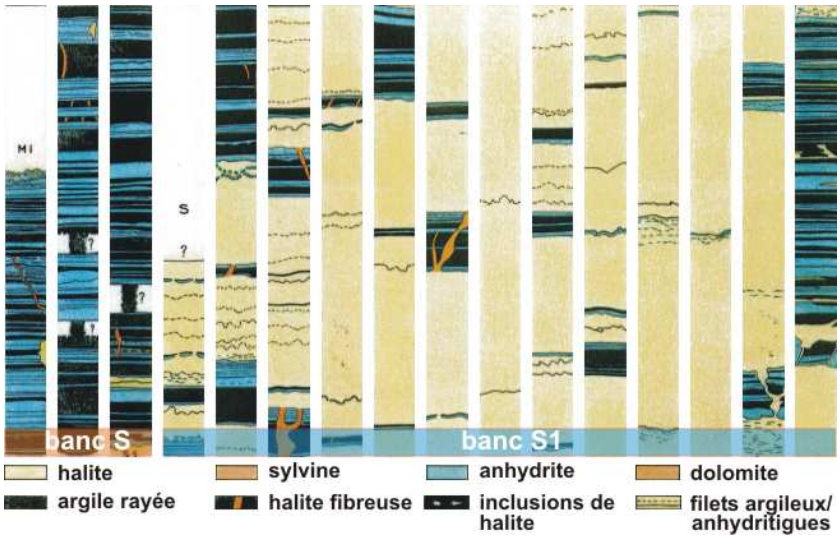

Figure 2 General stratigraphic situation

[Explanation: A) stratigraphy of the Mulhouse potash basin referred to [2], B) stratigraphy of the Wittelsheim basin referred to [12], C) lithologies and detail stratigraphy classification in the disposal area [2]]

The excavations of StocaMine are located in the footwall of a potash zone containing two sylvinite seams in rock salt interlayered by calcareous clay and anhydrite (Figure 2A) [12]. Details of the geologic/stratigraphic record are also reported in [12]. The rock salt formation of the disposal area is mainly inter-layered by calcareous clay (marl) and anhydrite [2].

Basically, no tectonic influence of the sub-horizontal, slightly NW dipping rock salt in the investigation area is known, although deep reaching, SW-NE oriented faults have been identified in other parts of the basin resulting in flexures in the evaporite layers. The hydrogeological situation within the evaporite formations was been characterised by [12] as normally water free. Only some small brine inclusions have been found during mining and minor amount were reported from the salt free marls of the Upper Salt Zone. Principally, the excavations of StocaMine are separated from groundwater bearing horizons by several 100 metres of low permeable rock salt and marl.

Figure 3 shows the location of the 7 test sites. All test sites are accessible by the shaft Joseph of the abandoned mine Amelie. The test sites named with T2 are situated in galleries in the direct vicinity of the disposal area. Whereas, the test sites named with T1 are located in the centre of the disposal area along the double gallery AJ1T/AJ1D. For sites T1-1 and T1-2, a massive pillar of a potash mining field in the hanging wall having the dimensions of approximately 230 m x 150 m has a rock mechanical relevance (see blue boundary in Figure 3).

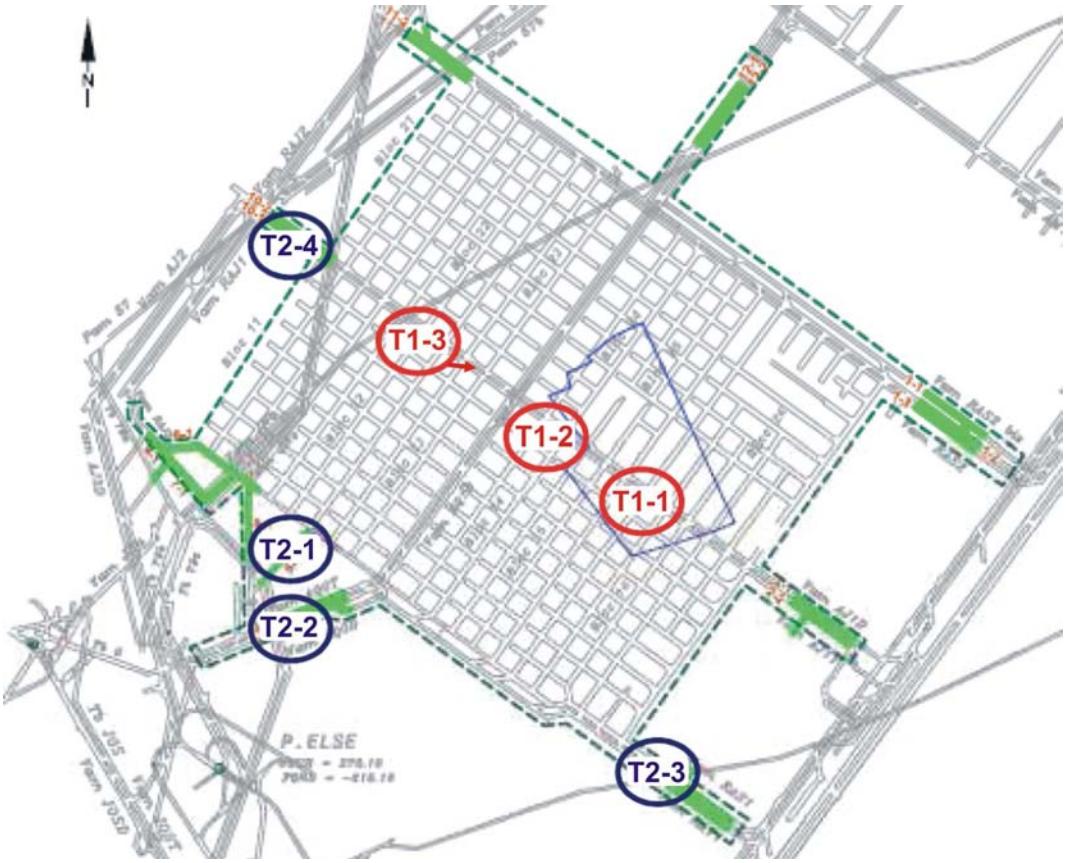

Figure 3 Location of test sites
[Explanation: blue boundary – massive pillar of a potash mining field in the hanging wall]

The Table 1 summarizes the information in respect to each site. Please see separate report parts for more detail information.

Table 1 Summarized site information

site	relative position[1]	gallery	excavation	amount boreholes	explored stratigraphy[2]	remarks
T1-1	centre	AJ1T/AJ1D (double)	mainly between Banc de 23 m and Banc de 25 m	2	S and S1	massive pillar of a potash mining field in the hanging wall
T1-2				2		
T1-3				2		
T2-1	vicinity	A-12 (single)		4	S1	-
T2-2		AQ0T/AQ0D (double)		9		-
T2-3		RAS1/RAT1 (double)	below Banc de 25 m	9		-
T2-4		AJ1T/AJ1D (double)	mainly between Banc de 23 m and Banc de 25 m	9		-

Generally, all boreholes at the test sites explore rock salt as well as the interlayered calcareous clay and anhydrite.

6 Drilling and work program

In preparation to the investigation, a working program was set up, discussed and consulted with StocaMine and MDPA [3]. On the 14th of February, 2013 an expansion of the working program for the last sites T1-2, T1-3 and T2-3 was agreed by StocaMine and MDPA [6].

In total, about 140 metres were drilled for 37 reference holes having a diameter of 70 mm in several drilling campaigns. Figure 4 depicts schematically the situation at the different sites.

A)

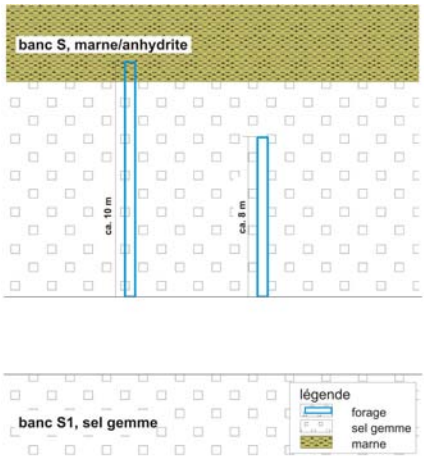

B)

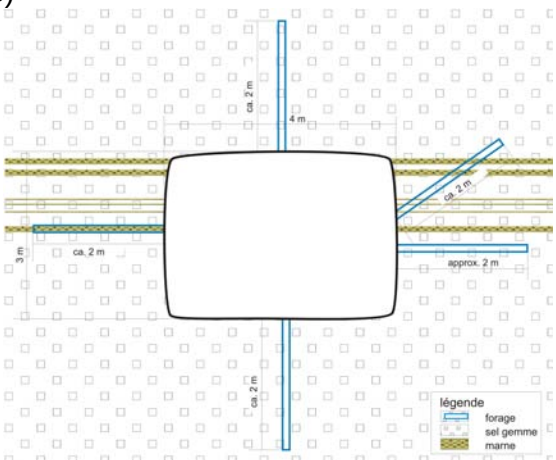

[1] in respect to the underground waste disposal

[2] referred to [2]

C)

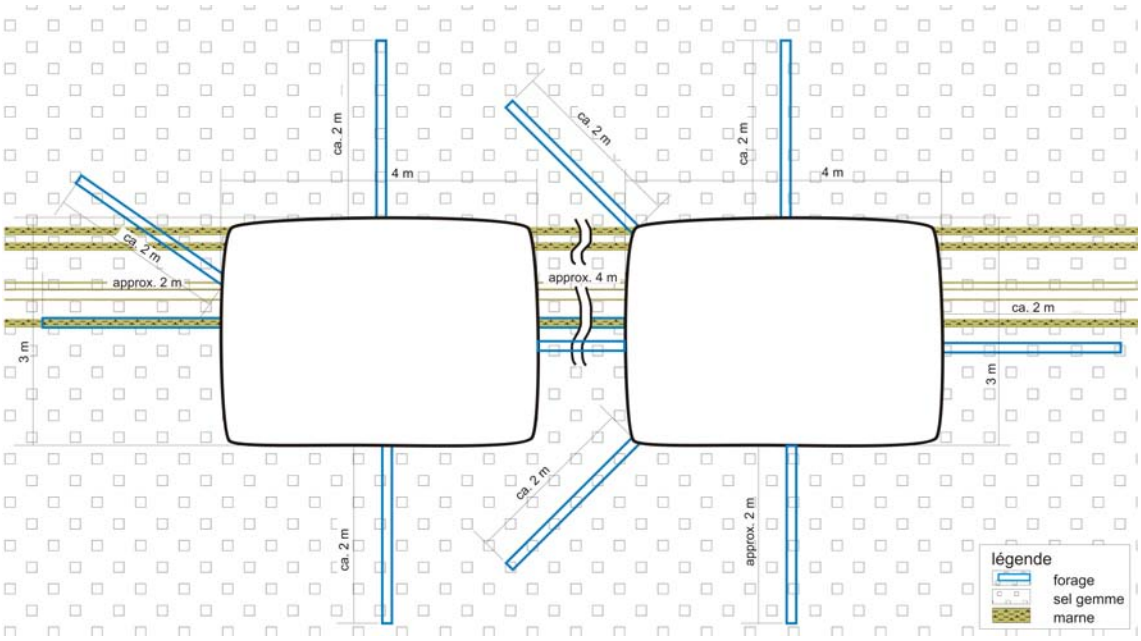

Figure 4 Position and orientation of reference holes at the sites

[Explanation: A) – sites T1-1, T1-2 and T1-3; B) site T2-1; C) sites T2-2, T2-3 and T2-4]

Between one and six measuring points were investigated in each reference hole. Hence, approximately 150 in situ permeability determinations were totally performed. For these determinations borehole packer tests were performed using double and quadruple borehole packers with < 70 mm in diameter. Basically, test intervals of about 0.18 m length were tested. However, if testing a whole borehole sequence from the packer end to final depth of the borehole even intervals of up to several metres length were integrally tested. Prior to the in situ permeability test, the reference hole was standardizing cleaned by dry pressurized air and surveyed by video endoscopy.

In addition to the in situ fluid tests in boreholes, laboratory investigations were performed in order to determine the brine content at the measuring point in the borehole. Therefore, the drilled cores were geological described, welded in plastic foil, transported, photographed and sampled for oven drying.

For more detail information on the drilling and work program, please read [4] and [6] as well as the separate report parts 2-8.

7 Description of analytic methods

7.1 Determination of permeability by in situ-Tests

The general, fluidic, initial situation for in situ permeability tests in boreholes can be characterised as follows:

- The tested rocks (rock salt and marl/clay) have very low permeabilities. Close to the contour the permeability may increase depended on the geologic situation, the mining site condition and the change in ground stress. This area is mainly signified as loosening or excavation damaged zone (EDZ). Due to contrasts in competence of rocks

within a sedimentary layering and the resulting differences in deformation behaviour of rock salt and intercalated marl/clay a loosening induced by relative movement along bedding planes in the sense of shear strain (simple shear) can not be excluded. Conditioned by the drilling process itself an additional loosening along the contour of the borehole has to be assumed.

- Basically, the tested rock salt with the exception of marl/clay can be considered as dry. The entry of moisture has be avoided and/or reduced by the use of dry pressurised air as drilling fluid and by an immediate sealing of the borehole or an instantaneous measurement. However, depended on the durability of the borehole the existence of moisture in the vicinity of the measuring point can not completely be excluded. Therefore, all in situ gas permeabilities have to be considered as effective gas permeability in dependence of the saturation with brine.

7.1.1 Description of test method – in situ permeability tests

In situ permeability tests exhibit fluidic in situ experiments. During these experiments an unsteady flow process is initiated in the pore space of the tested rock and recorded in its temporary development by measuring technique. Different fluids are in use. Thus, the performance of tests with different gases and liquids (commonly brines) is possible. The selection of a fluid is always use- and task-orientated.

Gas, especially dry pressurised air, exhibits an inert fluid in respect to the pore space of salty rocks and was often applied to many salt formations in the past (e.g. [14], [15], [16], [17], [18], [19], [20], [21]). Below only in situ permeability tests with gas will be discussed.

Due to the dependence of gas permeability on the liquid saturation and the circumstance that the existence of liquid in the pore space can never completely excluded the in situ determined gas permeability always exhibit an effective gas permeability. This permeability may decrease in the order of magnitude with increasing liquid saturation. Based on the lack of knowledge of time-dependent liquid saturation no evaluation of the influence of this effect is possible. In case of evidence of an elevated moisture influence based on the determination of brine content on core samples from the test site in situ permeability tests with brine as fluid are advised.

In situ permeability test can principally be performed as:

- pulse test (IT),
- constant pressure test (CP) and
- constant rate test (CR).

7.1.2 Borehole packer tests

7.1.2.1 Test method and experimental setup

The test methods (IT, CP, CR) differ in the temporally development of pressurisation. During pulse tests the defined volume of the test interval (so-called test room) is hermetically sealed by hydraulic inflatable packer segments and subsequently charged with a pressure impulse.

For constant pressure tests the test interval is permanently exposed to a constant pressure, whereas the test interval is loaded by a constant flow rate during the constant rate test.

The curves of pressure and flow rate are continuously recorded during the performance of the in situ experiment. Depending on the applied packer equipment (e.g. quadruple packer in Figure 5) the pressure in up to three additional, hermetically sealed intervals (so-called control rooms) can be controlled. The test equipment is explained more in detail in the chapter 7.1.2.3.

The in situ permeability tests within a test interval (MP – measuring point equates the central point of the test interval) are usually performed in to steps. During a pulse test the level of permeability at the measuring point will be determined in the first step (pre-test). In case of a proofed, rapid pressure decrease within a few seconds a main test will be performed as constant pressure test. However, if only a slow rate of pressure decrease will be proved the experiment (pre-test) will be continued as pulse test.

The test data are continuously recorded during the whole in situ experiment. The frequency of data recording will be adapted in a way that data within time intervals having great changes will be recorded in a sufficient frequency (minimal frequency of 1 Hz meaning one measurement per second).

The charge with pressure of the test interval leads to a cylindrical to spherical flow in the rock as schematically depicted in Figure 5 and Figure 9. Dependent on the permeability of the rock as well as the not a priori excludable existence of a secondary loosening zone around the borehole pressure reaction in the control intervals can be observed. This results consequently in interfering flow processes (interference). Figure 6 and Figure 7 are showing examples for measured data and the numerical evaluation by simulation model for pulse and constant pressure tests.

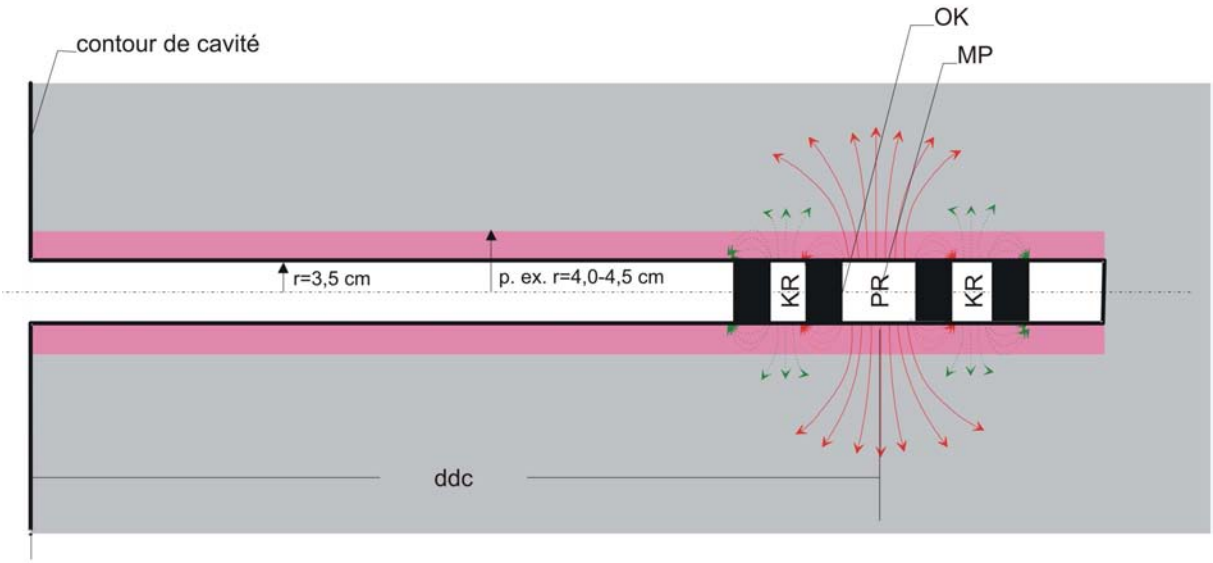

Figure 5 Schematic presentation of gas or fluid flow for a quadruple packer

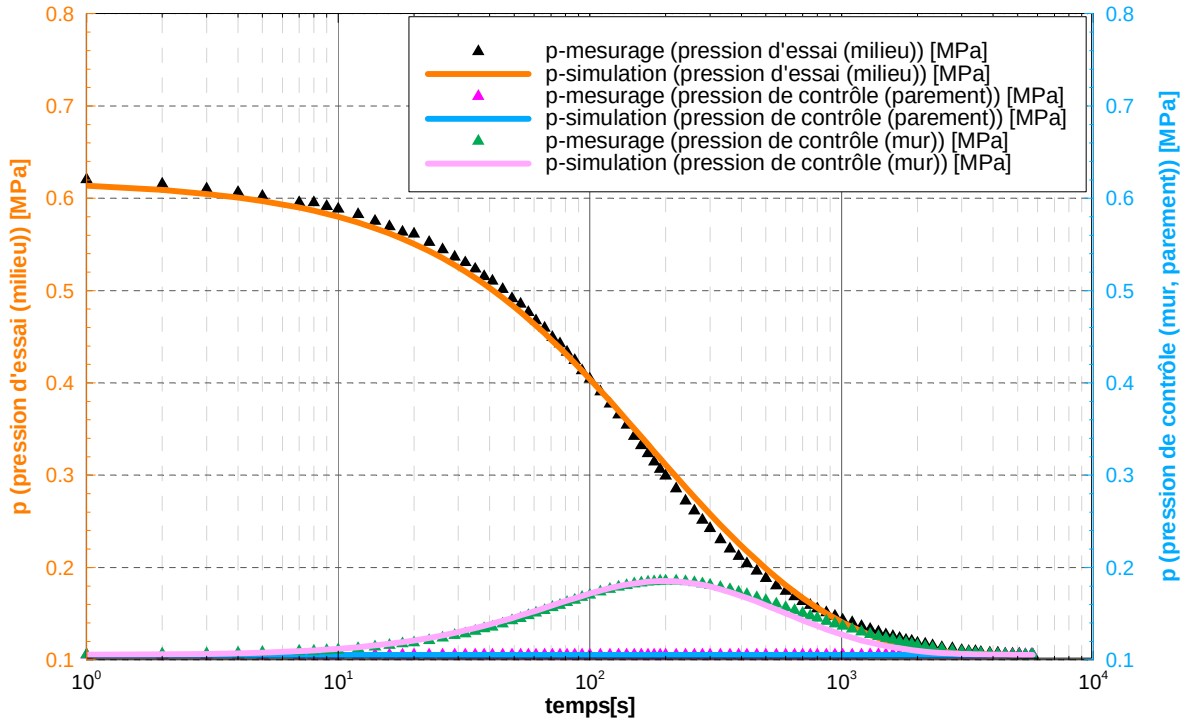

Figure 6 Example for a measurement and subsequent test evaluation of a pulse test applying a quadruple borehole packer

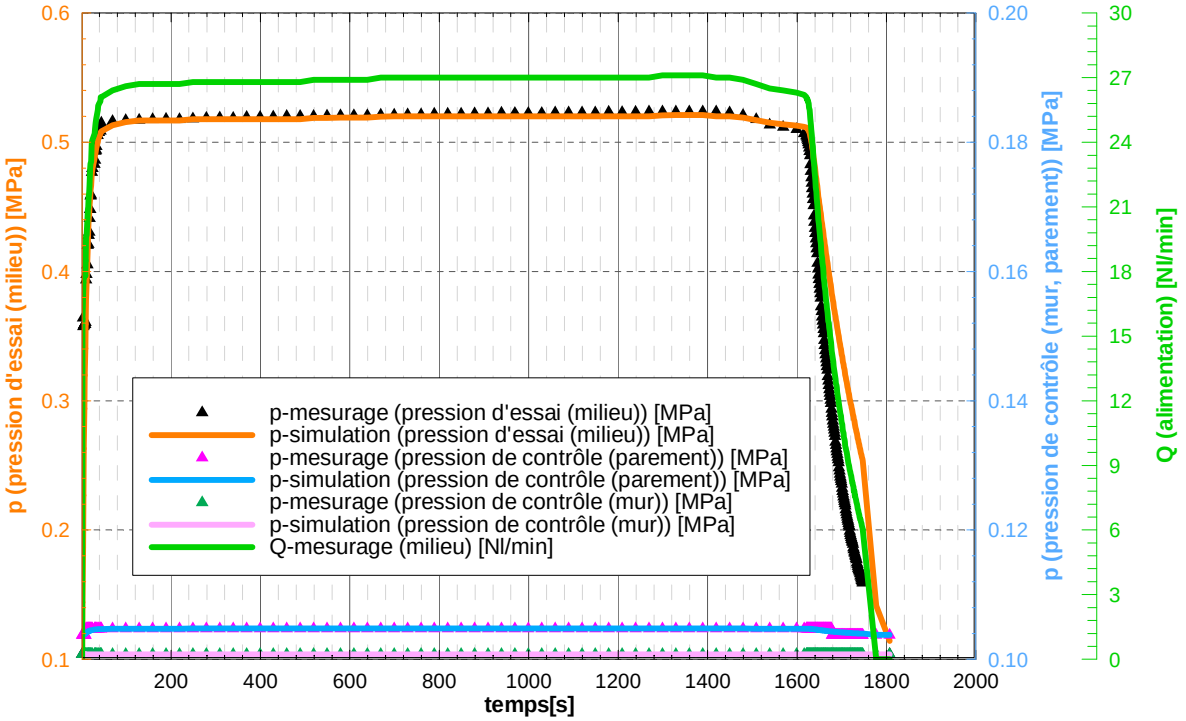

Figure 7 Example for a measurement and subsequent test evaluation of a constant pressure test applying a quadruple borehole packer

7.1.2.2 Test performance

Based on the description of the test method and the experimental setup in chapter 7.1.2.1 and chapter 7.1.2.3 the single steps of the different test designs for the determination of the in situ gas permeability will be presented in the following brief description.

Pulse test (gas)

Pulse tests as applied in boreholes in order to determine the in situ gas permeability are performed in following sub-steps:

- installation of the packer at the measuring point in the borehole, if necessary preventing of displacement of the packer in the borehole by an mechanical abutment (e.g. if whole borehole is pressurised),
- hydraulic inflation of packer elements, observation phase in order to guarantee a complete placing of the packer elements,
- charge of the test interval with a pressure impulse,
- time-dependent measurement of the test pressure and if applicable of the pressure reactions within the control intervals as well as of the air pressure, the hydraulic pressure in the packer elements and the air temperature,
- model-based evaluation of measured pressure data considering all knowledge of the site conditions and test performance.

Constant pressure/ rate test (Gas)

Constant pressure/ rate tests as applied in boreholes in order to determine the in situ gas permeability are performed in following sub-steps:

- installation of the packer at the measuring point in the borehole, if necessary preventing of displacement of the packer in the borehole by an mechanical abutment (e.g. if whole borehole is pressurised),
- hydraulic inflation of packer elements, observation phase in order to guarantee a complete placing of the packer elements,
- permanent exposure of the test interval to a constant pressure/ load of test interval by a constant flow rate,
- time-dependent measurement of the test pressure and if applicable of the pressure reactions within the control intervals as well as of the air pressure, the hydraulic pressure in the packer elements and the air temperature,
- model-based evaluation of measured pressure data considering all knowledge of the site conditions and test performance.

7.1.2.3 Test equipment

Generally, there are several packers (quadruple, double and single) for application in bore-holes with 42 mm and 70 mm in diameter available. Furthermore, special double packers applicable for bore diameters of 36 - 46 mm, 66 - 76 mm, 95 -105 mm and 127 - 137 mm supply more flexibility in use. The length of test intervals varies from 0.04 m to 1.0 m. Some packers are equipped with a central passageway for pressurisation or control of the bottom hole. Figure 8 shows some of the packer equipment. Simultaneous measurements at up to four sites or alternatively measurement of interference in up to four boreholes at one site are possible with the equipment for in situ gas permeability tests.

Figure 8 Selection of packer equipment with diameters of 42 mm and 70 mm

Additional to quadruple packers depicted in Figure 9 double and single packers are also in use depending on site conditions and measurement task. Double packers consist of two packer elements sealing the test interval. Whereas, single packers only have one packer element for sealing the bottom hole as integral test interval.

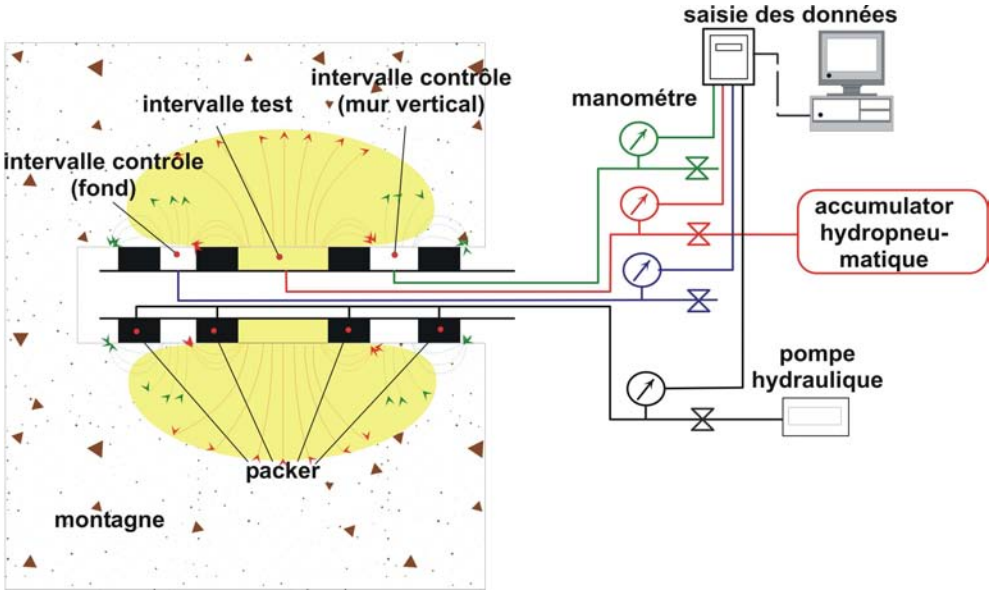

Figure 9 Experimental setup of in situ test applying a quadruple borehole packer

However, multi-packer systems (e.g. double, quadruple) equipped with a central passageway are usually applied for permeability tests of long borehole sections as test interval (pressurisation of the borehole). These packers are hydraulic deformed in the borehole and the hence arisen volume (down to the bottom hole) is been charged by pressure. In this configuration the length of the test interval is variable and depends on the distance of the first packer element from the bottom hole. However, it is essentially necessary to ensure the packer by a mechanical abutment at the collar (piling and rock bolts).

The feasibility of in situ permeability tests is depended on the depth of the measuring points, the quality of the reference hole and the bore diameter. Hence, in situ permeability tests have to be planed, proofed and designed considering the site conditions. Measurements in deep boreholes (l > 25 m) are principal feasible however, special equipment is necessary. This equipment actually allows the application double packers for gas and brine down to a depth of about 75 m.

Prior to measurement leak tests performed in frequent time intervals at the test site proof the necessary tightness of the assembled equipment. Additional leak tests are performed at lab in advance to a measurement campaign. During leak tests as well as in situ permeability tests it is possible to dope the gas by 1,1,1,2-Tetrafluorethane in order to detect leakages either at the equipment or at the collar. Even very low traces (> 1.5 ppm) of the tracer gas are detectable by the applied leak indicator and reveal leakages of the equipment or circulations of packer elements.

Piezoelectric pressure transducers having a precision of normally 0.1 % to 0.2 % are applied in order to record the temporal pressure development in the separate volumes (intervals) as well as in the packer elements. The measuring range of sensors is carefully fitted to the expected pressure ranges in dependence of the test pressure. The flow rate is recorded by thermal mass flow rate sensors having an accuracy of 1 % Rd (> 20 % of flow) and of 0.2 % FS (> 20 % of flow).

In situ gas permeability experiments can be performed with different gases. The test setup differs between pulse and constant pressure test only by an extern 20 MPa pneumatic source, a pressure control valve and a thermal mass flow rate sensor applied for constant pressure tests. In some cases this equipments is applied for pulse tests, too.

In general, the test setup for gas consists of a pressure controlling, measuring and a data acquisition unit as depicted in Figure 10. All components have to resist very corrosive site conditions; therefore they are designed from robust, water-tight and corrosion-resistant materials.

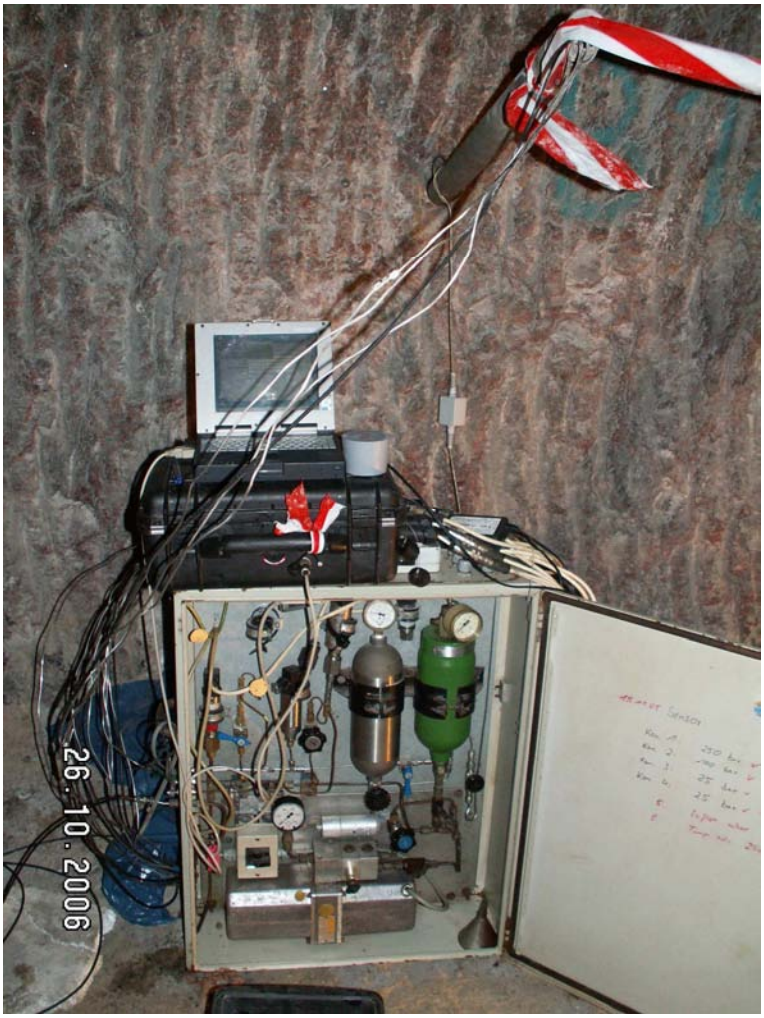

Figure 10 Measuring equipment for in situ permeability tests with gas

7.1.2.4 Data evaluation

In order to evaluate the measured data and determine the permeability a two-dimensional model in r-φ-z geometry (r-z profile) is built up considering the knowledge of the geometric structure of the flow space as well as of the properties of the fluid. The model can be variable fine discretised. In doing so, on one side the radius is spread in x-direction beginning from the bore centre and on the other side the distance to contour (face) is spread in y-direction (Figure 11). Applying a specific computer code the numerical solution of the partial differential equation (PDE) for the two-dimensional, radial-symmetrical flow of single phase (gas or liquid) can be simulated. The parameter permeability is determined by fitting measured and calculated pressure data. The computer code is combined with a parameter identification algorithm.

The fitting process is started beginning with a starting value of permeability. The permeability result is determined during the fitting process at which the measured and simulated pressure curves show the best fit. The target function of the fitting is the minimisation of the error square sum for both curves (least-squares method).

Figure 11 shows an example for the simulation of the radial-symmetrical flow during a bore-hole packer test, the model discretisation and the calculated, spatial pressure distribution.

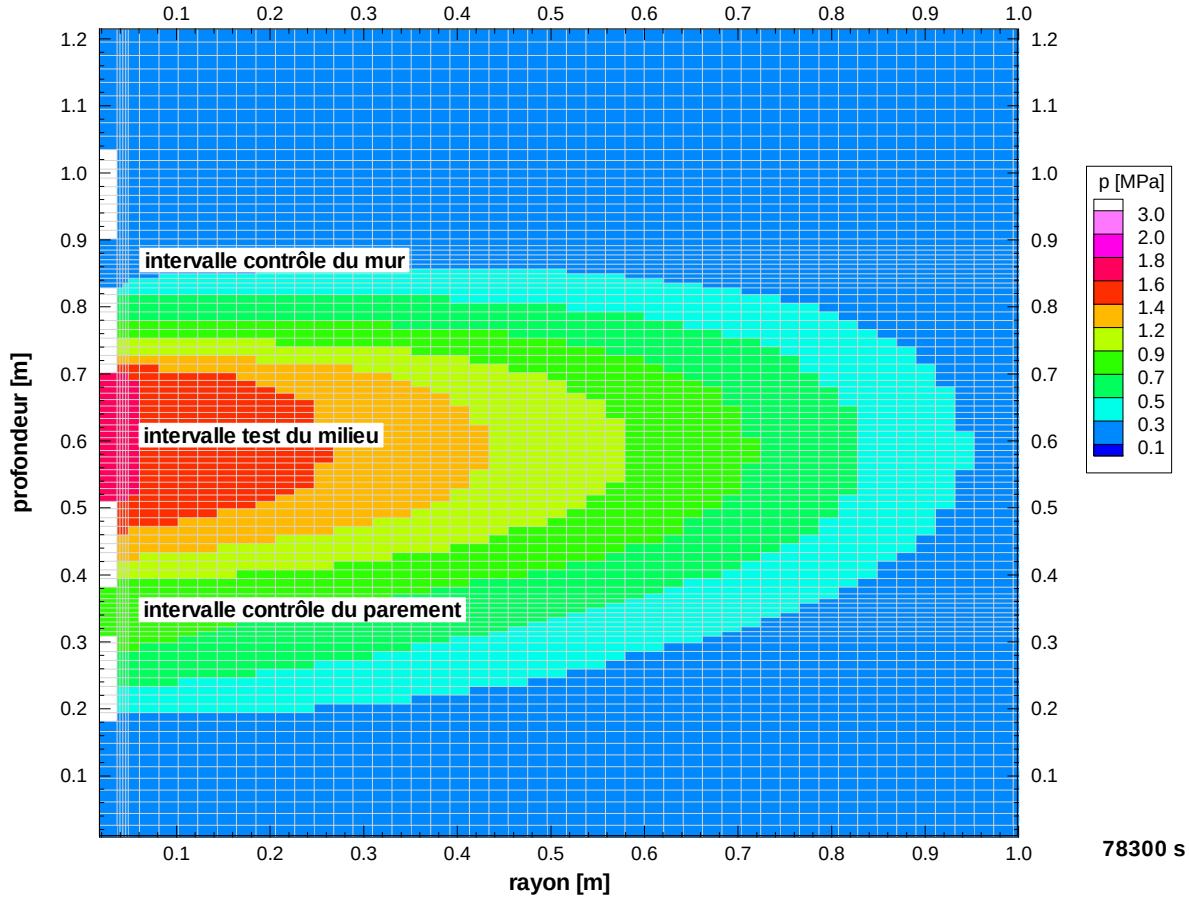

Figure 11 Test evaluations – model discretisation and simulated, spatial pressure distribution

- red: high pressure starting from test interval
- blue: initial (low) pressure in rock (air pressure)

7.2 Determination of brine content by oven drying

The determination of brine contents was carried out by oven drying at 105 °C [3]. The samples for drying were obtained from core material at the vicinity of the measuring point as far as possible. In order to consider the precipitation from brine in the pore space a mineralisation of 317.1 g/l and a density of 1.201 g/cm³ [22] were applied. These parameters are based on the assumption of saturated halite brine (equilibrium brine in respect to rock salt).

The brine content was calculated by:

$$w_L = \frac{m_L}{m_{s,korr}} \quad (1)$$

w_L	-	brine content	-
m_L	-	mass of brine	g
$m_{s,korr}$	-	corrected dry mass	g

8 In situ and laboratory results

All results inclusively in situ and lab protocols are presented in detail in the report parts 2-8.

8.1 Site investigation T1

The results of sites T1-1, T1-2 and T1-3 are summarised because similar geological site conditions (bank S1 / bank S) apply for all three sites. The focus of the investigations was the characterisation of permeability conditions of the marl as well as of the vertical hydraulic conditions at the test sites (see chapter 4). Figure 12 represents the result regarding to the general geological situation (details in report parts 2-4).

A)

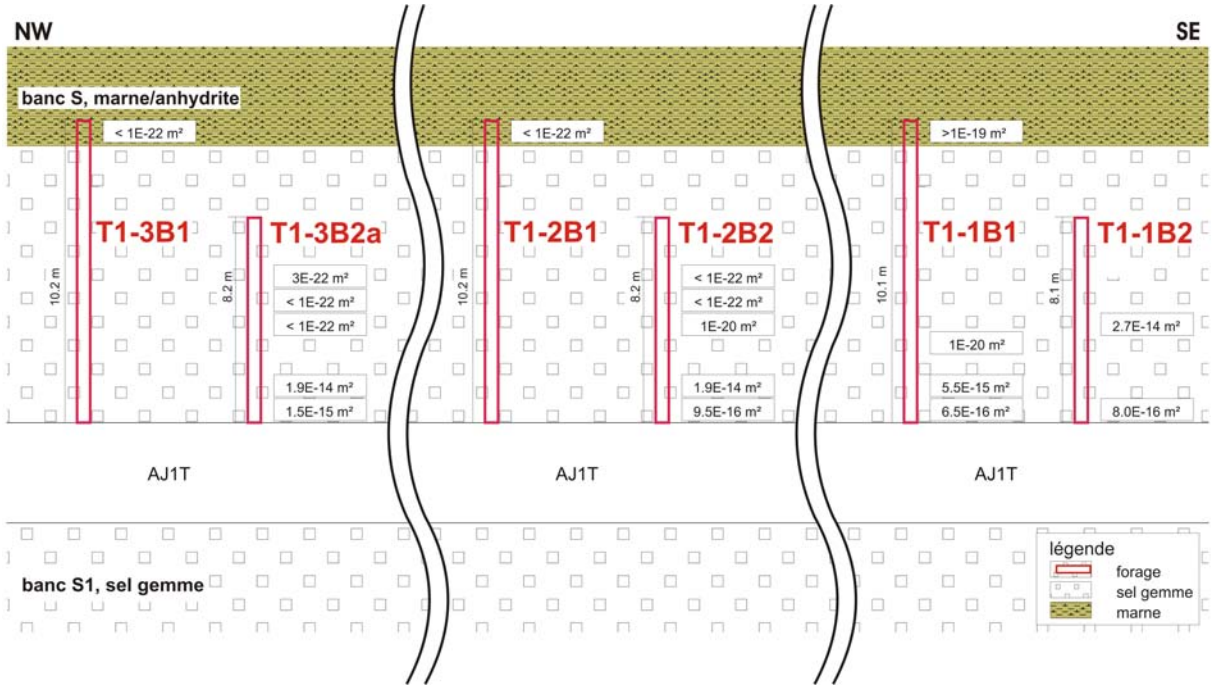

B)

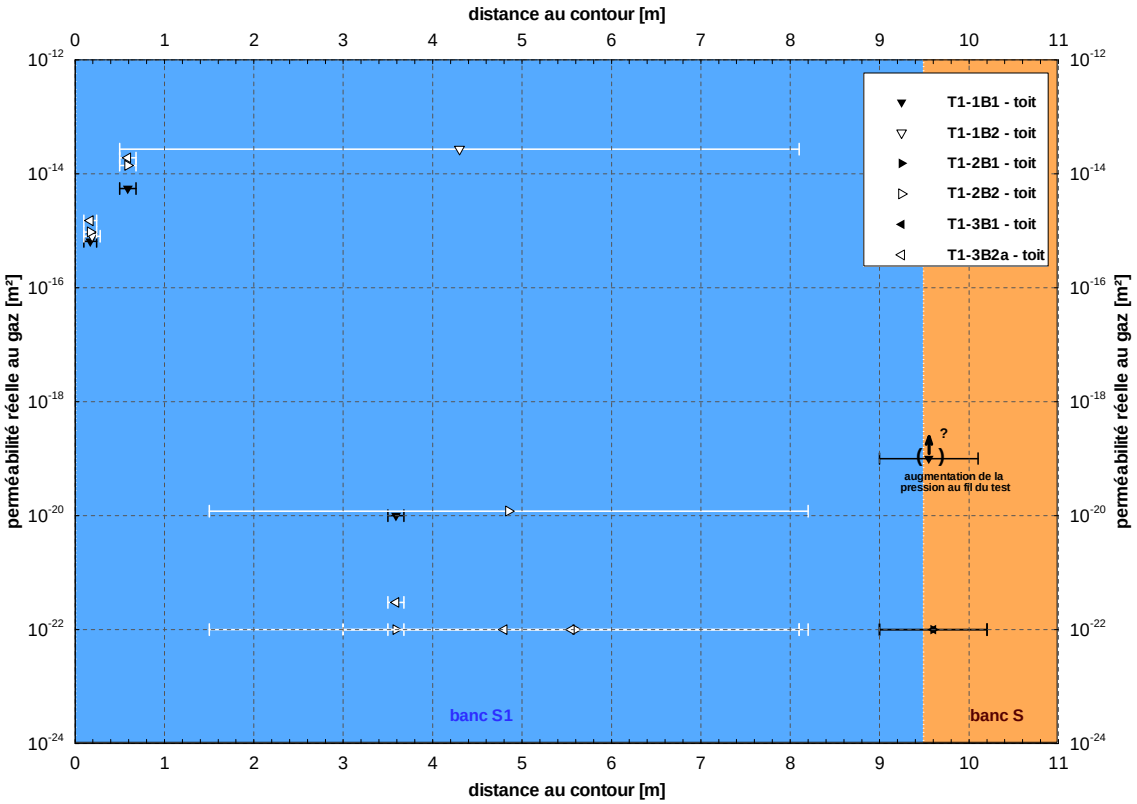

Figure 12 Results of in situ gas permeability in the roof at T1-1, T1-2 and T1-3
[Explanation: A) schematic profile of drift showing effective gas permeabilities, B) diagram k_{eff} vs. distance]

Generally, there was a level of elevated permeability (6.5E-16 m² to 1.9E-14 m²) detected in bank S1 within distances up to approximately 0.6 m as seen in Figure 12. Whereas, the permeability level in bank S1 in distances > 1.5 m are predominately low (≤ 2E-20 m²). However, the measurement T1-1B2-050-G1 with the test interval from about 0.5 m to about 8 m exhibits an exception with a permeability of 2.7E-14 m². This is interpreted to be mainly caused by an influence of high permeabilities within the range from 0.5 m to 1 m. However, evaluated permeabilities (e.g. bedding, joints and fissures) in distances > 1 m can not be excluded. The change from bank S1 to bank S in a distance of approximately 9.5 m is characterised by a low permeability of < 1E-22 m² for sites T1-2 and T1-3. Permeability levels of > 1E-19 m² were yielded for site T1-1. This result has to be considered with a certain uncertainty caused by pressure increase due to gas emission from marl layers (see report part 2).

In total 18 measurements were carried out in the roof at all three sites. Figure 13 shows the frequency distribution of the permeability results.

classement	fré-quence	fréquence statistique cumulée
≤ 1E-22	6	33.33%
≤ 1E-21	1	38.89%
≤ 1E-20	1	44.44%
≤ 1E-19	2	55.56%
≤ 1E-18	0	55.56%
≤ 1E-17	0	55.56%
≤ 1E-16	0	55.56%
≤ 1E-15	3	72.22%
≤ 1E-14	2	83.33%
≤ 1E-13	3	100.00%
> 1E-13	0	100.00%
nombre	18	

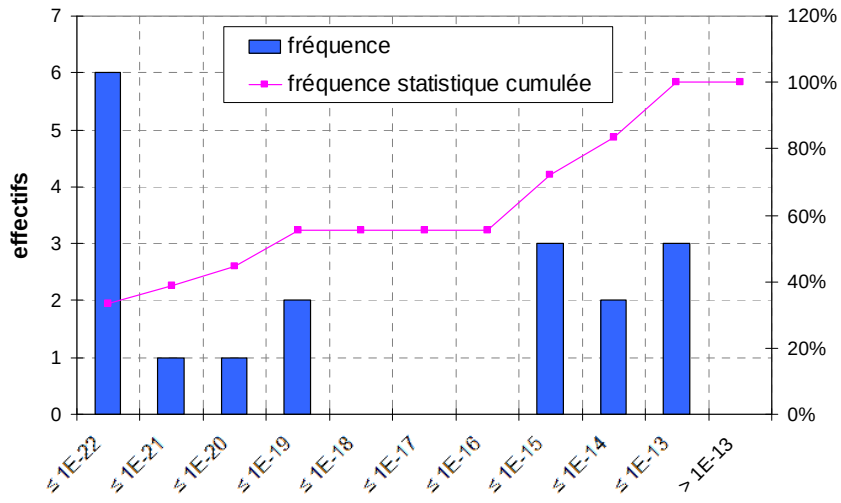

Figure 13 Frequency distribution of effective gas permeability at sites T1-1, T1-2 and T1-3

The unsymmetrical frequency distribution accommodates that on one hand permeability depends on distance and on the other hand on geology.

A direct comparison between the sites in respect to the permeability conditions is only be possible comparing the results of comparable measurements (measurement points at ca. 0.1 m, ca. 0.5 m, ca. 3.5 m and ca. 9.5 m) for each site (Figure 14).

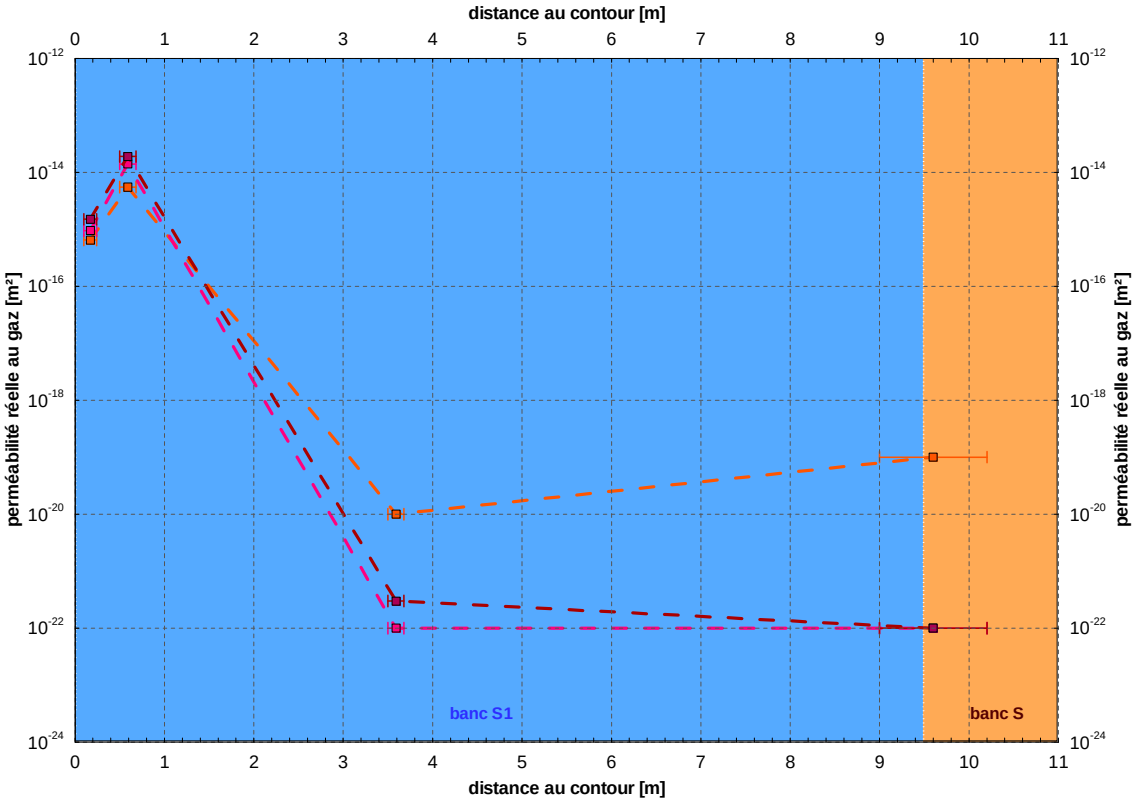

Figure 14 Comparison of permeability conditions of sites T1-1, T1-2 and T1-3

Figure 14 shows there is no great difference in permeability condition and trend between the three sites. The permeability > ca. 3.5 m is generally < 1E-18 m², whereas it seems to be slightly evaluated at site T1-1.

8.2 Site investigation T2

The site investigations at the four sites named with T2 were performed with the proposition to characterise the spatial permeability distribution in dependence on the distance to contour k = f(dtc) prominently in the rock salt. Therefore, the investigations were carried out site-dependent (roof, face, floor level, gallery corner and pillar) in order to define the lateral hydraulic conditions.

8.2.1 Site investigation T2-1

Fifteen measurements were performed in four boreholes at site T2-1 situated in a single gallery (see chapter 6). The measurements can be distinguished in four times roof, four times floor level and seven times face. Generally, the results vary from 7E-22 m² to 3E-14 m². Figure 15 from report part 5 shows the results of the in situ permeability tests at site T2-1 in respect to the principal geologic situation and to the spatial permeability distribution.

A)

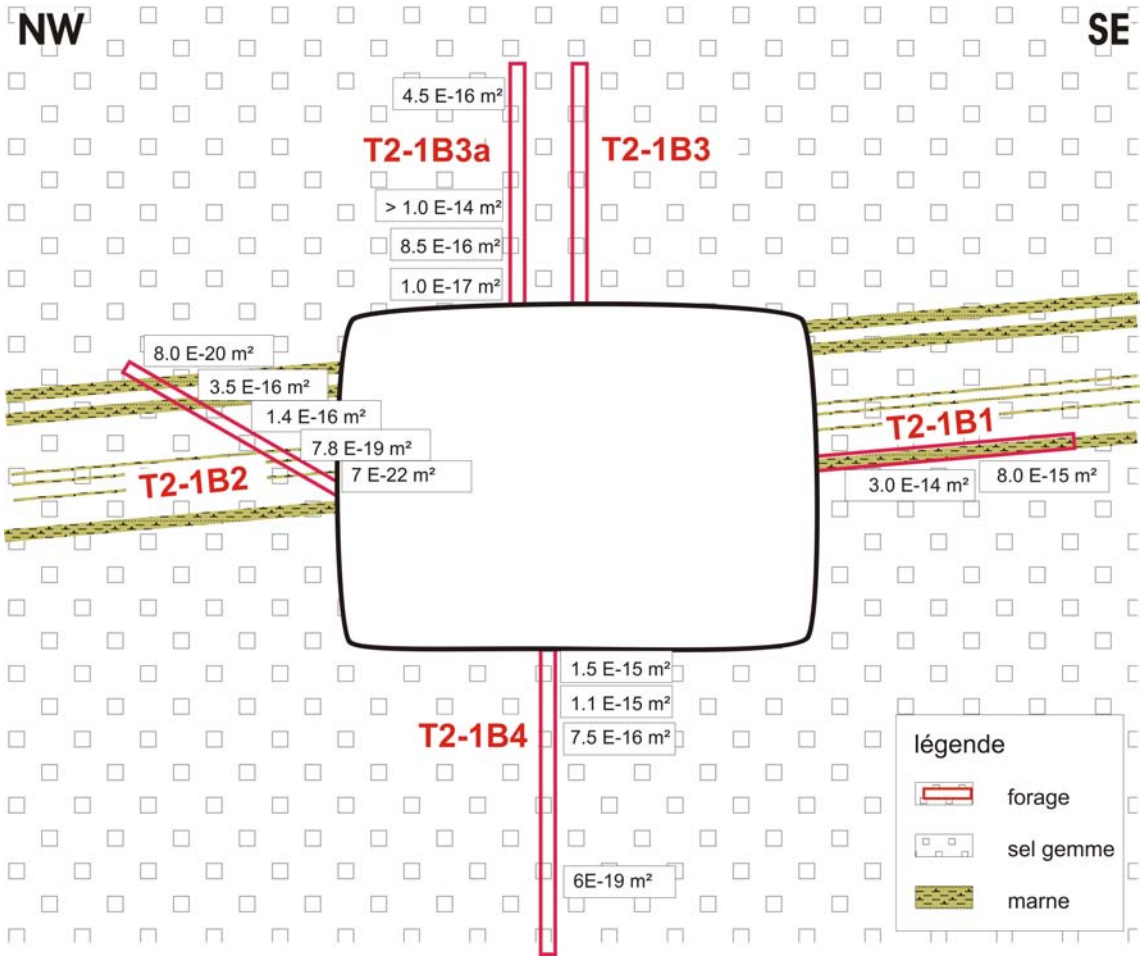

B)

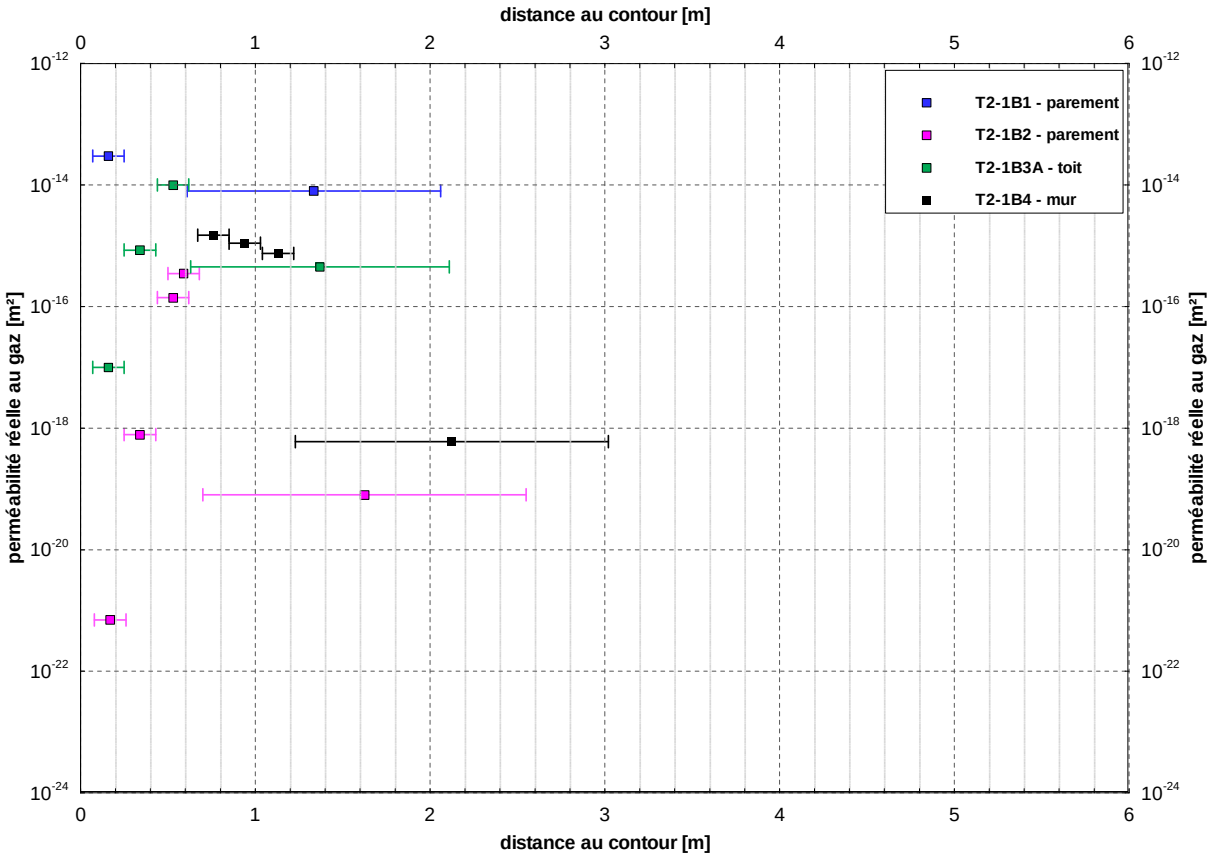

Figure 15 Results of in situ-gas permeability tests at site T2-1

[Explanation: A) Schematic profile of drift showing effective gas permeabilities, B) diagram k_{eff} vs. distance]

The frequency distribution without consideration of site condition and distance to contour is depicted in Figure 16.

classement	*fré-quence*	*fréquence statistique cumulée*
≤ 1E-22	0	0.00%
≤ 1E-21	1	6.67%
≤ 1E-20	0	6.67%
≤ 1E-19	1	13.33%
≤ 1E-18	2	26.67%
≤ 1E-17	1	33.33%
≤ 1E-16	0	33.33%
≤ 1E-15	5	66.67%
≤ 1E-14	3	86.67%
≤ 1E-13	2	100.00%
> 1E-13	0	100.00%
nombre	15	

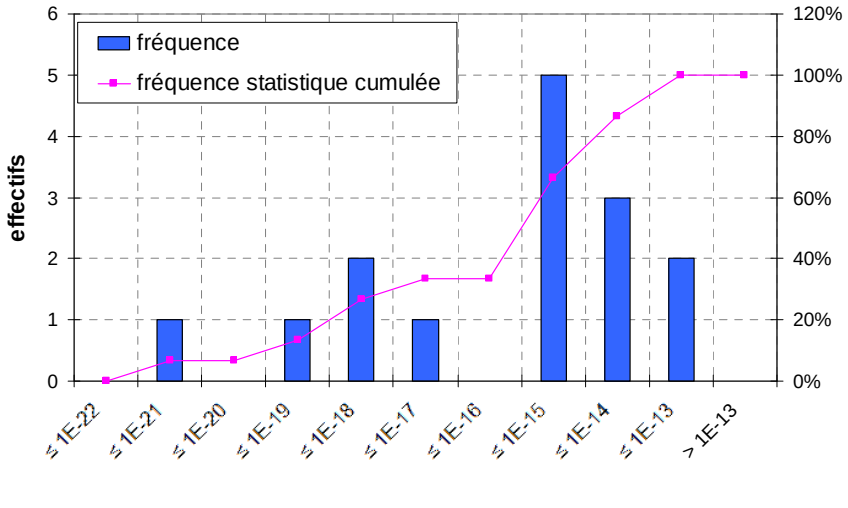

Figure 16 Frequency distribution of effective gas permeability at sites T2-1

For the interpretation of the gas permeability results please see report part 5 and chapter 9.

8.2.2 Site investigation T2-2

Site T2-2 is located in a double gallery named AQ0T/AQ0D. Twelve measurements were performed in three boreholes at AQ0T, whereas 24 measurements were carried out in six boreholes at AQ0D (in sum 36 measurements, four per borehole). In respect to the site conditions (collar) it is possible to classify the measurements as follows:

- roof: eight measurements (two boreholes)
- floor level: eight measurements (two boreholes)
- face: eight measurements (two boreholes)
- face (pillar): four measurements (one borehole)
- gallery corner: eight measurements (two boreholes)

In general the permeability results show a variation within the range of < 1E-22 m² and 6.6E-14 m². The spatial permeability distribution as well as the general geological situation for the 36 permeability results in the double gallery at site T2-2 is presented in Figure 17 (from report part 6).

A)

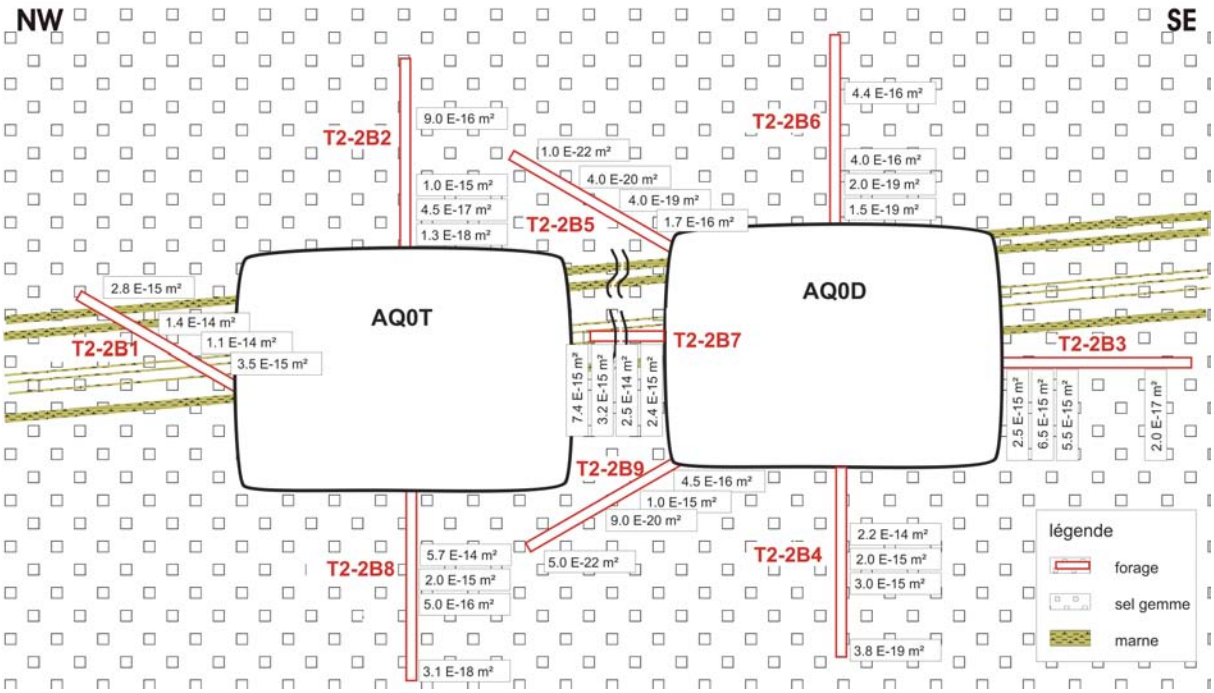

B)

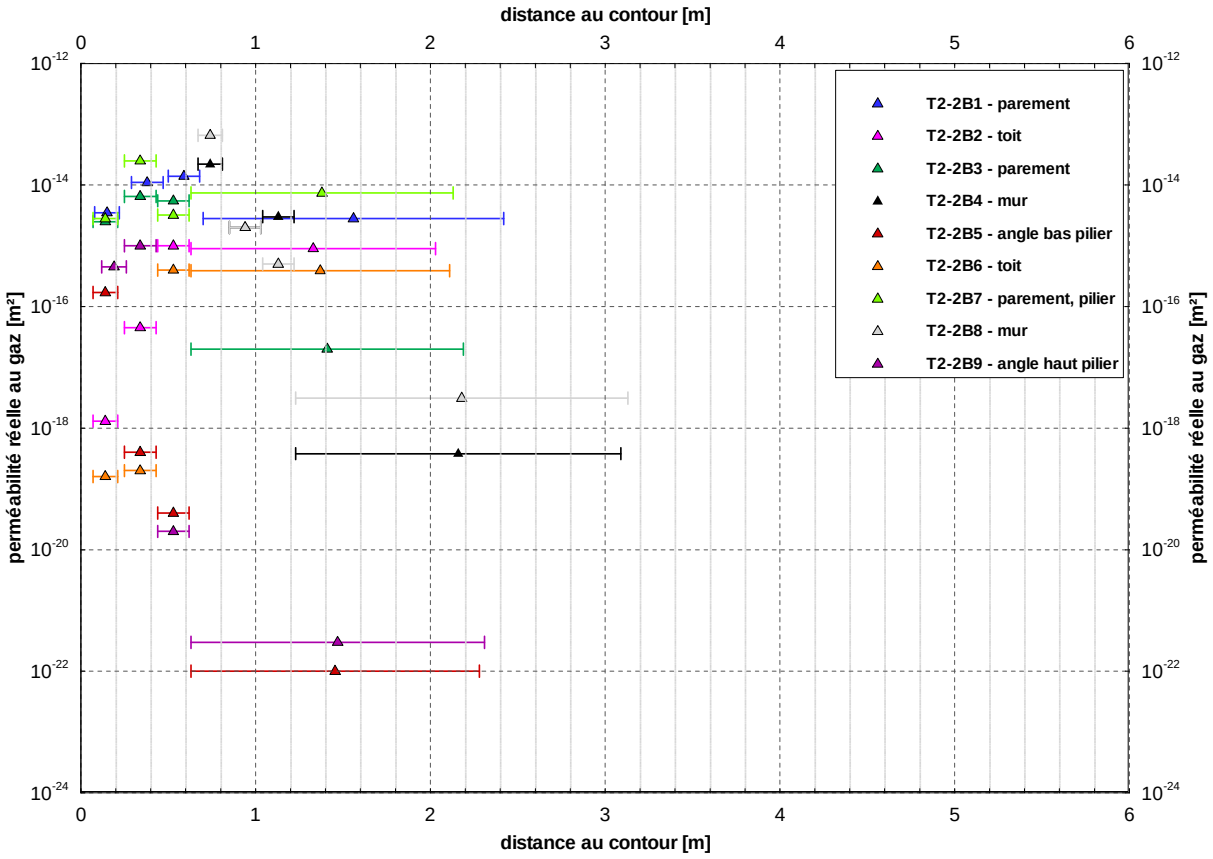

Figure 17 Results of in situ gas permeability tests at site T2-2

[Explanation: A) Schematic profile of drift showing effective gas permeabilities, B) Diagram k_{eff} vs. distance]

Figure 18 depicts the frequency distribution of all results.

classement	*fré-quence*	*fréquence statistique cumulée*
≤ 1E-22	1	2.78%
≤ 1E-21	1	5.56%
≤ 1E-20	0	5.56%
≤ 1E-19	2	11.11%
≤ 1E-18	4	22.22%
≤ 1E-17	2	27.78%
≤ 1E-16	2	33.33%
≤ 1E-15	8	55.56%
≤ 1E-14	11	86.11%
≤ 1E-13	5	100.00%
> 1E-13	0	100.00%
nombre	36	

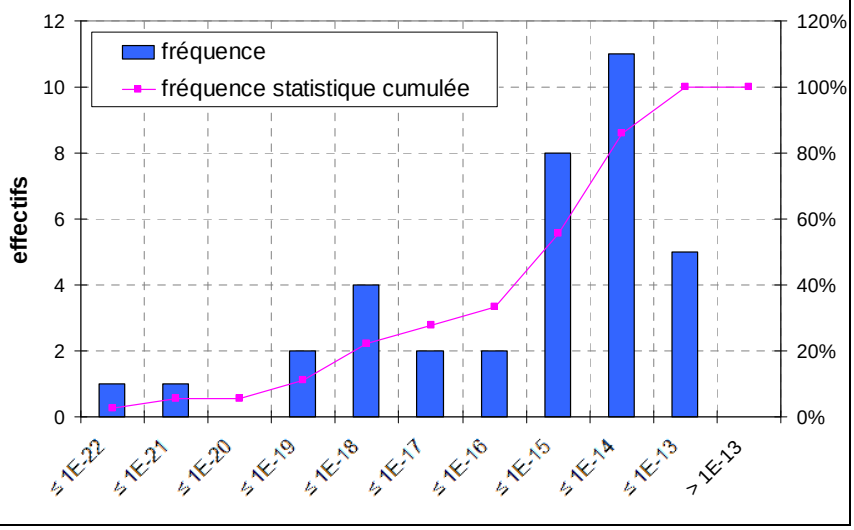

Figure 18 Frequency distribution of effective gas permeability at sites T2-2

For details it is referred to report part 6. The interpretation of the gas permeabilities in respect to dependencies on site conditions (collar) and on distance will follow in chapter 9.

8.2.3 Site investigation T2-3

Analogue to site T2-2 the site T2-3 is situated in a double gallery. The distribution of boreholes is similar to the site T2-2 (B1 to B6 at RAT1 and B7 to B9 at RAS1). However, the excavations of double gallery RAS1/RAT1 are located below Banc de 25 m in difference to site T2-2 and T2-4 (see chapter 5). Based on [6] eight measurement points were additionally investigated. Thus, the 44 measurements can be separated in:

- roof: twelve measurements (two boreholes)
- floor level: teen measurements (two boreholes)
- face: teen measurements (two boreholes)
- face (pillar): four measurements (one borehole)
- gallery corner: eight measurements (two boreholes)

The margin of deviation of permeability results is defined by < 1E-22 m² and 2.1E-13 m² at site T2-3. The 44 results of permeability tests are depicted in Figure 19 (from report part 7) in order to present their spatial distribution and relation to general geology at site T2-3.

A)

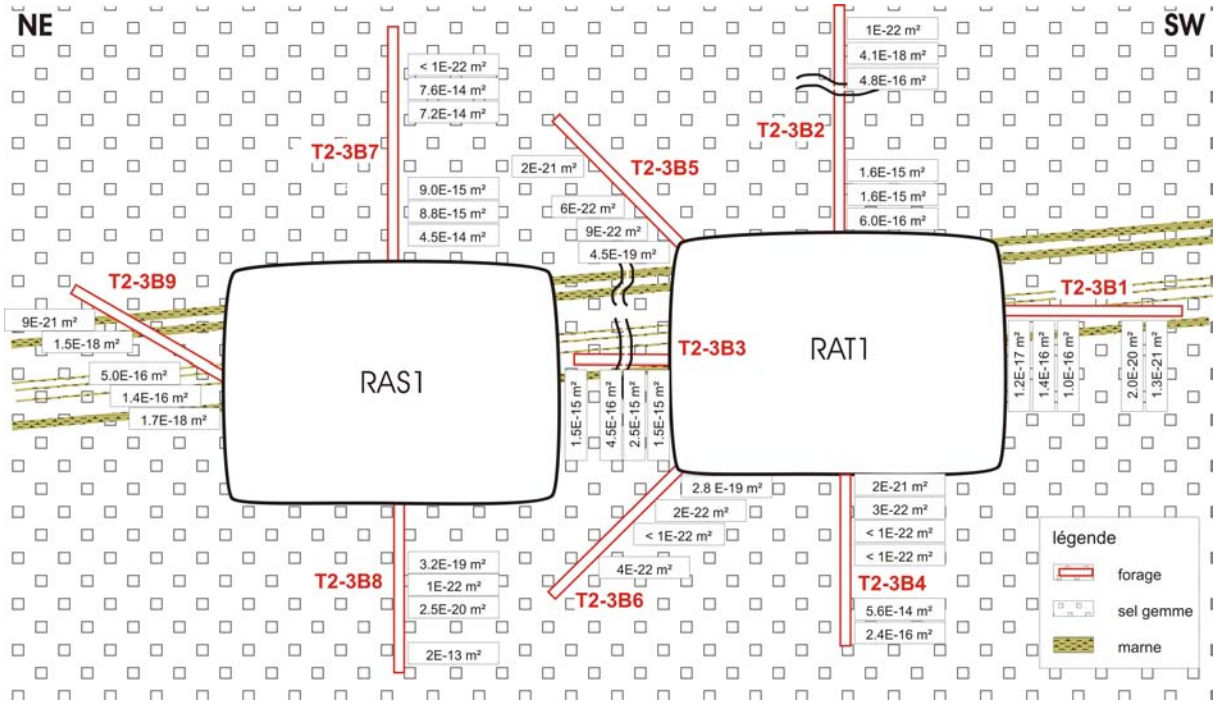

B)

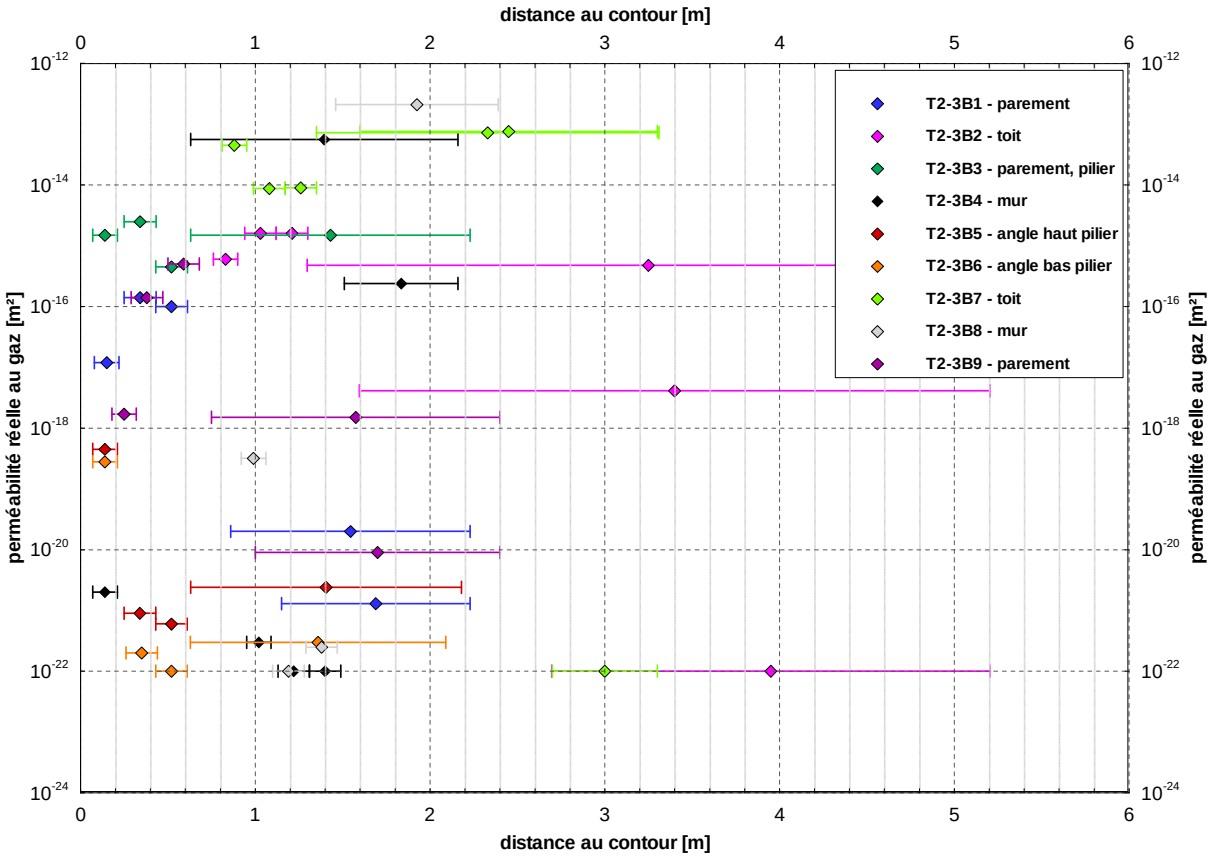

Figure 19 Results of in situ gas permeability tests at site T2-3

[Explanation: A) schematic profile of drift showing effective gas permeabilities, B) diagram k_{eff} vs. distance]

An unsymmetrical frequency distribution is revealed by Figure 20.

classement	*fré-quence*	*fréquence statistique cumulée*
≤ 1E-22	6	13.64%
≤ 1E-21	6	27.27%
≤ 1E-20	3	34.09%
≤ 1E-19	2	38.64%
≤ 1E-18	3	45.45%
≤ 1E-17	3	52.27%
≤ 1E-16	2	56.82%
≤ 1E-15	7	72.73%
≤ 1E-14	7	88.64%
≤ 1E-13	4	97.73%
> 1E-13	1	100.00%
nombre	44	

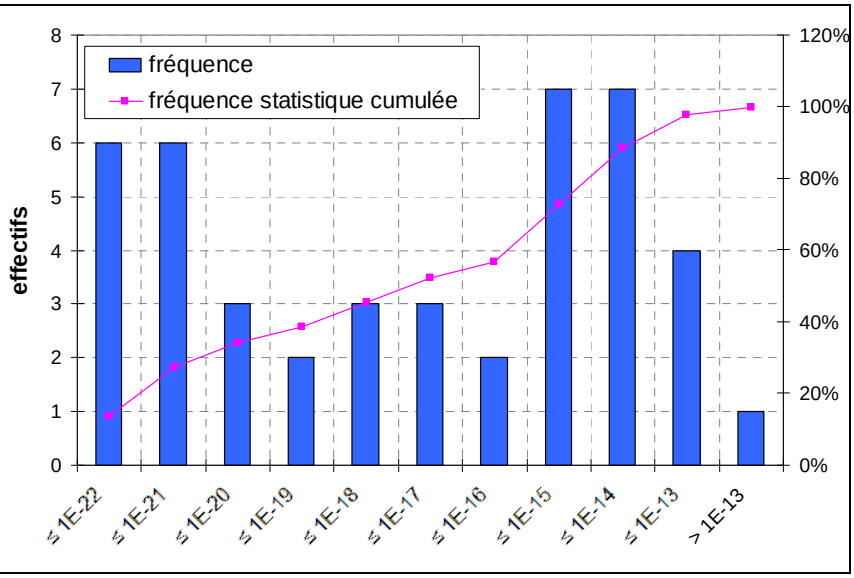

Figure 20 Frequency distribution of effective gas permeability at sites T2-3

The difference in frequency distribution compared to Figure 18 and Figure 22 is partly due to the reported additional eight measurements predominately in distances to contour approximately > 1 m.

Report part 7 reports more details on the in situ measurements at site T2-3. For interpretation of the gas permeabilities depend on site conditions (collar) and on distance please see chapter 9.

8.2.4 Site investigation T2-4

Finally, the site T2-4 is located in the same double gallery as the sites T1 (AJ1T/AJ1D). However, the location is outside of the disposal area in its NW vicinity (chapter 5).

Similar to T2-2, twelve measurements were performed in three boreholes at AJ1T, whereas 24 measurements were carried out in six boreholes at AJ1D (in sum 36 measurements, four per borehole). These measurements can be distinguished as follows:

- roof: eight measurements (two boreholes)
- floor level: eight measurements (two boreholes)
- face: eight measurements (two boreholes)
- face (pillar): four measurements (one borehole)
- gallery corner: eight measurements (two boreholes)

Compared to T2-3 the permeability results deviate within the similar range of < 1E-22 m² and 1.4E-13 m², whereas the permeability range at site T2-2 is slightly smaller (< 1E-22 m² and 6.6E-14 m²). Figure 21 shows the permeability results from report part 8 at site T2-4.

A)

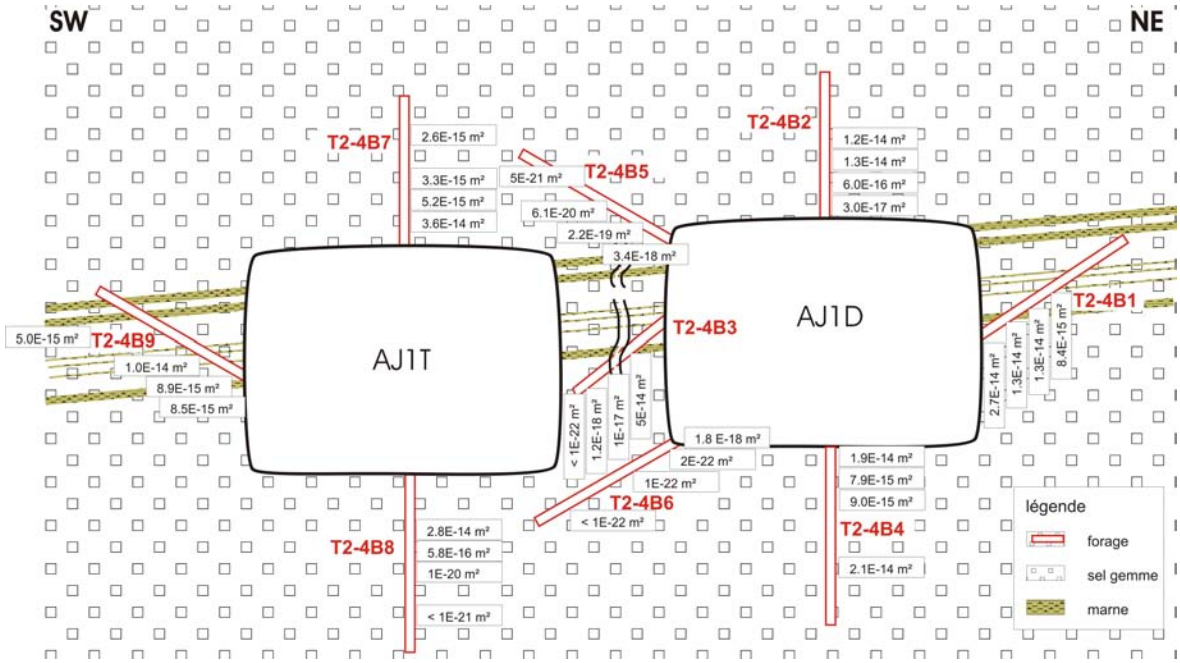

B)

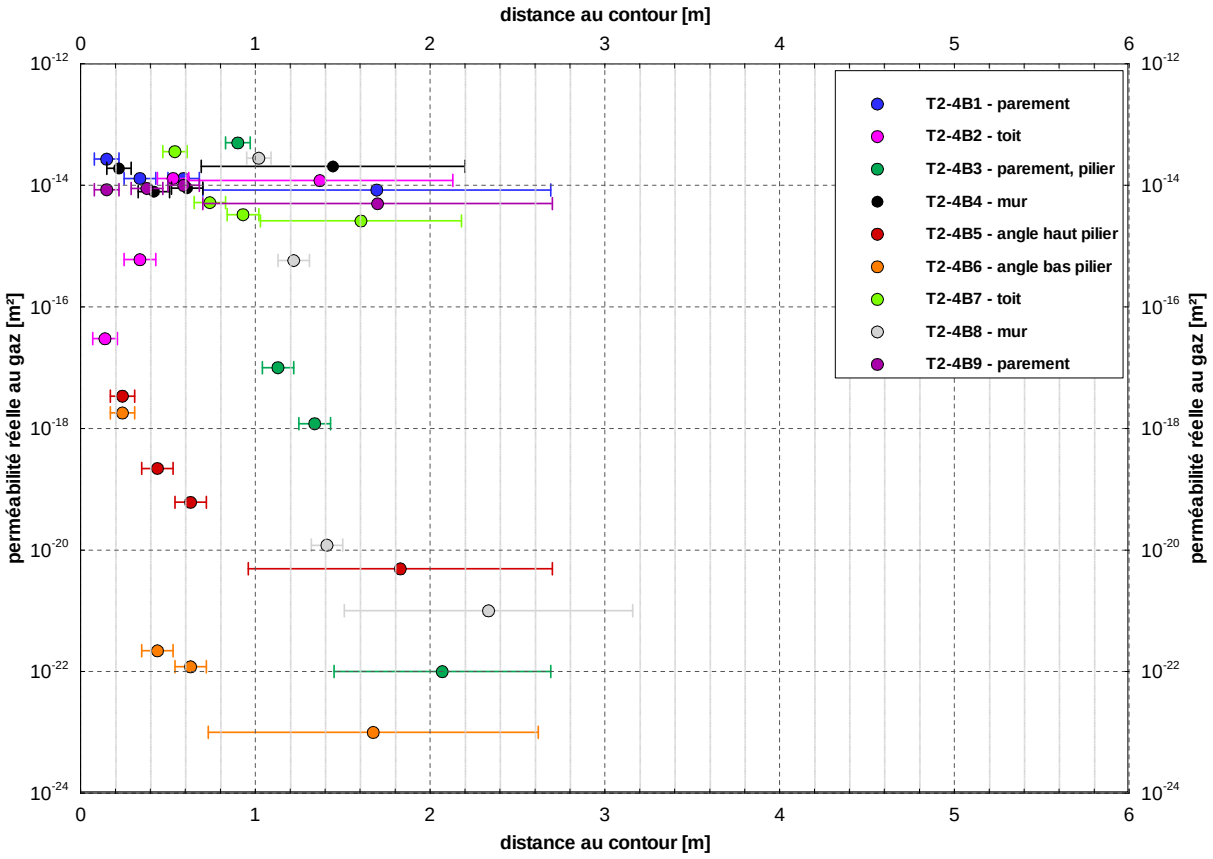

Figure 21 Results of in situ gas permeability tests at site T2-4

[Explanation: A) schematic profile of drift showing effective gas permeabilities, B) diagram k_{eff} vs. distance]

Figure 22 shows a similar frequency distribution for T2-4 as for T2-2 (Figure 18).

classement	*fré-quence*	*fréquence statistique cumulée*
≤ 1E-22	3	8.33%
≤ 1E-21	2	13.89%
≤ 1E-20	2	19.44%
≤ 1E-19	1	22.22%
≤ 1E-18	1	25.00%
≤ 1E-17	4	36.11%
≤ 1E-16	1	38.89%
≤ 1E-15	2	44.44%
≤ 1E-14	10	72.22%
≤ 1E-13	9	97.22%
> 1E-13	1	100.00%
nombre	36	

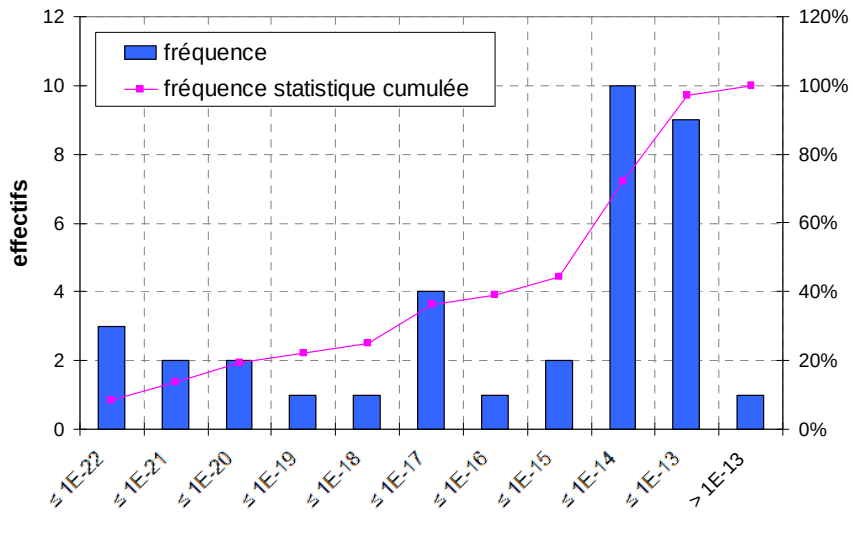

Figure 22 Frequency distribution of effective gas permeability at sites T2-4

More details on the permeability results from site T2-4 are cover in report part 8. Dependencies on site conditions (collar) and on distances to contour will be considered in chapter 9.

8.3 Laboratory investigations on core material from all sites

In total 198 samples were taken from core material in order to evaluate the brine content of rocks at the investigated sites. The goal of these investigations was to detect evaluated brine contents in order evaluate the in situ measured gas permeabilities in respect to the possibility of influence by liquid saturation in the sense of effective gas permeability.

Core samples were generally distinguished in marl, rock salt with certain amount of marl an, more or less pure rock salt. Figure 23 depicts the sampled lithologies.

A) B) C)

Figure 23 Sampled lithologies

[Explanation: A) marl sample ± anhydrite, B) rock salt with certain amount of marl, C) visually pure rock salt]

The core samples were investigated by oven drying referred to chapter 7.2

The Figure 24 presents all brine contents from the report parts 2, 3 and 4 ([9], [10] and [11]) versus the distance to contour for the three sites T1.

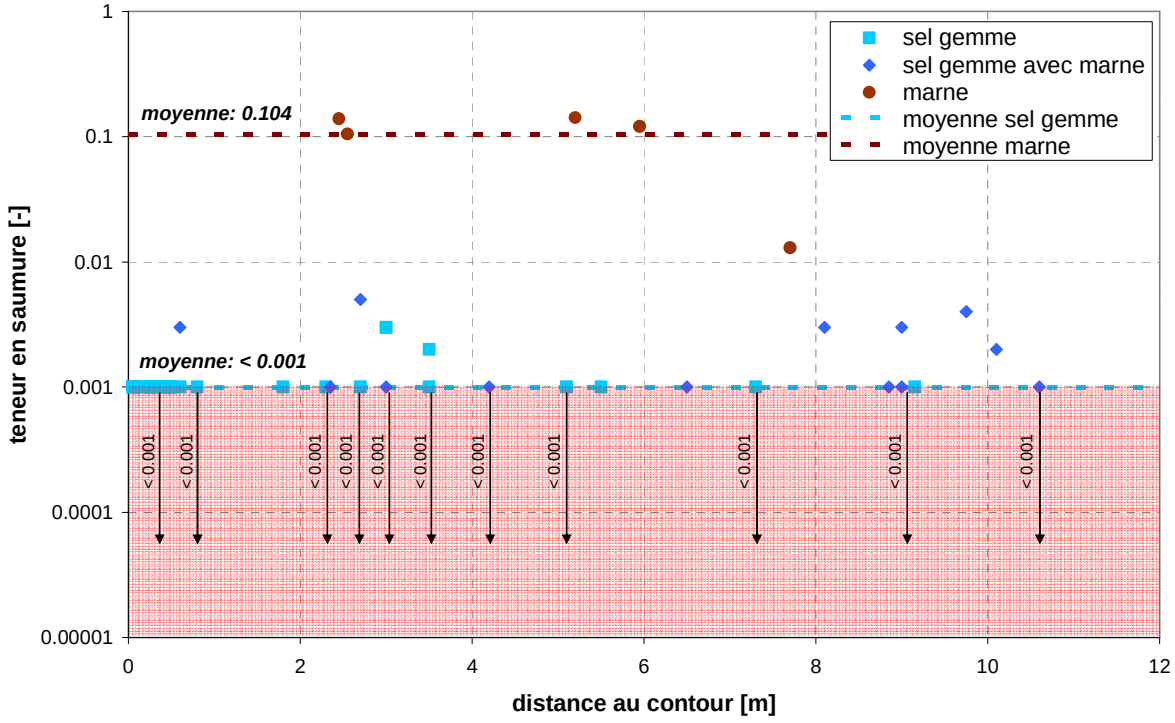

Figure 24 Brine content vs. distance to contour for sites T1

From 45 samples, brine contents > 1 wt % were only yielded for five marl samples as some one can see in Figure 24. All other analyses from rock salt and rock salt with certain amount of marl yielded brine contents < 1 wt % whereas, the bulk of values are even lower than 0.1 wt %. However, the following samples have brine contents between 0.1 wt % and 1 wt %.

Table 2 Samples of rock salt and rock salt with certain amount of marl from sites T1 having a brine content between 0.1 wt % and 1 wt %

borehole	cored section	sample ID	distance to contour (*)	brine content	additional information
-	-	-	[m]	[-]	-
T1-1B1	CS9	P224-14/5	ca. 8.1	0.003	broken core, smell of bitumen
		P224-14/6	ca. 8.85	0.001	ca.8.8-8.5 m marl
	CS10	P224-14/4	ca. 9.75	0.004	ca. 9.55-9.65 m marl
	CS11	P224-14/1	ca. 10.1	0.002	broken core material
T1-2B1	CS10	P224-38/5	ca. 9	0.003	broken core material, rock salt, strongly porous, ca. 8.65-8.75 m marl
T1-2B2	CS1	P224-35/2	ca. 0.25	0.001	broken core material, rock salt, smell of bitumen
	CS4	P224-35/6	ca. 2.7	0.005	broken core material, rock salt, ca. 2.45-2.5 m and ca. 2.7-2.75 m marl
T1-3B1	CS4	P224-36/2	ca. 3	0.003	broken core, rock salt
	CS5	P224-36/3	ca. 3.5	0.002	
T1-3B2	CS2	P224-37/4	ca. 0.6	0.003	broken core, rock salt, impurity by marl

The elevated brine content (Table 2) is assumed to be caused by a certain amount of marl within the rock salt samples.

To demonstrate the differences in brine content in respect to different lithologies mean values were calculated for marl with about 10.4 ± 5.3 wt % (n=5) and for rock salt < 0.1 wt % (n=27). No mean value was calculated for samples of rock salt with a certain amount of marl because these samples are representing rock mixtures with varying content of the components. However, basically these samples tend to slightly evaluated brine contents due to their marl content as seen in Figure 24 and Table 2.

The brine content of 153 samples from the four sites T2 are summarised and graphically analysed versus the distance to contour in Figure 25. The report parts 5, 6, 7 and 8 ([5], [6], [7]) are reporting more details.

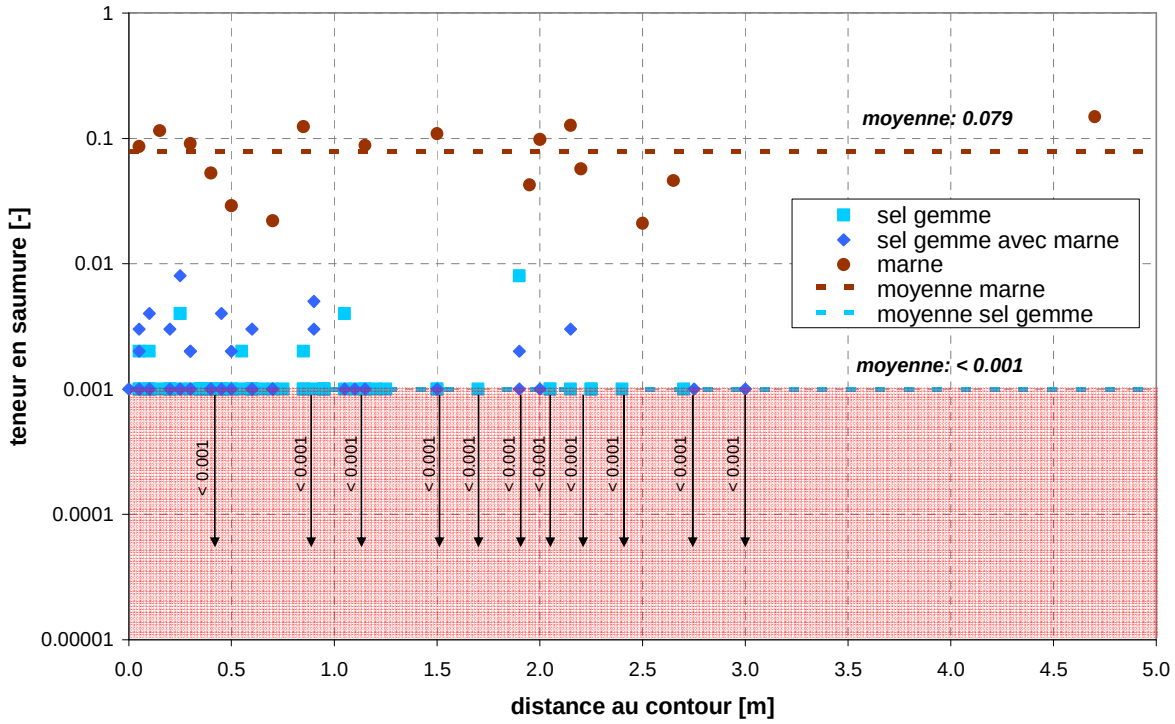

Figure 25 Brine content vs. distance to contour for sites T2

In principal the situation at the sites T2 resembles those at the sites T1 (compare Figure 25 with Figure 24). Brine content reaches values > 1 wt % only for marl samples (16 samples). For all other analysed samples values < 1 wt % were obtained. Samples having slightly elevated brine content are listed in Table 3.

Table 3 Samples of rock salt and rock salt with certain amount of marl from sites T2 having a brine content between 0.1 wt % and 1 wt %

borehole	cored section	sample ID	distance to contour(*)	brine content	additional information
-	-	-	[m]	[-]	-
T2-4B1	CS1	P224-10/1	ca. 0.1	0.003	rock salt, thin marl layers, heavy jointed
	CS4	P224-10/8	ca. 1.9	0.008	rock salt
T2-4B3	CS2	P224-20/2	ca. 1.05	0.004	rock salt, macroscopic pores
T2-4B4	CS1	P224-13/2	ca. 0.25	0.004	rock salt, macroscopic pores
T2-4B6	CS1	P224-22/2	ca. 0.35	0.001	rock salt
T2-4B9	CS1	P224-25/3	ca. 0.5	0.008	rock salt, impurified by marl, macroscopic pores
T2-3B2	CS1	P224-27/2	ca. 0.25	0.004	rock salt with marl bands
T2-3B7	CS2	P224-32/4	ca. 0.7	0.005	compact rock salt, heavy porous marl band at ca. 0.5 m, smell of bitumen
	CS5	P224-32/8	ca. 2	0.001	compact rock salt, marl bands at ca. 1.75 m and ca. 2 m, marl striae beginning at ca. 2.1 m, partly heavy porous
T2-3B9	CS2	P224-34/2	ca. 0.2	0.002	compact rock salt, smell of bitumen, from ca. 0.6-0.7 m wet
T2-2B2	CS1	P224-16/1	ca. 0.1	0.002	rock salt

borehole	cored section	sample ID	distance to contour(*)	brine content	additional information
-	-	-	[m]	[-]	-
		P224-16/2	ca. 0.35	0.001	
		P224-16/3	ca. 0.55	0.002	
T2-2B3	CS1	P224-8/1	ca. 0.05	0.002	rock salt with marl striae
		P224-8/2	ca. 0.3	0.002	
		P224-8/3	ca. 0.5	0.002	
	CS2	P224-8/7	ca. 0.85	0.002	rock salt, at 0.7-0.75 m and at 0.9-1.0 m jointed
	CS4	P224-8/5	ca. 1.9	0.003	rock salt with marl striae, heavy porous, wet
		P224-8/6	ca. 2.15	0.003	
T2-2B4	CS1	P224-7/1	ca. 0.05	0.002	broken core material, rock salt heavy smell of bitumen
T2-2B7	CS1	P224-6/1	ca. 0.05	0.002	rock salt with marl striae, P224-6/2 heavy smell of bitumen
		P224-6/2	ca. 0.3	0.001	
	CS2	P224-6/4	ca. 0.7	0.003	rock salt with marl striae, P224-6/4 heavy smell of bitumen, at ca. 0.75-0.9 m highly porous, probably by leaching, > 0.9 m highly porous, wet
		P224-6/6	ca. 1.1	0.004	
T2-1B2	CS1	P224-2/1	ca. 0.1	0.003	rock salt with marl striae, at ca. 0.2 m smell of bitumen
		P224-2/3	ca. 0.4	0.002	

Whereas, the slightly elevated brine content at T1-sites is only assumed to be caused by certain amounts of marl within rock salt analyses evidence for the existence of partly visible pore space in combination with wetness was reported in almost pure rock salt as well as in impure rock salt from T2-sites.

The mean value calculated from brine content of marl samples at sites T2 (bank S1) is with approximately 7.9 ± 4.1 wt % (n=16) slightly lower than this at T1 (bank S). However, this might be explained by the difference in the amount of analyses (5 samples at T1 compared to 16 samples at T2).

9 Interpretation of results in relation to the overall situation

9.1 Sites investigation T1

9.1.1 Permeability conditions in the roof

Figure 26 shows the change in permeability with increasing distance to contour in the roof independent from test site for all three T1 sites.

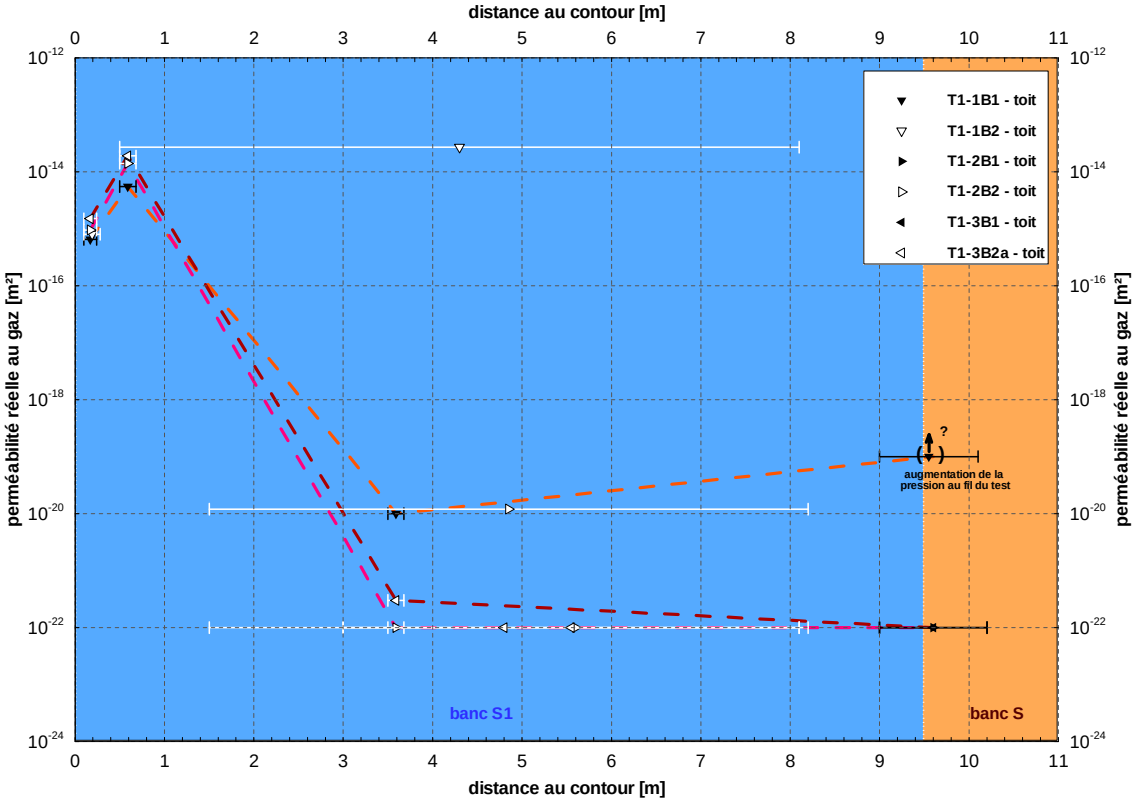

Figure 26 Effective gas permeability vs. distance to contour at T1 – roof

As seen in Figure 26, there is a good correlation between the results from all sites (T1-1, T1-2 and T1-3). The profiles from T1-1B1, T1-2B2 and T1-3B2 are showing similar permeability trends for the sedimentary sequences of bank S1. The range close to the contour (< 0.5-1.0 m) is characterised by an increase in effective gas permeability with the distance to contour. Based on the data on brine content (chapter 8.3), there is no evidence for an increased brine content at these measurement points in the vicinity of the drift (e.g. caused by air humidity). This is why we exclude an important influence of brine content to the effective gas permeability at this stage.

However, the measurements within the contour near range of the roof principally revealed a higher permeability level of > 6E-16 m² (T1-1B1-010-G1 in [9]). This is interpreted as loosening in the sense of the excavation damaged zone (EDZ). After this range the permeability decreases to very low values of ≤ 1E-20 m² (T1-1B1-350-G in [9]). However, the transition in permeability from > 1E-18 m² to < 1E-18 m² seems to occur earlier at sites T1-2 and T1-3 than at T1-1 somewhere between ca. 0.6 m and ca. 1.5 m (top of test intervals of T1-2B2-150-G in [10] and T1-3B2a-150-G in [11]). This may be caused by the lack of measurements at T1-1 in the range between ca. 0.6 m and ca. 3.5 m.

No pressure increase due to gas emission from the interbedded marl/anhydrite strata of bank S was observed during measurements T1-2B1-900-G1 and T1-3B1-900-G1. This is in contradiction to the equivalent measurement at site T1-1.

The measured effective gas permeabilities in the roof at the sites T1 can generally be distinguished in:

- distance to contour < ca. 0.6 m => elevated permeability level (> 6E-16 m²) due to loosening (EDZ)
- distance to contour > ca. 1.5 m => permeability level (≤ 1E-20 m²) whereas, pressure increase during test complicated evaluation of T1-1B1-900-G and T1-2B2-150-G

Generally, the rock salt without impurities of marl seems to have mainly low brine content (mean value < 0.1 wt %). However, the brine content of the marl locally rises up to maximal 14.2 wt % and has an average of 10.4 ± 5.3 wt % (n=5).

9.2 Sites investigation T2

9.2.1 Permeability conditions in the roof

Figure 27 shows the change in permeability with increasing distance to contour in the roof independent from test site for all four T2 sites.

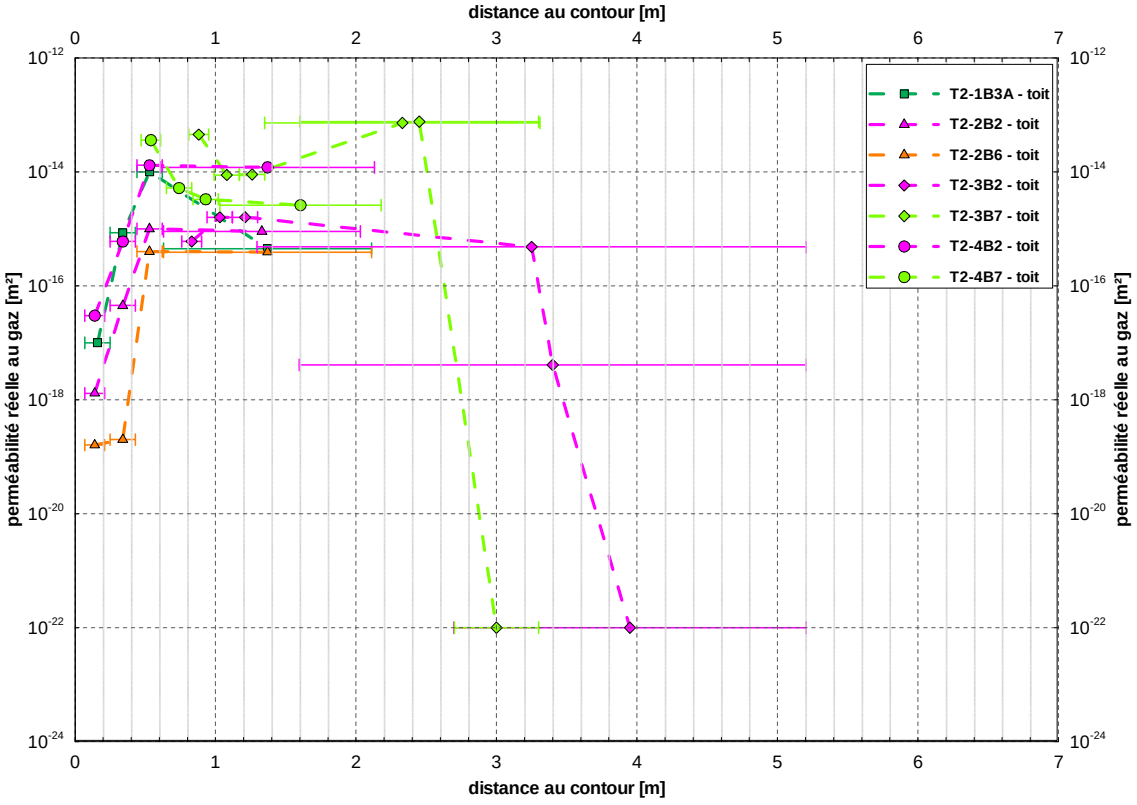

Figure 27 Effective gas permeability vs. distance to contour at T2 – roof

As seen in Figure 27, there is a good correlation between the measurements at all T2-sites (T2-1, T2-2, T2-4 and the first measurement points of the profiles from site T2-3). Basically, all seven permeability profiles show more or less similar conditions. The extended profiles of site T2-3 are showing a similar permeability level at distances < ca. 2 m. However, they reveal a permeability decrease to values of ≤ 1E-22 m² at distances > ca. 2 m.

Generally, the effective gas permeability increases with the distance to contour in the roof within the distance range from 0 m to about 2 m. As the extended profiles from site T2-3

show decreases the effective gas permeability within the distance range from about 2 m to about 5 m. Based on the data on brine content (chapter 8.3) there is no evidence for an increased brine content at these measurement points in the vicinity of the drift (e.g. caused by air humidity). This is why we exclude an important influence of brine content to the effective gas permeability at this stage.

The high effective gas permeabilities at MP4 (0.63 m to final depth) at sites T2-1, T2-2 and T2-4 might be caused by local higher permeabilities along small marl layers (e.g. bedding planes). The shifted profile in T2-4B7 however reveals a decrease in permeability with distance to contour within the interval of initial MP4 (0.63 m to final depth). However, the measurement T2-4B7-103-G testing an interval from 1.04 m to final depth still yielded a relative high effective gas permeability of 2.6E-15 m². Testing intervals having a larger distance to contour (e.g. T2-3B2-160-G, T2-3B2-270-G, T2-3B7-270-G) revealed a decrease in permeability down to values of ≤ 1E-22 m² as assumed in [7].

9.2.2 Permeability conditions in the face

Figure 28 shows the change in permeability with increasing distance to contour determined in all face boreholes from all test sites.

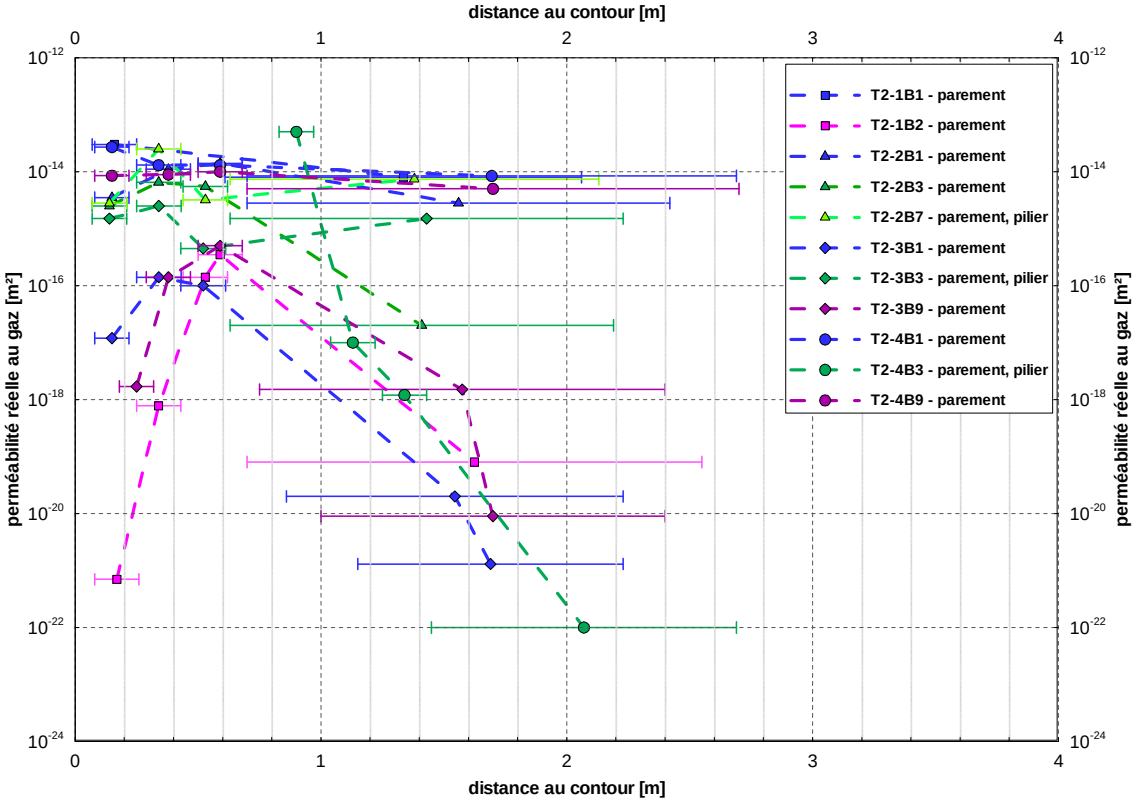

Figure 28 Effective gas permeability vs. distance to contour at T2 – face

As depicted in Figure 28 the bulk of results are showing effective gas permeabilities > 1E-15 m². A second group of measurements includes the complete measurements in the borehole T2-1B2, T2-3B1 and T2-3B9, MP4 in borehole T2-2B3 and the last 3 measure-

ments in T2-4B3. Principally, we assume higher local permeabilities along marl layers (e.g. bedding planes) as reason for the frequently observed relative high permeability level.

In the range from 0 m to ca. 0.6 m, permeability in boreholes T2-1B2, T2-3B1 and T2-3B9 increases with distance to contour. Based on the data on brine content (chapter 8.3) there is no evidence for an increased brine content at these measurement points in the vicinity of the drift (e.g. caused by air humidity). This is why we exclude an important influence of brine content to the effective gas permeability at this stage.

Measurements with smaller test intervals in a distance from 1.2 m to 2 m (MP2 and MP3 in T2-4B3) were suggested to specify permeability conditions in these intervals (e.g. [7]). Analogue to the measurements in the floor level MP3 in T2-4B3 reveals a transition in permeability from > 1E-18 m² to ≤ 1E-18 m² within a distance from ca. 1.2 m to 1.4 m which is in good concordance with the results from MP4 in T2-2B3, MP4 in T2-3B9 and MP4 in T2-1B2. However, at this stage it is impossible to say whether this observation only relates to T2-4B3 or is valid in a similar pattern for the other boreholes too.

9.2.3 Permeability conditions in the floor

The permeability conditions in the floor are shown for all T2-sites in Figure 29.

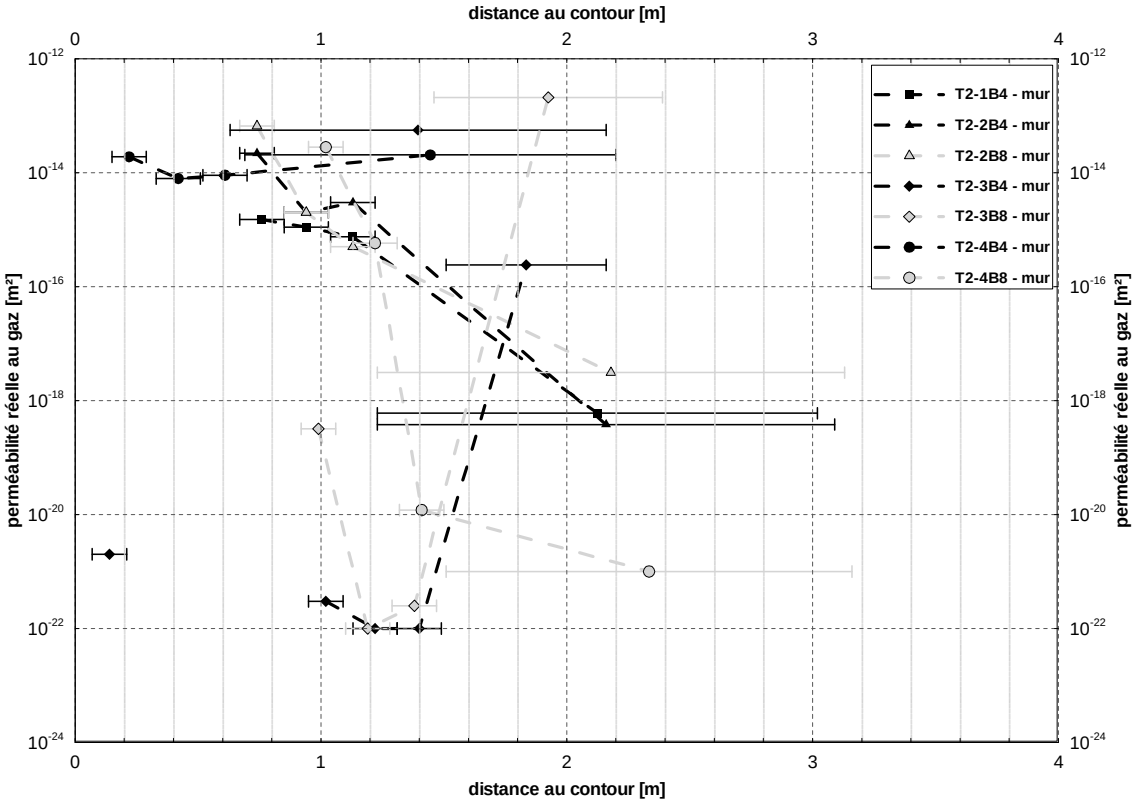

Figure 29 Effective gas permeability vs. distance to contour at T2 – floor

Three permeability profiles (T2-1B4, T2-2B4 and T2-2B8) start at ca. 0.6 m because the lower ranges were characterised by visible loosening of ground (e.g. cracks, fissures). That is why the planed profiles of measurement were completely shifted by about ca. 0.6 m. The profile in T2-4B8 was also shifted. However, the visible loosening of ground (e.g. cracks, fissures) was extended to about 1.0 m. Whereas the profile in T2-4B4 begins at about 0.15 m because no visible loosening of ground (e.g. cracks, fissures) was observed. The profiles at site T2-3 were shifted by about 0.85 m or 0.88 m, respectively. Shifting of profiles was cleared with the client.

Analogue to the situation discussed for the roof, there is again a good correlation between the results for T2-1 and the results for T2-2. However, permeability decreases with distance to contour in the floor. This is a permeability trend which is expected caused by loosening of ground due to excavation (EDZ).

For site T2-4 the transition in permeability from values of > 1E-18 m² to values ≤ 1E-18 m² occurs at a distance between ca. 1.13 m and ca. 1.5 m (MP2 and MP3 in T2-4B8) as Figure 29 reveals. On the other hand, measurements with in the range from ca. 0.15 m to ca. 0.7 m in T2-4B4 yielded relative high permeabilities from 7.9E-15 m² to 1.4E-14 m² showing that shifting of the other profiles was reasonable. MP4 in T2-4B4 (from ca. 0.69 m to ca. 2.2 m) is not in contradiction to the measurements at T2-1 and T2-2 or in T2-4B8 but is simply more affected by higher permeabilities within the range of ca. 0.69 m to ca. 1.13 m (compared to MP2 in T2-4B8) than MP4 in the other boreholes. Therefore, the results of T2-4 correlate to the general observed trend of permeability distribution and supply essential information for the range > ca. 1.2 m (T2-4B8) and for the range < ca. 0.6 m.

Based on these observations we assume relative high permeabilities between 0 m and ca. 1.13 m (> ca. 1E-15 m²), a transition in permeability from values of > 1E-18 m² to values ≤ 1E-18 m² somewhere between ca. 1.13 m and ca. 1.5 m and relative low permeabilities << 1E-18 m² for distances > ca. 1.5 m in the floor level. This is not applicable if changes in geology occur with distance to contour as both profiles from site T2-3 (T2-3B4 and T2-3B8) are showing. The different geological situation in the floor level of site T2-3 is depicted in Figure 30 where an intercalation of marl and anhydrite was drilled at the bottom of the bore-holes.

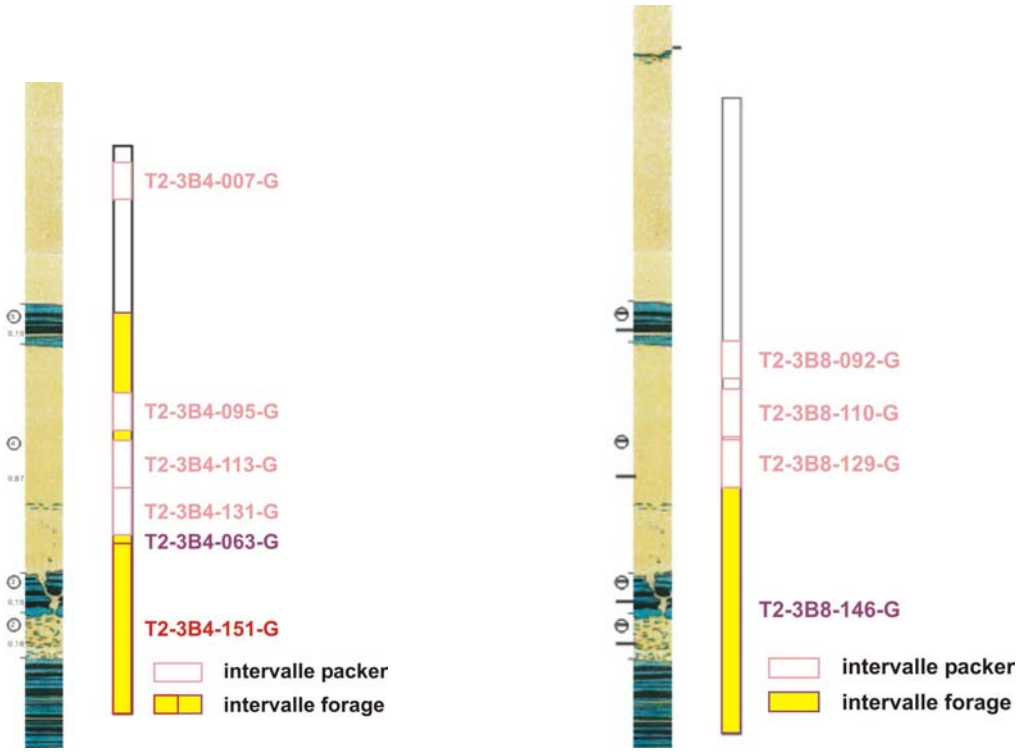

A) T2-3B4 B) T2-3B8

Figure 30 Schematic geological situation in the floor level of site T2-3 situated about 25 m in the footwall of the potash excavation

After a permeability level < 1E-18 m² at about 1 m distance to contour (T2-3B4-095-G or T2-3B8-092-G) the permeability decreases to values ≤ 1E-22 m² and finally increases to values > 1E-18 m² at T2-3B4-151-G or T2-3B8-146-G. Correlating these permeability results with the geological situation in Figure 30 we interfere that high permeability at the boundary faces either between rock salt and marl and/or between marl and anhydrite at the end of the bore-holes are accounting for yielded high permeability levels of effective gas permeability at T2-3B4-151-G and T2-3B8-146-G. This change in geology was observed in video inspection (see photographs in report part 7 [8], Table 1).

Furthermore, the additional measurements in borehole T2-3B4 at distances from ca. 0.07 m to ca. 0.14 m and from ca. 0.63 m to ca. 2.16 m are showing the occurrence of distance ranges (small intervals, T2-3B4-007-G) having low permeability (assumed to be pure rock salt) and other ones (large intervals, T2-3B4-063-G) having high permeability. Especially the comparison of the result of T2-3B4-063-G from 0.63 m to 2.16 m with the results from T2-3B4-095-G, T2-3B4-113-G and T2-3B4-131-G (small intervals) illustrates the effects of integral measurements in large borehole intervals. Whereas the measurement T2-3B4-063-G is characterized by high permeabilities presumably at boundary faces within the distance ranges from ca. 0.63 m to ca. 0.9 m and from ca. 1.5 m to ca. 2.16 m, the measurements of small intervals (T2-3B4-095-G, T2-3B4-113-G and T2-3B4-131-G) reveal low to very low permeabilities (pure rock salt) within the distance range from ca. 0.63 m to ca. 2.16 m.

9.2.4 Permeability conditions in the corners

Figure 31 shows the change in permeability with increasing distance to contour in the drift corners.

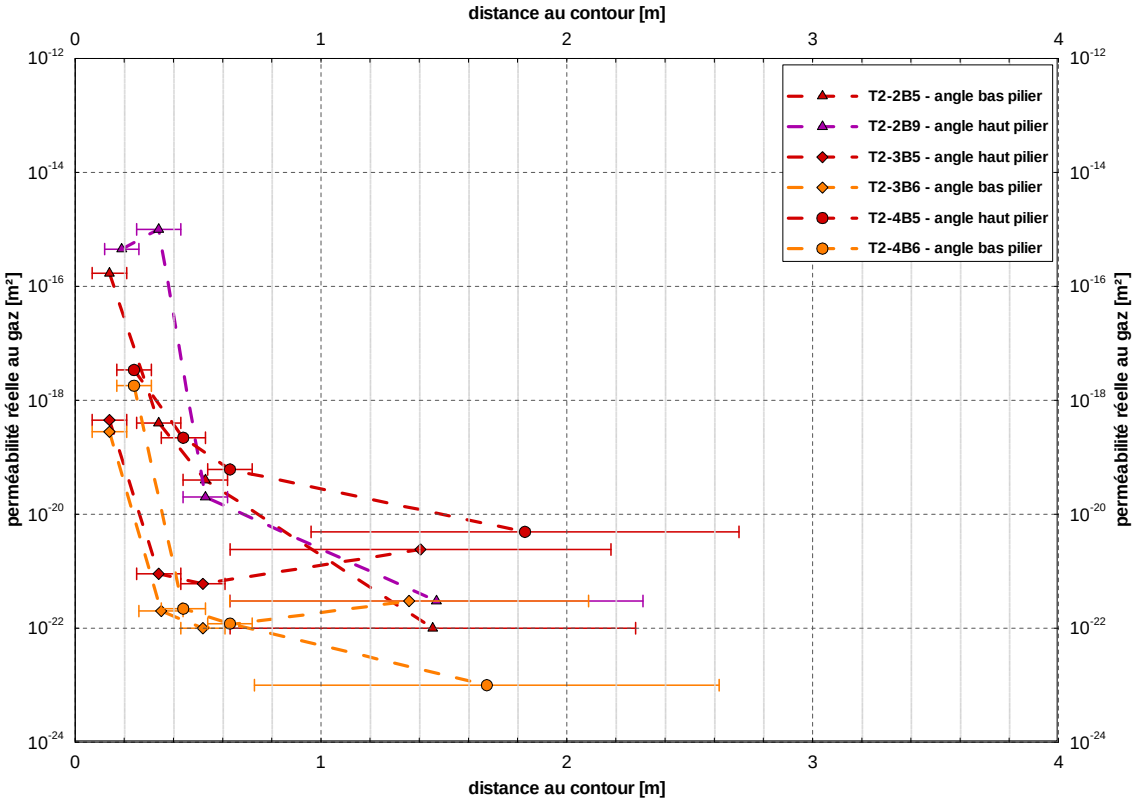

Figure 31 Effective gas permeability vs. distance to contour at T2 - corner

The permeability conditions in the drift corners were investigated at sites T2-2, T2-3 and T2-4. The permeability decreases with distance to contour as expected. The same general permeability trend was observed at all T2-sites. We assume the influence of high geomechanical stress in the drift corners limiting dilatancy in the roof and the floor regions of the pillar.

9.2.5 Permeability conditions in the pillar

At last Figure 32 shows the effective gas permeability vs. distance to contour only for the three T2-sites being located in double galleries.

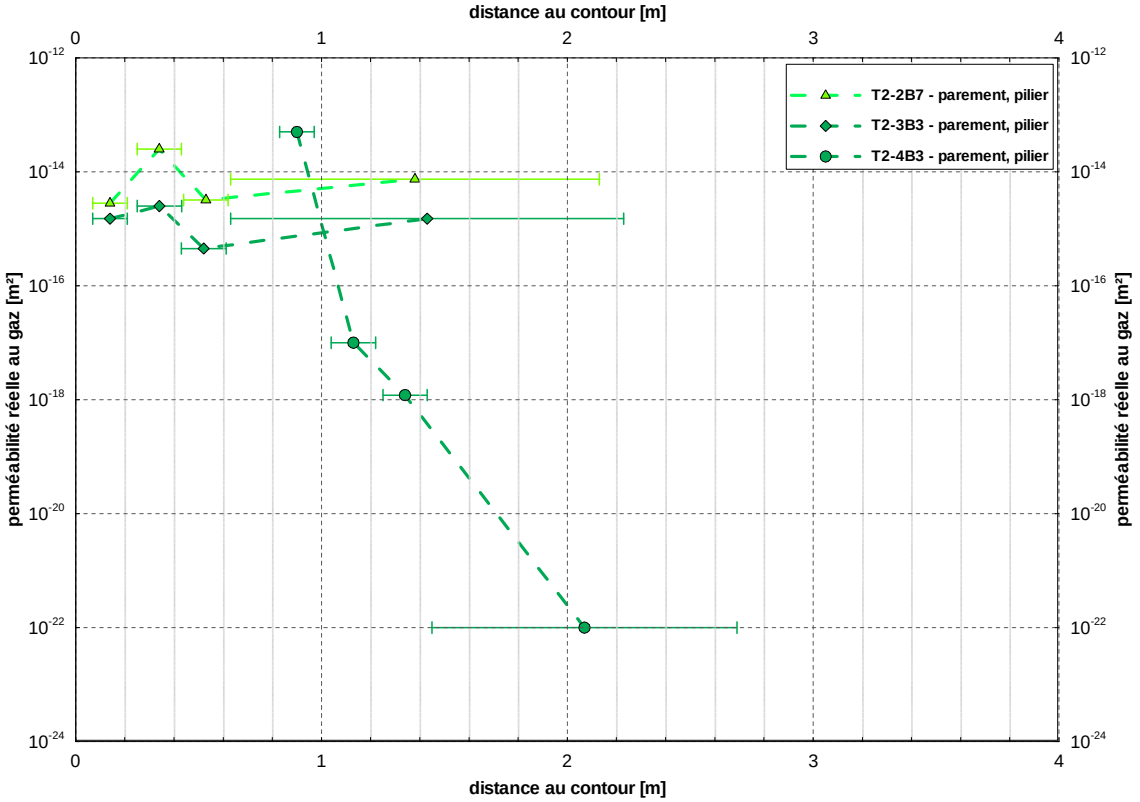

Figure 32 Effective gas permeability vs. distance to contour at T2 – face, pillar

The comparison of the results from boreholes T2-2B7, T2-3B3 and T2-4B3 (Figure 32) with the results from other face boreholes (Figure 27 in chapter 9.2.2) reveals that there is no evidence for particular higher permeabilities in the pillars of the double galleries (between AQ0T and AQ0D or AJ1T and AJ1D) compared to the massive drift faces.

9.3 Permeability conditions in the roof – comparison between T1- and T2-sites

The measurements in the roof give the opportunity to examine the general permeability situation and to analyse whether there exist differences in permeability distribution between T1- and T2-sites.

As Figure 33 reveals there is no conspicuous difference between the permeability profiles from T1-sites and from T2-sites. Basically, the only difference is that generally deeper measurement points were investigated in 8 m to 10 m deep boreholes at T1-sites whereas, the depth of measurement points at T2-site were mainly limited by a borehole depth of about 2 m to 2.5 m. Deeper boreholes were only be investigated at site T2-3 (up to 5.2 m).

That is why the general permeability situation in the roof can be summarised considering results from T1- and T2-sites as follows:

- range dtc < ca. 1.5 m: level of effective gas permeability mainly > 1E-16 m² (except some measurement points having a distance to contour lower than 0.4 m at T2-sites),
- range ca. 1.5 m < dtc < ca. 2.5 m: transition of level of effective gas permeability from > 1E-16 m² to < 1E-22 m² and

– range dtc > ca. 1.5-2.5 m: level of effective gas permeability mainly < 1E-22 m² (permeability tests T1-1B1-900-G and T1-2B2-150-G were influenced by gas emission)

On one hand, the ground close to the contour at T1-sites shows the analogue high level of effective gas permeability as at T2-sites (see measurement points T1-1B1-010, T1-1B1-050, T1-1B2-010, T1-1B2-050, T1-2B2-010, T1-2B2-050, T1-3B2a-010 and T1-3B2a-050). On the other hand, investigations in deeper boreholes at T2-sites (see T2-3B3 and T2-3B7) revealed a decrease in the level of the effective gas permeability with depth.

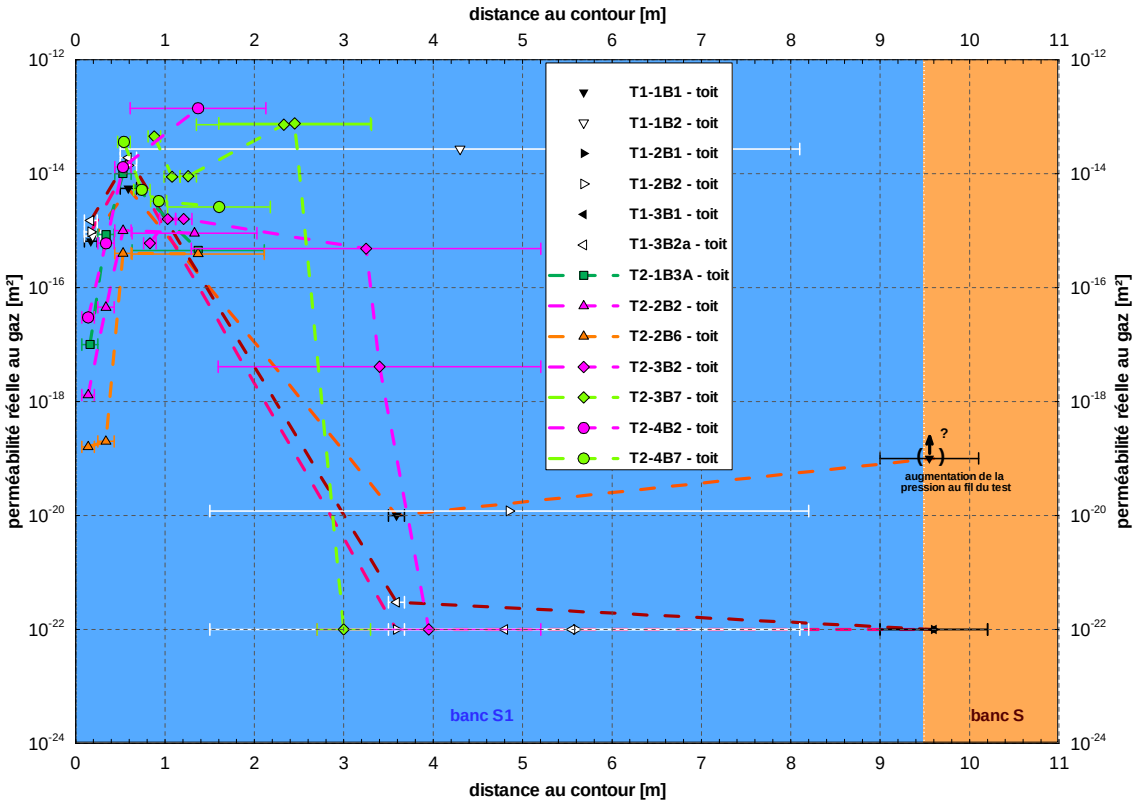

Figure 33 Effective gas permeability vs. distance to contour – comparison of permeability distribution in the roof at T1- and T2-sites

10 Summary

The results of the performed tests and investigations can be summarised as follows:

- Permeability profiles measured in layered rocks are dependent on the geomechanical site condition. Differences were found in respect to the collar (roof, face including pillar faces, floor level and drift corners). By this reason a comparison of permeability conditions in respect to the collar across all sites is admissible.
- The level of permeability depends on the distance to contour caused by loosening (EDZ). Generally, the permeability level within the first metre from the contour is > 1E-16 m² for the most performed tests. Some measurement points (roof: 6 points, face: 5 points and floor: 1 point) however yielded permeabilities ≤ 1E-16 m². At this stage it is assumed that the lower permeabilities are representing weakly to undeformed parts of pure rock salt (dependency on geology).
- The level of permeability in layered rocks depends on the geological site condition. Elevated permeabilities were measured in case of changes in lithology and/or in competence contrasts (rheological behaviour in case of deformation). The dependency of permeability on geology was demonstrated by the measurements T2-3B4-151-G and T2-3B8-146-G where permeabilities > 1E-16 m² were proved in a distance > ca. 1.5 m whereas the bulk of permeabilities in distances > ca. 1 m show values ≤ 1E-16 m² and often ≤ 1E-18 m².
- Based on the measured data showing often an inhomogeneous permeability distribution the following generalised distribution is assumed:
  - roof T1: < ca. 1.0-1.5 m => mainly elevated
  - roof T2: < ca. 1.5-2.0 m => mainly elevated
  - face: < ca. 1.0-1.5 m => mainly elevated
  - floor: < ca. 1.0-1.5 m => mainly elevated (geology caused elevation > 1,5 m possible, ca. 1.5-2.25 m)
  - corner: < ca. 0.25-0.5 m => mainly elevated (no geology dependence observed, assume the influence of high geomechanical stress in the drift corners limiting dilatancy)
- The permeability trends for the drift corners exhibit the expected behaviour of permeability dependent on the distance to contour (permeability decrease with distance).
- The permeability level in the roof at sites T1 is apparently low (≤ 1E-20 m²) in a distance to the contour of > ca. 1.5 m.
- The general permeability situations investigated in the roof boreholes at T1- and T2-sites are compatible.
- No evidence was found for particular high permeabilities within the pillars of double galleries in comparison to massive gallery faces. The permeability levels are equal within the first metre (> 1E-16 m²).
- The brine content of rock salt is generally low < 0.1 wt % and has mainly no major effect on effective gas permeability. However, the brine content can increase up to values between 0.1 wt % and 1 wt % if macroscopic pores are present. In case of impurity of rock salt by marl, intercalation of marl or presence of pure marl the brine content even rises up to 14.2 wt % (possible influence of analyses by drying of crystalline water at 105 °C).

11 Indexes

11.1 References

[1] StocaMine (2012): Order JR/CT156-12. StocaMine, France, 9th of October, 2012

[2] Rybka, S. (1981): Bassin Potassique de Mulhouse – Répertoire des bancs de halite et d'insolubles au–dessus et au-dessous des couches potassiques. Mines de Potasse d'Alsace S.A., Département Geologie, France

[3] DIN 18121, Teil 1 (1998): Baugrund; Untersuchung von Bodenproben - Wassergehalt - Teil 1: Bestimmung durch Ofentrocknung. DIN Deutsches Institut für Normung e. V., Berlin.

[4] IBeWa-1 (2012): Determination of in situ permeability in the StocaMine. Work program, IBeWa Consulting Germany on behalf of StocaMine, France, Order JR/CT156-12, 26th of October, 2012, 15 p.

[5] IBeWa-2 (2013): Preliminary results of sites T2-1 and T2-2. Interim report, IBeWa Consulting Germany on behalf of StocaMine, France, Order JR/CT156-12, 17th of January, 2013, 22 p.

[6] IBeWa-3 (2012): Determination of in situ permeability in the StocaMine. Work program, IBeWa Consulting Germany on behalf of StocaMine, France, Order JR/CT156-12, 14th of February, 2013, 19 p.

[7] IBeWa-4 (2013): Preliminary results of site T2-4. Interim report, IBeWa Consulting Germany on behalf of StocaMine, France, Order JR/CT156-12, 25th of March, 2013, 17 p.

[8] IBeWa-5 (2013): Preliminary results of site T2-3. Interim report, IBeWa Consulting Germany on behalf of StocaMine, France, Order JR/CT156-12, 23rd of April, 2013, 20 p.

[9] IBeWa-6 (2013): In situ permeability investigations at site T1-1. interim report, IBeWa Consulting Germany on behalf of StocaMine, France, order JR/CT356-12, 7th of May, 2013, 7 p.

[10] IBeWa-7 (2013): In situ permeability investigations at site T1-2. interim report, IBeWa Consulting Germany on behalf of StocaMine, France, order JR/CT356-12, 7th of May, 2013, 7 p.

[11] IBeWa-8 (2013): In situ permeability investigations at site T1-3. interim report, IBeWa Consulting Germany on behalf of StocaMine, France, order JR/CT356-12, 7th of May, 2013, 7 p.

[12] Ercosplan (2010): Backfilling of Underground Waste Disposal StocaMine, Wittelsheim/France. feasibility study, Ercosplan Ingenieurgesellschaft Geotechnik und Bergbau mbH, Erfurt / Germany, EGB 07-042, p. 16-20

[13] Walter, R. (1992): Geologie von Mitteleuropa. Schweizerbat'sche Verlagsbuchhandlung, Stuttgart, 561 p.

[14] Cosenza, Ph.; Ghoreychi, M.; Bazargansabet, B. (1997): Mesure de la perméabilité in situ du sel. Revue Francaise de Geotechnique, Nr. 79 (1997).

[15] Förster, S. (1970): Dichtheitsprüfung des Jüngeren Steinsalzes im Schacht Burggraf. Bergakademie Freiberg, Sektion Geotechnik und Bergbau, Lehrstuhl für Tiefbohrtechnik und Erdölgewinnung.

[16] Förster, S. (1985): Gasdruckbelastbarkeit und Rißbildung der für die unterirdische Gasspeicherung bedeutsamen Salinargesteine des Zechsteins. Dissertation, Bergakademie Freiberg, Sektion Geotechnik und Bergbau; veröffentl. in: Leipzig : VEB Deutscher Verlag für Grundstoffindustrie, Freiberger Forschungsheft A 724.

[17] Häfner, F.; Belohlavek, K.-U.; Förster, S.; Pohl, A.; Behr, A. (2001): In situ Ermittlung von Strömungskennwerten natürlicher Salzgesteine in Auflockerungszonen gegenüber Gas und Salzlösungen unter den gegebenen Spannungsbedingungen im Gebirge. Abschlussbericht 2001, TU Bergakademie Freiberg, Institut für Bohrtechnik und Fluidbergbau.

[18] Häfner, F.; Förster, S.; Pohl, A.; Behr, A. (1998): Dichtheitsuntersuchungen der Ortsbrust EU, 1. Teilbericht zum BMBF- und TMLNU-geförderten Vorhaben, Förderkennzeichen 02 C 0527 6, In-situ-Ermittlung von Strömungskennwerten natürlicher Salzgesteine in Auflockerungszonen gegenüber Gas und Salzlösungen unter den gegebenen Spannungsbedingungen im Gebirge, April 1998.

[19] Stormont, J.C. (1997a): Conduct and interpretation of gas permeability measurements in rock salt. Int. J. Rock Mech. & Min. Sci. Vol. 34, No 3-4, paper No. 303.

[20] Stormont, J.C. (1997b): In Situ Gas Permeability Measurements to Delineate Damage in Rock Salt. Int. J. Rock Mech. Min. Sci. Vol. 34, No. 7, 1997.

[21] Weber, J.R.; Wallner, M. (1998): Hydraulische Untersuchungen im Grubengebäude Morsleben. Bundesanstalt für Geowissenschaften und Rohstoffe, Hannover.

[22] Kaltofen, R.; Schumann, K.; Ziehmann, J. (1962): Tabellenbuch Chemie. VEB Deutscher Verlag für Grundstoffindustrie, Leipzig

11.2 List of Figures

11.3 List of Tables

11.4 Abbreviations

B	-	borehole
CP	-	constant pressure test
CR	-	constant rate test
CS	-	cored section
dtc / ddc	-	distance to contour / distance du conteur
EDZ	-	excavation damaged zone
FS	-	full scale
IBeWa	-	IBeWa Consulting
IT	-	pulse test
KR	-	control interval
MDPA	-	Mines de Potasse d'Alsace
MP	-	measuring point (equates the central point of test interval)
OK	-	upper limit of test interval
PDE	-	partial differential equation
PR	-	test interval
T	-	test site